Dissertations   Electronic Theses and Dissertations

2015

Synchrophasor Assisted Efficient Fault Location Techniques In An Active Distribution Network

Anil Khanal
North Carolina Agricultural and Technical State University

Synchrophasor Assisted Efficient Fault Location Techniques in an Active Distribution Network

Anil Khanal

North Carolina A&T State University

A dissertation submitted to the graduate faculty

in partial fulfillment of the requirements for the degree of

DOCTOR OF PHILOSOPHY

Department: Electrical and Computer Engineering

Major: Electrical Engineering

Major Professor: Dr. Gary L Lebby

Greensboro, North Carolina

2015

The Graduate School
North Carolina Agricultural and Technical State University

This is to certify that the Doctoral Dissertation of

Anil Khanal

has met the dissertation requirements of

North Carolina Agricultural and Technical State University

Greensboro, North Carolina
2015

Approved by:

_____   _____
Dr. Gary L. Lebby   Dr. Ali R. Osareh
Major Professor   Committee Member

_____   _____
Dr. Robert Y. Li   Dr. Jung H. Kim
Committee Member   Committee Member

_____   _____
Dr. John C. Kelly, Jr.   Dr. Clinton B. Lee
Department Chair   Committee Member

_____
Dr. Sanjiv Sarin
Dean, The Graduate School

Biographical Sketch

Anil Khanal was born to Ananda Prasad Khanal and Padma Khanal. He is the husband to Milu Neupaney Khanal. He is the brother of one sister Jyoti Bhattarai and two brothers: Amit Khanal and Avash Khanal. In 1999 he graduated as an electrical engineer from Karnataka Regional Engineering College, India. He worked in a transmission line project for Instalaciones Abengoa Inabensa S.A. from 1999 to 2002. From 2002 to 2004 he held the teaching and a network support engineering positions for a Computer Point (P) Ltd. He worked as an optimization and planning engineer in Spice Nepal (P) Ltd, a telecommunication company implementing GSM network from 2004 to 2006. He joined the masters in electrical engineering in 2007 and graduated in 2008 from University of Bridgeport, CT with an MSEE degree in power system. In Fall 2011 he joined the PhD program with North Carolina A and T State University and currently working towards his graduation. His concentration is in renewable energy and synchrophasor. Mr. Khanal is also a student member of Institute of Electrical and Electronics Engineering Society.

Dedication

This thesis is dedicated to my wife, Milu Neupaney Khanal who has greatly supported me throughout my graduate school since 2007. She has been a constant source of inspiration for me to make me choose this option and ever since has always stayed by my side. Her constant cheering and her strong held belief in me actually gave me strength to propel ahead during my lowest phases in my life. I cannot thank her enough for her immense contributions to make this day come true.

Acknowledgments

I would like to thank my advisor, Dr. Gary Lebby, for taking me as his student in his program . He has inspired me to work hard to excel more by examples and deeds but verbally. His general phrase "Publish or Perish" always kept me on check that I should never be the one who perishes. I am also totally grateful for the freedom he gave me to choose and work in the area I enjoyed the most. It was wonderful having him as my advisor. I would also like to thank Dr. Kim, Dr. Li, Dr. Osareh for their time and valuable advice. I have had further acquaintance with them while I took their classes . Those experiences were truly amazing. I would like to thank Dr. Clinton Lee for being my advisor. Though I did not have the opportunity to attend his class, I came to know him closely when I worked for him as his teaching assistant. Those experiences were very good. I would also like to extend my gratitude to Dr. John Kelly and the Electrical Engineering Department for financially supporting me through the better part of this program. I would further like to thank Dr. Sanjiv Sarin and the Graduate School for granting me the opportunity to pursue my PhD here at North Carolina A and T State University. The invitation to enroll and the financial support for a year were the turning point in my decision making. Lastly I would like to thank my colleague Mr. Emmanuel Oleka for his immense support and readiness to help whenever I needed one. His energy and the quest for knowledge were the door openers in many cases when I thought I had hit the dead end. I would once again like to thank Dr. Lebby for providing me the resources I needed for my research such as Biologically Inspired Energy and Engineering Systems (BIEES) laboratory facilities which gave me ground to prove myself. Out of school premises, I was constantly guided to stay on my path of success and for that reason I would like to thank my wife Milu.

Table of Contents

List of Figures

List of Tables

List of Abbreviations

CCVT	Coupling Capacitor Voltage Transformer
CHP	Combined Heat and Power
CIGRE	Council on Large Electric Systems
DER	Distributed Energy Resources
DFT	Discrete Fourier Transform
DG	Distributed Generation
DSP	Digital Signal Processing
FFT	Fast Fourier Transform
FTU	Feeder Terminal Unit
GA	Genetic Algorithm
GHG	Green House Gas
GIS	Geographical Information System
GPS	Global Positioning System
IEEE	Institute of Electrical and Electronics Engineers
IF	Instantaneous Frequency
IGBT	Integrated Gate Bipolar Transistor
IP	Instantaneous Phase
LL	Line to Line
LLG	Line to Line to Ground
LTC	Load Tap Changer
PDC	Phasor Data Concentrator
PEV	Pluggable Electric Vehicle

PMU   Phasor Measurement Unit

PPS   Pulse per Second

PV   Photo-Voltaic

RFE   ROCOF Error

RGA   Refined Genetic Algorithm

ROCOF   Rate of Change of Frequency

SLG   Single Line to Ground

SPC   Static Power Converter

THD   Total Harmonic Distortion

TVE   Total Vector Error

UTC   Universal Time Coordinated

WAMS   Wide Area Measurement System

Abstract

Reliability of an electrical system can be improved by an efficient fault location identification for the fast repair and remedial actions. This scenario changes when there are large penetrations of distributed generation (DG) which makes the distribution system an active distribution system. An efficient use of synchrophasors in the distribution network is studied with bidirectional power flow, harmonics and low angle difference consideration which are not prevalent in a transmission network. A synchrophasor estimation algorithm for the P class PMU is developed and applied to identify efficient fault location. A fault location technique using two ended synchronized measurement is derived from the principle of transmission line settings to work in a distribution network which is independent of line parameters. The distribution systems have less line length, harmonics and different sized line conductors, which affects the sensitivity of the synchronized measurements, Total Vector Error (TVE) and threshold for angular separation between different points in the network. A new signal processing method based on Discrete Fourier Transform (DFT) is utilized to work in a distribution network as specified in IEEE C37.118 (2011) standard for synchrophasor. A specific P and M classes of synchrophasor measurements are defined in the standard. A tradeoff between fast acting P class and detailed measurement M class is sought to work specifically in the distribution system settings which is subjected to large amount of penetrations from the renewable energy.

CHAPTER 1

Introduction

Distribution engineering is a complex science that involves striking a balance between multiple objectives that includes: power quality, reliability, efficiency, voltage regulation, safety to the general public, environmental impacts, aesthetics and cost [1]. The distribution network will be changed from radial network into multi-source network after DG connection. This change has a significant impact on the traditional relay protection, making the FTU-based distribution network automation feeder protection and fault location program more complex [2]. Fault location techniques are used in power systems for accurate pinpointing of the fault position. It helps fast repair to restore power system, improves system availability and performance as well as reduces operating costs, saves time and expense of crew searching in bad weather and tough terrain, aids crew in disturbance diagnostics by identifying temporary faults and detecting weak spots.

Synchronized Phasor Measurement Units aids some relief with real time measurement in the network.

1.1 Problem Description

This research has focused on two aspects of fault location using synchronized phasor measurement. First one is to analyze synchrophasor deployment in the transmission line and transform the model to the distribution system. Second, it improves on the signal processing techniques that is most suited to the distribution system.
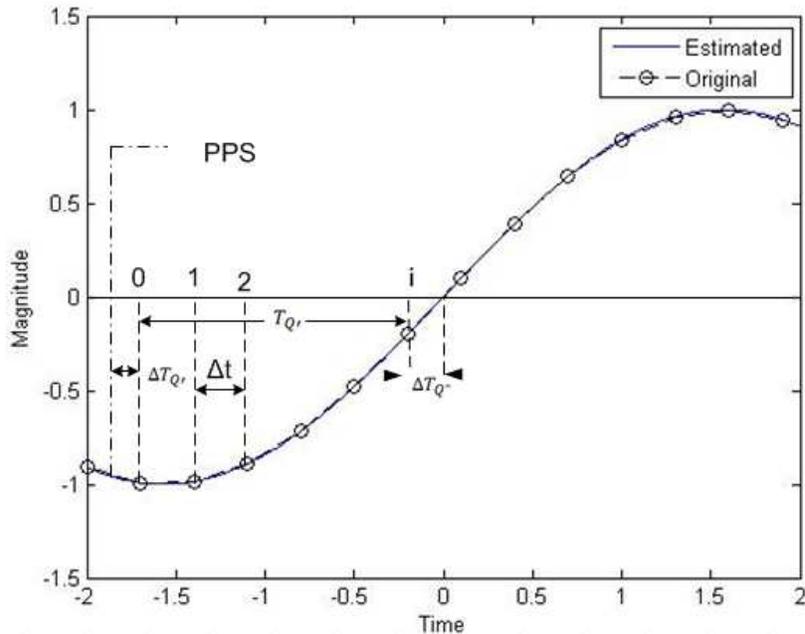
Figure 1.1: Synchrophasor phase estimation technique

The transmission system being operated at very high voltages and traverse a long distances, have their synchrophasor standard defined by IEEE C37.118 (2005) which obviously misses the precise standard needed by protection class (P) suited for distribution system. The distribution system have less line length and uses different sized conductor so the R/X ratios are different than the transmission line. The angle difference between two points in the network are too small to trigger an alarm and activate the subsequent automated protection protocols.

The second part of this research looks precisely into the signal processing techniques so as to address the problems faced by the previous synchrophasor standard. The latest standard IEEE C37.118 (2011) addresses the issue of TVE and Angular Deviation Threshold. A new algorithm is proposed using One Cycle Discrete Fourier Transform. This algorithm works in two step. First it finds the fundamental frequency tone of the signal in a Fourier domain and second, it reconstructs the tone of that fundamental frequency in a time domain for better phase

estimation. Figure 1.1 shows the tone reconstructed signal with phase correction at the start of the PPS from the GPS. The phase correction formulation is defined as in equation 1.1.

$$\varphi_1 = \frac{3}{2}\pi - 2\pi f_0\left(T'_{\varphi 1} + \Delta T'_{\varphi 1} + \Delta T''_{\varphi 1}\right) \tag{1.1}$$

where

$$T'_{\varphi 1} = i\Delta t$$

$$\Delta T'_{\varphi 1} = k\frac{1}{f_{clock}}$$

$$\Delta T''_{\varphi 1} = \Delta t\frac{s[i\Delta t]}{|s[i\Delta t] - s[(i+1)\Delta t]|}$$

The estimation of $T'_{\varphi 1}$ is realized by means of a counter that estimates (with the pointer k) the time interval between the PPS rise and the first acquired sample of the $s(t)$. This counter is associated to the clock frequency f_{clock} . The term $\frac{3}{2}\pi$ in equation 1.1 is needed in order to estimate the synchrophasor phase angle in agreement with the time reference defined in IEEE C37.118 (2011). The factors $s[i\Delta t]$ and $s[(i+1)\Delta t]$ are signal value of ith and (i+1)[th] samples.

1.2 Motivation

The motivating factor for me to take on this venture are my natural inclinations and interest towards renewable energy, as well as the collective advantages it brings to the society . The conventional source of energy is depleting every day by our growing consumptions. To fulfill the ever increasing demand of energy in this growing world, some alternative has to be sought before we burn all our conventional resources. On the other hand the burning of the conventional fuel lead us to degraded environmental conditions such as GHG emission, the

global warming phenomenon and the associated drastic changes in the climatic condition worldwide [3].

The interest part of this motivation is that, I had always wanted to work towards improving fault location techniques for an enhanced reliability of our distribution system in the face of large penetrations from the renewable energy. Since its inception, the fault location techniques has evolved through different phases. The use of synchronized measurement using PMUs for fault location applications looked promising and above all, the major contribution of this is credited to the virtue of synchrophasors voltage and current measurement technique itself. The technology is new and promising to be explored further and as well strengthens my research objectives.

The renewable energy resources which are a part of DG find their way in the distribution system as their integration point because these generations are more site specific, for example solar PV installations, wind turbine installations, small hydro plants etc. With the increasing amount of DGs in the distribution network the conventional distribution system has bidirectional flow of power and it needs more sophisticated approach to monitor and control the network changes and behavior.

1.3 Contribution

The area of interest impacted directly by this research are three fold. First the economical placement of the synchrophasor in the distribution network gives distribution network planner a cost optimized solution to monitor the health of the network. The real time monitoring by synchrophasor which are designed to work specifically under distribution system environment, saves time and money in terms of fault location techniques. Second, the new algorithm specific

for distribution system derived and retrofitted from the transmission network allows efficient fault location techniques and complies with the IEEE C37.118 (2011).

Third, the work at hand provides a small subset towards realizing a smart electric grid. With the work on active distribution system, deployment of PMUs and efficient signal processing techniques developed here helps integrate and manage the system with distributed resources efficiently and effectively. Some already accomplished tasks in these areas are the following publications which contributes in the field of Energy Economics and Optimization.

(A. Khanal, G. Lebby et. al) Optimal Placement of Phasor Measurement Units for Maximum Network Observability Using Python Gurobi. Conference: IAJC Orlando Fl, 25th Sep-27th Sep 2014.

(A. Khanal, G. Lebby et. al) Impact of Wind Energy on Cost and Balancing Reserves. Conference, ICEEE Miami Fl, 09th Mar-10th Mar 2015.

1.4 Dissertation Scope

This dissertation plans on achieving an efficient fault location algorithm in an active distribution network. It plans on developing a signal processing techniques in estimating synchronized phasor suited for distribution network with bi-directional power flow scenario. Synchrophasor estimation is done by implementing one cycle DFT. The PMUs are further subdivided into different performance classes such as P (Protection) class PMU and M (Measurement) class [4] depending on the precision and speed required by different applications. In this study the work is carried out with the P class PMU which is prompt to respond for the actions that requires high speed and fast decision. It focuses more on speed than on precision of measurement. It closely follows IEEE C37.118(2011) guidelines for the P class PMUs. Anything

outside of the P class are not the scope of this dissertation. The standard for synchrophasor does not specify the out-of-band interference testing for a P class PMU, so it also remains out of the scope of this dissertation.

The development of this algorithm is for the implementation for fault location techniques improvement on the distribution network. It plans to compare all other algorithms for the same purpose and proves the efficiencies of the proposed algorithm.

1.5 Dissertation Outline

This dissertation is organized in the following way. Chapter 1 describes the problem at hand and portrays the interest and the motivation to work towards solving this problem. It outlines the necessary contributions in the area after the successful implementation of this algorithm. In chapter 2 the author gives brief descriptions on the background of the related topics. Since this venture is related to the efficient fault location techniques in an active distribution network, it describes the relevant topics such as smart power systems followed by renewable distributed generations giving an emphasis on the issues. It points out the most common problems encountered and describes the nature in an elaborate way. It delves deeper into faults and its sources in the distribution network.

Further it describes the technology introduced to eradicate or mitigate the above mentioned problems. Such technology implemented here are in the form of synchronized phasor measurement techniques, which are described in detail and the extent of its implementations are assessed to provide clear understanding of the problems at hand. Chapter 3 gives the relevant literature review incorporating the area of interest in this field. Chapter 4 describes in details the methodology used to achieve this goal. In chapter 5, the methodology described earlier is further

implemented into a realistic network to apply the algorithm and preset the conditions for bigger experiments. In chapter 6, the results are discussed with its outcome when implemented in a bigger network. The statistical analysis is provided to compare and authenticate the findings in this area. Finally Chapter 7 concludes this dissertation with possible future endeavor.

CHAPTER 2

Background

2.1 Smart Power System

In [5] the authors points out the electric power system delivery as the greatest and most complex machine ever built. It consists of wires, cables, towers, transformers and circuit breakers—all bolted together in some fashion, as shown in figure 2.1.

Markets   Operation Center   Power Generation Plant   Transmission   Power Distribution Center   Customer Use

Electricity flows only in single direction
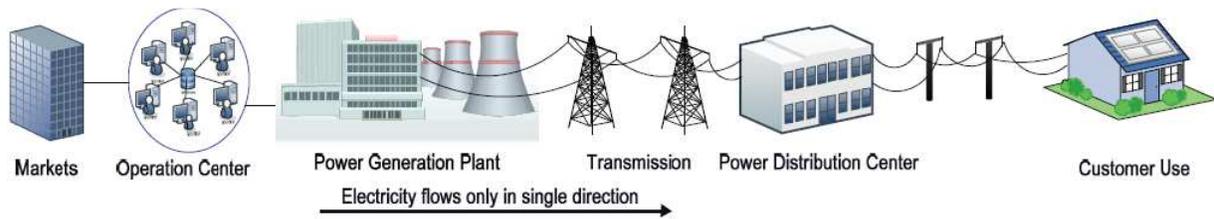
Figure 2.1: Conventional power system [5]

The conventional grid is a robust system. The penetration from renewable energy into the distribution system changes the fundamental settings of the conventional distribution system and challenges the robustness it possess. The distribution system in the past and in most countries even now uses a top down power flow model. For example the energy is produced in a generation units and transmitted through transmission network to the distribution network and eventually to the customers. The concept and increasing practices of using site specific distributed renewable energy generators nearer to the customer and load changes the working principle of the distribution network. The simple unidirectional protection devices fails to respond when the power is flowing in both directions. The non dispatchable nature of these generations are hard to account for reliability of the services and are more prone to the faults due

to the mismatches in the generation and the load. To accommodate these renewable energies and yet maintain the same level of reliability in the distribution network, a fundamental changes are required. These changes have evolved since its inception and are still working towards the betterment of the network in the power system. The smart grid initiative addresses these issues and makes recommendations to various aspects of the system.

A smart grid is an electricity network that can intelligently integrate the actions of all users connected to it - generators, consumers and those that do both in order to efficiently deliver sustainable, economic and secure electricity supplies [6]. A smart grid can:

- Better facilitate the connection and operation of generators of all sizes and technologies

- Allow consumers to play a part in optimizing the operation of the system

- Provide consumers with greater information and choice of supply

- Significantly reduce the environmental impact of the whole electricity supply system

- Deliver enhanced levels of reliability and security of supply.

The conceptual model of a smart grid is shown in figure 2.2.
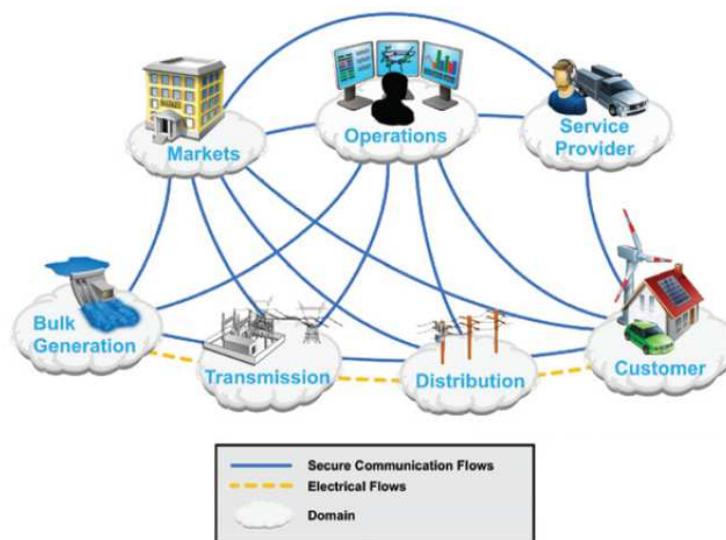
Figure 2.2: Conceptual model of a smart grid [5]

The distribution system are the major sources to contribute on the reliability issues. According to [7] about 80 percent of reliability factors are distribution system generated. This scenario even worsens when there are large penetrations from the renewable energy. The effect of different type of DGs and their impacts are explored in the next section. But before that, the process of transformation of the distribution network into an active distribution network is important and are considered here first.

The Distribution networks in the past were used as a passive networks which employed 'Fit and Forget' strategy. As the time advanced, the complications in the distribution system also advanced and now the majority of transmission network responsibilities such as constraint management, power flow, contingency analysis and balancing role have been assigned to the distribution network [6] . Beside these existing transmission network responsibilities, the increasing number of DGs, the intelligent residences and commercial buildings services and the need for the local generations to support the local loads during out-of-the-mains conditions due to the tremendous increase in PEVs charging also came to the distribution system. The role of an active distribution networks according to [5] are:

- Effective and coherent visibility of the various devices for timely decision making and information flow

- Centralized control replaced by a distributed control architecture

- Retrofit design for compatibility of all functions and devices

- On-line control, management and optimization of new functionality based on communication protocol, communication capacity, communication reliability and cost

2.2 Distributed Generation

Active distribution network operation requires accurate control of the available DERs in order to optimally dispatch power flow, keep bus voltages within specified limits and particularly in islanding condition, maintain the network frequency [8]. The IEEE defines distributed generation (DG) as the generation of electricity by facilities that are sufficiently smaller than central generating plants so as to allow interconnection at nearly any point in a power system [9].

The CIGRE working group has set its definition of DG [10] to be generation that is (1) not centrally planned (2) not centrally dispatched (3) usually connected to the distribution network (4) smaller than 50–100 MW. In [11] author points out that the DG is growing in a very fast pace as an alternative generating resources and as the ratio of DG over total system capacity increases, the impact on various system aspects becomes significant. Due to the variability and uncertainties of DG, the integration have impacts on reliability, operating efficiency, power quality and many other aspects of power systems.

The reference [9] points out the benefit of DG as i) High efficiency in CHP. ii) Enhanced reliability as a standby or emergency generation. iii) Cost effective source of energy for peak shaving purpose. iv) Reduction in loss due to grid support. v) Grid investment deferment. vi) Green power due to subsidized renewable energy strategy. vii) Mass production does not burden customers and viii) High quality supply for premium power. Barker and de Mello et. al. [12] further states that these benefits can be available only when the DG sources are reliable, dispatchable and of the proper size and at the proper locations. Taking these factors into the consideration we have looked further into these issues which are explained in detail in the following sections.

2.3 Types of Green Power Generators

Mozina et.al [13] classifies the different types of green distributed generation or renewable energy by working principles as i) Induction type, example: wind power. ii) Synchronous type, example: internal combustion engine, small hydro, gas turbines. iii) Asynchronous type (SPC), example solar, PV, fuel cell and wind.

For Induction type generators the excitation are provided externally by system VAr drain. These are less costly than synchronous machines since no excitation system or control is needed and also no sync equipments are needed to operate. But it is limited in size to less or equal to 500 kVA and also may cause ferro resonance after disconnection from utility. Figure 2.3 and 2.4 shows the induction type generator with specific wind generator. Wind generator can be pitch regulated, squirrel cage, induction generator and direct grid connected.
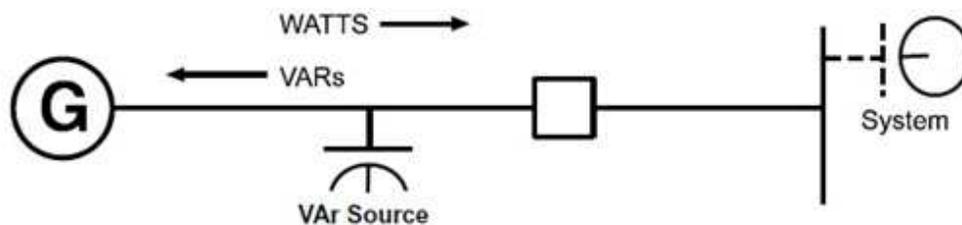
Figure 2.3: Excitation provided by system VAR drain [13]
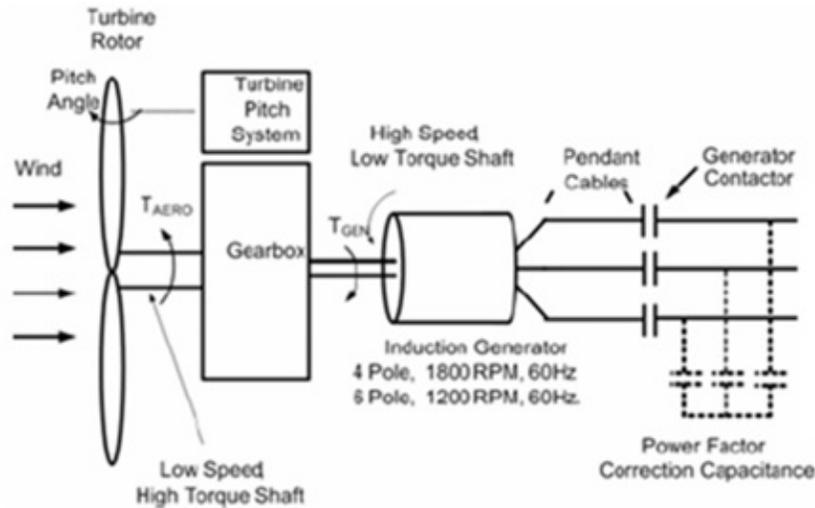
Figure 2.4: Wind turbine [13]

For synchronous generators the excitation is provided by DC field. This generator needs to synchronize with the utility system. Figure 2.5 shows the synchronous generator system with DC excitation.
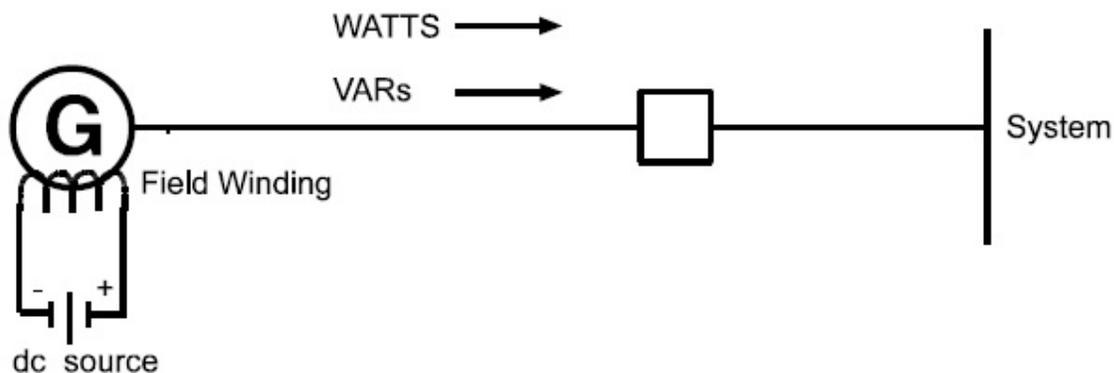
Figure 2.5: Synchronous machine with DC excitation [13]

Asynchronous type generators or SPC converts generator frequency to system frequency (dc-ac or ac-dc) as this generator is asynchronously connected to the power system. It may be self-commutating (needs sync relay) or maybe line-commutating (no sync relay needed). Figure 2.6 shows the asynchronous generator.
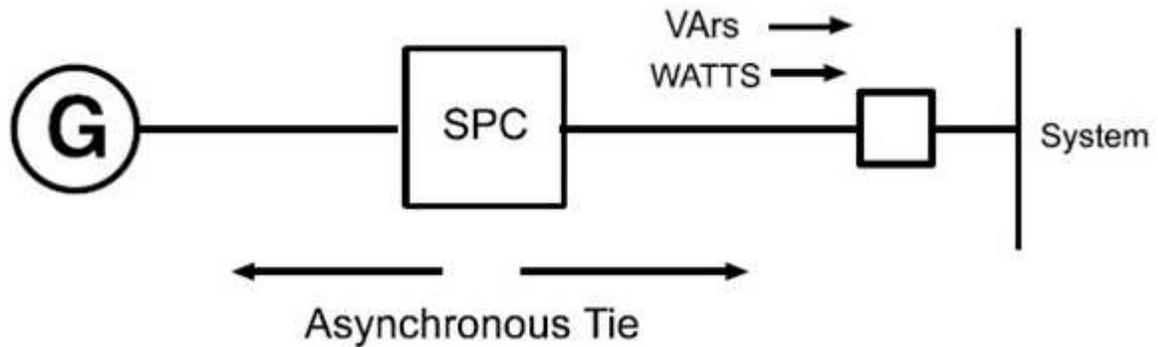
Figure 2.6: Asynchronous generator [13]

2.4 DG Interconnection with the Grid-An Issue

2.4.1 Islanding

Islanding occurs when the distributed generators continues to energize a portion of the utility system that has been separated from the main utility system. The separation from the mains could be due to the operation of a breaker, fuse, or automatic sensationalizing switch. Manual switching could also lead to islanding. Islanding can occur only if the generator can self excite and sustain the load in the islanded section. In most cases it is not desirable for a DG to island with any part of the utility system because this can lead to safety and power quality problems that will affect the utility system and load [12]. If an island develops on a feeder, the islanded DG units will quickly drift out of phase with the utility system during this loss-of-mains. When a reclose occurs, the utility will connect out of phase with the island if reclose blocking into an energized circuit is not provided at the breaker control. This can cause damage to utility equipment, the DG units supporting the island, and customer loads. Islanding also

increases the likelihood that DG sources may be allowed to subject the island to out of range voltage and frequency conditions during its existence and it can pose a serious safety threat during downed conductors and utility repair operations since the public and utility workers may be exposed to circuits that otherwise would be de-energized. Finally, islanding can hinder service restoration by requiring line crews to spend extra time disabling the island conditions.

On the other hand islanding can be used to the utilities advantage by allowing it to work safely isolated with the utility grid. The implementation of DG can increase reliability of electric service if units are configured to provide "backup- islands" during upstream utility source outages [12].
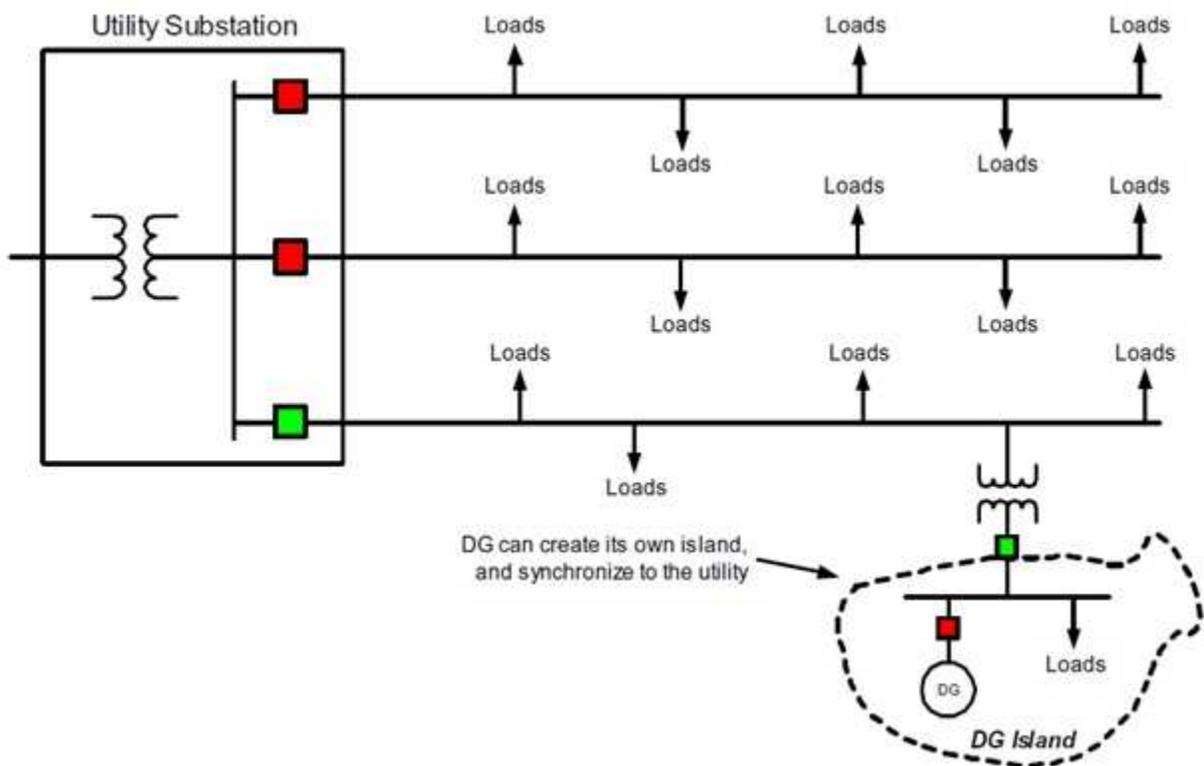
Figure 2.7: Island operation with DG [12]

Figure 2.7 shows the scheme where an upstream automatic switch is used to island a section of a distribution feeder. For this approach to work the switch must open during upstream faults and the generators must be able to carry the load on the islanded section maintaining suitable voltage and frequency levels at all islanded loads. A DG assigned to carry the island must be able to restart and pickup the island load after the switch has opened. Power flow analysis of island scenarios must be performed to insure that proper voltage regulation is maintained and to establish that the DG can handle inrush current during starting of the island. The DG unit must be able to load follow during islanded operation and the switch will need to sense if a fault current has occurred downstream of the switch location and send a signal to block islanding if a fault has occurred within the island zone. When utility power is restored on the utility side, the switch must not close unless the utility and island are in synchronism. This requires measuring the voltages on both sides of the switch and transmitting that information to the DG unit supporting the island so that it can synchronize with the utility and allow reconnection [12].

2.4.2 Voltage Regulation

In the conventional distribution network the voltage regulation is done by On Load Tap Changing Transformers, Line Regulators and Switched Capacitors on substation and feeder respectively. The introduction of DG in the network introduces the bi-directional power flow scenario which interferes with the effectiveness of standard voltage regulation practices [12]. This impact is further assessed with the example shown below in figure 2.8.
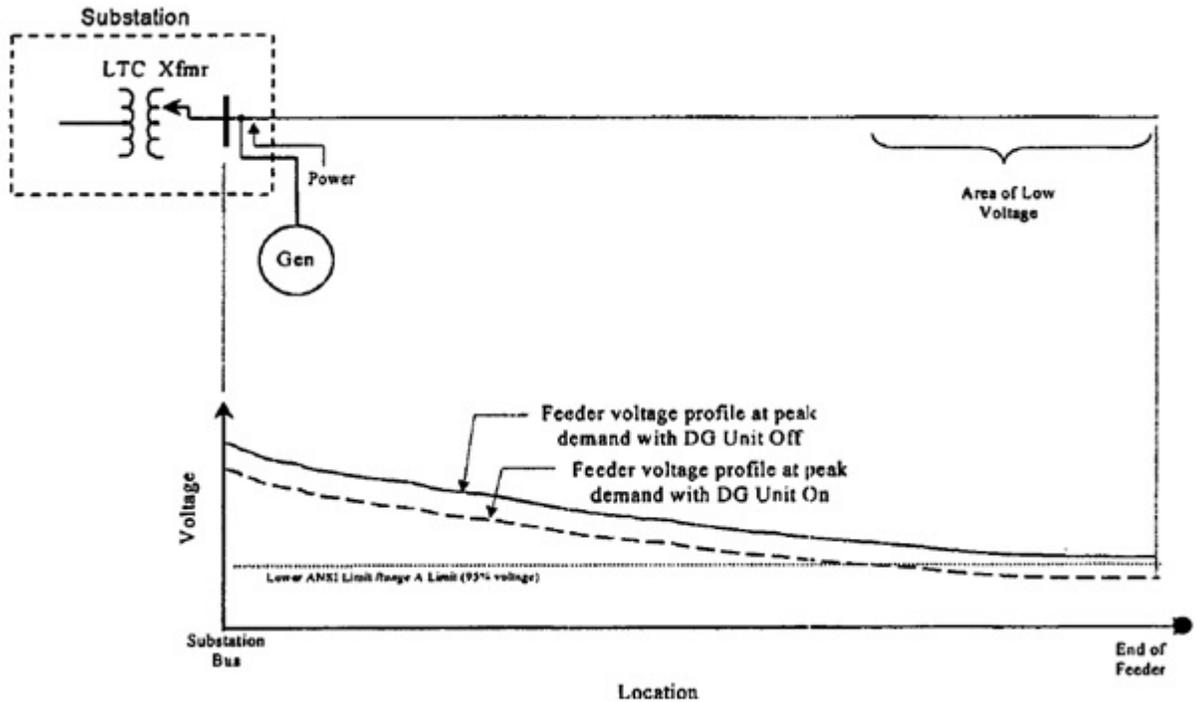
Figure 2.8: DG unit interfering with the voltage regulation [12]

An LTC transformer or a voltage regulator is used to regulate the voltage profile over the predefined length of the line. The voltage profile is considerable throughout the length of the line as it is evident from the figure above. When DG is added at the downstream of this substation or the line regulator, then this regulation control is unable to measure feeder demand properly. The impact of DG makes the voltage lower at the feeder side. The voltage is reduced because the DG reduces the observed load at the line drop compensator control. This confuses the regulator into setting a voltage lower than is required to maintain adequate service levels at the tail end of the feeder. As also mentioned by [14] the solution to this problem is to move the DG to the upstream of the regulator. In other words the smooth operation of distribution network depends on the location of DGs so does the fault occurring with this condition. So the incompatibility of the DG could both cause high or low voltage problems but also DG, when properly placed could compensate for the losses.

2.4.3 Harmonics

Distributed generators introduces harmonics when they are connected to the distribution system. The type and severity will depend on the power converter technology and interconnection configuration of these system. Inverters also have harmonic current contributions to the utility system. New inverter designs are based on IGBTs that uses pulse width modulation to generate the injected sine wave and these newer inverters are capable of generating a very clean output and they satisfy IEEE 519-1992 requirements [12]. Table 2.1 shows such requirements.

Table 2.1: Harmonic current injection requirements for DGs as per IEEE 519-1992 [12]

Harmonic Order	Allowed Level Relative to Fundamental(Odd Harmonics)
<11th	4%
<11th to <17th	2%
<17th to <23rd	1.5%
<23rd to 35th	0.6%
35th or greater	0.3%
Total Harmonic Distortion	5%

Any DG installation design should be reviewed to determine its compliance with IEEE 519 [15] and whether harmonics will be confined to the DG site or also be injected into the utility system. For larger DG units or cases involving complex harmonic problems, measurements and modeling of the system harmonics may be required to assess conditions. Any analysis should consider the impact of DG currents on the background utility voltage distortion

levels. The limits for utility system voltage distortion are 5% for THD and 3% for any individual harmonic [12].

2.4.4 Impact on Short Circuit Levels

The fault contribution from a large DG unit can alter the short circuit levels enough to cause fuse-breaker mis-coordination though this effect may not be seen with a small DGs [12]. This could affect the reliability and safety of the distribution system. Figure 2.9 shows a fused lateral on a feeder where fuse saving scheme or the fault selective relaying is utilized. If a DG units are added to the system, the fault current may become large enough that the lateral fuse no longer coordinates with the feeder circuit breaker during the fault [12]. This would lead to unnecessary fuse operations and decreased reliability on the lateral.
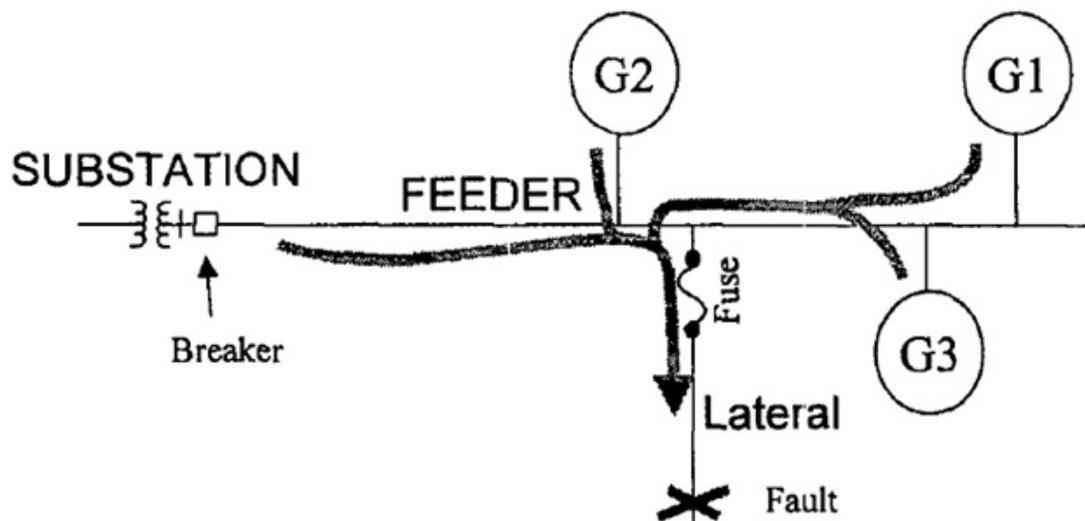
Figure 2.9: Fused lateral on a feeder where fuse saving scheme or the fault selective relaying is utilized [12]

Typical short circuit levels of DG power converters are characterized in table 2.2 below from [12].

Table 2.2: Short circuit levels of DG power converters

Type of Generator	Fault Current into shorted bus terminals as percent of rated output current
Inverter	100-400% (Duration will depend on controller settings and current may even be less than 100% for some inverters)
Separately excited synchronous generator	Starting at 500-1000% for the first few cycles and decaying to 200-400%
Induction generator of self excited synchronous generator	500-1000% for first few cycles and decaying to a negligible amount within 10 cycles.

For inverters, the fault contributions will depend on the maximum current level and duration for which the inverter manufacturer's current limiter is set to respond. On some inverters fault contributions may last for less than a cycle, in other cases it can be much longer. For synchronous generators, the current contribution depends on the pre-fault voltage, sub transient and transient reactance of the machine, and exciter characteristics. Induction generators can also contribute to faults as long as they remain excited by any residual voltage on the feeder. For most induction generators, the significant current would only last a few cycles and would be determined by dividing the pre-fault voltage by the transient reactance of the machine, Even

though a few cycles is a short time, it is long enough to impact fuse-breaker coordination and breaker duties in some cases [12].

2.4.5 Grounding and Transformer Interface

Distributed generation must be applied with a transformer configuration and grounding arrangement compatible with the utility system to which it is to be connected otherwise the voltage swells and over voltages may be imposed on the utility system that damages utility or customer equipments [12]. Table 2.3 shows some transformer arrangements used for DG sites.

Table 2.3: Transformer arrangements for DG sites [12]

Transformer Configuration	Comments
Delta/Wye-Grounded Or Delta/Delta	Both of these will not provide effective grounding unless a suitably sized primary side grounding bank is provided adjacent to the step-up transformer
Wye-Grounded/Wye-Grounded	Provides effective grounding only if a suitable sized grounding bank is provided or if the generator is Wye-Grounded and meets neutral impedance requirements.
Wye-Grounded /Delta	Typically provides effective grounding regardless of generator grounding arrangement

Most of the distribution systems are four wire multi-grounded neutral systems which are effectively grounded with respect to the substation source. For a single line to ground fault, this

arrangement limits the voltage rise on un-faulted phases to about 125 to 135% of the pre-fault condition. By IEEE definition [16], effective grounding means that the positive sequence reactance is greater than the zero sequence resistance $X_1 > R_0$ and the zero sequence reactance is less than three times the positive sequence reactance $3\ X_1 > X_0$. Use of a DG source that does not appear as an effectively grounded source connected to such systems may lead to over voltages during line to ground faults on the utility system [12].

2.5 Faults

A fault created by the short circuit event is the disturbance which are frequent and common for utility, transmission and grid operators. Faults can be classified as phase-to-ground, phase-to-phase, phase-to-phase-to-ground, three phase fault or three phase to ground fault. From the system operator point of view the accurate estimation of its location is crucial for timely restoration of services. There are different techniques for the fault location. Most popular among them are impedance based techniques. There are types of fault location algorithm that utilizes single ended voltage and current or double ended voltages and currents.

2.5.1 Single-Ended Fault Location Technique

Single ended methods are simple as compared to the double ended methods. They do not require communication links between the ends of the faulted line. This makes single-ended methods attractive for application in protective relays and single-ended fault locators. The need for only one device on the local end makes these methods less costly. Single-ended fault location schemes are generally impedance based schemes. These types of schemes require the measurement of voltage (phase to ground) and current of each phase from one end of the faulted

circuit to calculate the apparent impedance from that terminal. This method requires fault type identification prior to applying the different algorithms of fault location. If the fault resistance is assumed to be zero, then the impedance calculation outlined in table 2.4 can be used to estimate the fault location [17].

Table 2.4: Simple impedance equations [18]

Fault Type	Positive Sequence Impedance Equation mZ_{1L}
A-ground	$\dfrac{V_a}{I_a + k3I_0}$
B-ground	$\dfrac{V_b}{I_b + k3I_0}$
C-ground	$\dfrac{V_c}{I_c + k3I_0}$
a-b or a-b-g	$\dfrac{V_{ab}}{I_{ab}}$
b-c or b-c-g	$\dfrac{V_{bc}}{I_{bc}}$
c-a or c-a-g	$\dfrac{V_{ca}}{I_{ca}}$
a-b-c	$\dfrac{V_{ab}}{I_{ab}}$ or $\dfrac{V_{bc}}{I_{bc}}$ or $\dfrac{V_{ca}}{I_{ca}}$

Where,

$k = \dfrac{Z_{OL} - Z_{1L}}{3Z_{1L}}$ and Z_{OL} is the zero-sequence line impedance.

Z_{1L} is the positive-sequence line impedance.

m is the per unit distance to fault (for example: distance to fault in kilometers divided by the total line length in kilometers).

I_0 is the zero sequence current.

From [19] the errors encountered during the use of this simple methods are outlined below:

- Pre-fault Load current, and unbalance in the load current

- Fault resistance, which can be high especially on distribution circuits

- Wrong type of fault is identified

- Mutual coupling, especially zero sequence mutual coupling for faults involving ground

- Model errors

- Instrument transformer errors

Figure 2.10 shows the one-line circuit and representation of a line fault [17] and [20].
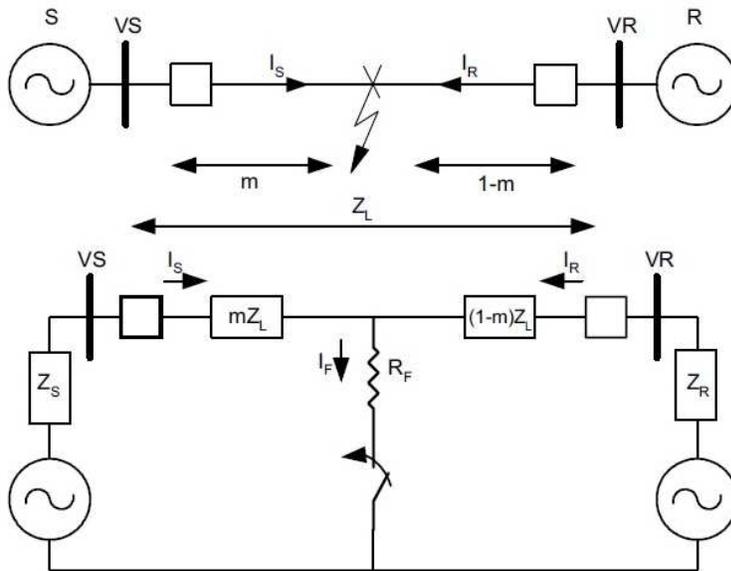
Figure 2.10: One-line and circuit representation of a line fault [17]

2.5.1.1 Simple Reactance Method

With the simple reactance method, the device measures the apparent impedance, then determines the ratio of the measured reactance to the reactance of the entire line [17]. This ratio is proportional to the distance to the fault. This method assumes that the current through the fault resistance is in phase with the current at the measurement point, and there is no load prior to the fault. The reactance algorithm compensates for the fault resistance by measuring only the imaginary part of the apparent line impedance Z_G . Equation 2.2 shows the per unit distance-to-fault.

$$m = \frac{Im\frac{V_G}{I_G}}{Im(Z_L)} \qquad (2.2)$$

For the line-ground fault (a-g), the calculation is as shown in equation 2.3.

$$m = \frac{Im\frac{V_G}{I_{G_a}+k_0 I_R}}{Im(Z_L)} \qquad (2.3)$$

Where,

k_0 is $\frac{Z_{0L}-Z_{1L}}{3Z_{1L}}$ and residual current $I_R = 3I_0$.

The value or the positive-sequence impedance in the numerator can be obtained from table 2.4 for the different types of fault. Different methods and algorithms used in determining the fault type play a very important role in this method. An error in the fault type identification leads to the incorrect estimation of the fault distance which makes it less attractive [19].

2.5.1.2 One -Ended Method without Source Impedance

This method is also referred to as Takagi method. This method was first described by T. Takagi with Tokyo Electric Power in 1982. Since then, many researchers have used it as a basis for one-ended fault location methods that do not utilize source impedance. Since up to this point we have, $\frac{V_S}{I_S} = Z_{FS} = mZ_L + \frac{I_F}{I_S}R_F$. If I_F and I_s are not in phase, then $\frac{I_F}{I_S}R_F$ is a complex number. This could cause errors in any reactance based fault location method. Takagi method separates a single phase circuit with a fault into two circuits, a load flow component circuit and a fault component circuit. The load flow component is the pre-fault circuit. This method requires pre-fault and fault data. It improves upon the simple reactance method [21] by reducing the effect of load flow and minimizing the effect of fault resistance.

2.5.1.3 One -Ended Method with Source Impedance

Single-ended fault location algorithms that do not utilize source impedance can create considerable error if the current in-feed from the remote end is significant and the fault impedance cannot be ignored. This in-feed current creates a difference in the magnitude and angle between the fault current and the current at the local end where the fault location algorithm is applied.
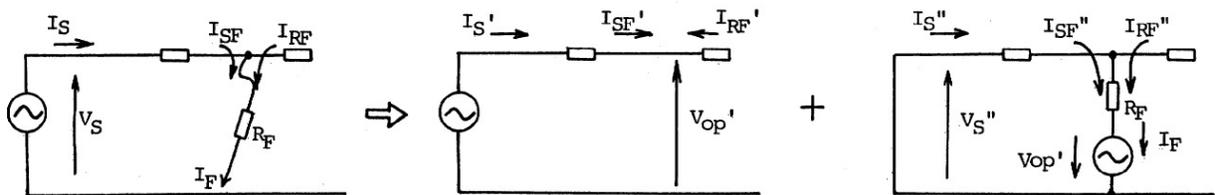
Figure 2.11: Two equivalent circuit for fault [21]

Reference [22] describes more elaborately the one ended method with the source impedance. Referring to the leftmost figure of figure 2.11 and rightmost figure of figure 2.11 the following relationship can be realized as shown in equation 2.4.

$$\frac{I''_S}{I_F} = \frac{(1-m)Z_L + Z_R}{Z_s + Z_L + Z_R} \tag{2.4}$$

The ratio of $\frac{I''_S}{I_F}$ is defined as the fault distribution factor D_s . $D_s = \frac{I''_S}{I_F}$. Using symmetrical components, we can extract the following relationships for a phase-to-ground fault $I_F = 3I_0$ and $I^+ = I^- = I^0$. Where, I^+ , I^- and I^0 are positive-sequence, negative sequence and zero sequence current respectively. Since we have $V_s = m \, Z_L I_s + I_F R_F$, we can obtain equation (2.4) by substituting the fault current from the distribution factor relationship.

$$V_s = mZ_L I_F + \left(\frac{I''_F}{D_s}\right) R_F \tag{2.5}$$

Substituting the distribution factors D_S with its value obtained earlier we get equation 2.6.

$$m^2 = \left(\frac{V_s}{I_s Z_L} + \frac{Z_R}{Z_L} + 1\right)m + \left(\frac{Z_R}{Z_L} + 1\right)\frac{V_s}{I_s Z_L} - R_F \frac{I''}{I_s Z_L}\left(\frac{Z_s + Z_R}{Z_L} + 1\right) = 0 \tag{2.6}$$

Equation 2.6 has a real part and an imaginary part that equals zero. R_F and m are the two unknown variables, therefore it is possible to solve for m. The above method requires the

knowledge of the source impedance on both ends of the faulted transmission line. This is a required setting in the device to perform this algorithm. The problem here is that if this setting is not accurate, then this method will produce errors. System configurations and operating conditions can change and affect the source impedance settings.

2.5.2 Multi-Ended Fault Location Technique

Single-ended fault location methods have deficiencies due to uncertainties of fault resistance, load and angle mismatch of in-feed currents resulting in fault voltage angle mismatch between the end where the fault is located and the fault location point. As communication technologies advanced, it became possible to get fault measurements from both ends of the faulted transmission line. This includes voltages and currents. In figure 2.10, using quantities from both ends of the line, the fault point voltage can be easily described by forming two equations for voltage loops, one from each end of the line, as follows.

$$V_f = V_s - mZ_L I_s \tag{2.7}$$

$$V_f = V_R - (1 - m)Z_L I_R \tag{2.8}$$

The above two equations can be solved simultaneously to find the fault location m.

$$m = \frac{\left(\frac{(V_s - V_R)}{Z_L}\right) + I_R}{I_s + I_R} \tag{2.9}$$

Some of the benefits of the using the above fundamental technique and described in [18] are:

- Simplicity

- Insensitivity to the external system (source impedance are not needed)

- Insensitivity to load flow

- Unaffected by the fault resistance

- Fault type identification is not needed

By using the positive-sequence or negative-sequence quantities in equation 2.9, the need for fault type identification is eliminated. This improves the accuracy of these methods as the zero-sequence component can introduce errors due to uncertainty of the zero-sequence network. These uncertainties stem from unbalanced loading and mutual coupling. Another benefit of not needing fault type identification is the possible poor performance of fault type identification methods for evolving faults. Evolving faults are those that start as one type, but change into another type of fault.

2.5.3 Other Fault Location Techniques

2.5.3.1 Voltage Only Method

This fault location method assumes a new bus inserted into the existing bus impedance network. This method allows for direct modification of the bus impedance matrix. Following the modification, basic three-phase analysis of the fault is performed. Three phase, positive, negative and zero-sequence component fault voltages are calculated. Positive, negative and zero-sequence

component fault currents are also calculated in terms of the sequence voltages and the modified bus impedance matrix.

This method is used for locating faults using voltage magnitude from one bus and further use least squares method to solve the three phase voltage equations and the fault current equation for the unknowns of fault resistance and fault location. The drawback of this method is the need to identify the fault type so that the correct set of equations can be applied. Other error sources are the estimation of small fault resistance for three phase faults, and assuming of 1 p.u. pre-fault voltage.

2.5.3.2 Travelling Wave Method

This method captures the surges (or traveling waves) on the transmission line following a fault which is a high frequency wave. Capturing can be done using current transformers or voltage transformers. Recently, CCVT has become widely used by utilities. The winding of the CCVTs may prevent the unit from reproducing these transients on the secondary windings of the CCVT. Additionally, the stronger the bus, the lower the surge voltages are. Therefore, current transients may be more appropriate for the purpose of fault location. Sensors are used to capture the surge pulses. When the pulses are captured, the distance to the fault can be calculated with the information regarding the speed of traveling wave.

Traveling wave methods are also divided into single-ended and two-ended methods. Single-ended methods rely on the surge created by the fault, and the reflection again from the same fault after it reaches the recording end of the transmission line. This method measures the time between the consecutive captured surges and calculates the distance to the fault based on the time difference. A problem could arise if the fault is not capable of reflecting the wave back

due to the arc extinguishing. Single-ended methods can be degraded by reflections from other sources such as tapped load, stations, or line taps [19].

Two-ended fault location methods are more accurate. This is due to insensitivity to reflection sources mentioned above. Two-ended methods capture the first wave initiated by the fault at both ends of the transmission line. Using the data from both ends, it is fairly simple to calculate the distance to the fault. However, two-ended fault location methods requires twice the hardware needed for a single ended method. Although the fault location analysis does not need to be run online, a communication link still needs to exist to obtain the recorded data from both ends of the transmission line. All traveling wave methods requires high accuracy clocks and usually special fault location equipment capable of detecting the leading edges of the high frequency surges [19].

2.5.3.3 Series Compensated Lines

Series capacitor banks can offer steady-state and transient problems to current or impedance-based fault location technique. For impedance-based fault locating, the proper location of the potential transformers used by the fault locator can eliminate the steady-state problem. Series compensator cancels some of the impedance of the line and make the line appear shorter. This increases the amount of transferable real power on the line.

During transmission line faults, high fault current will pass through the capacitors. The impedance of the capacitor will cause a voltage to be developed across the capacitor. The capacitor needs to be protected against this over-voltage.
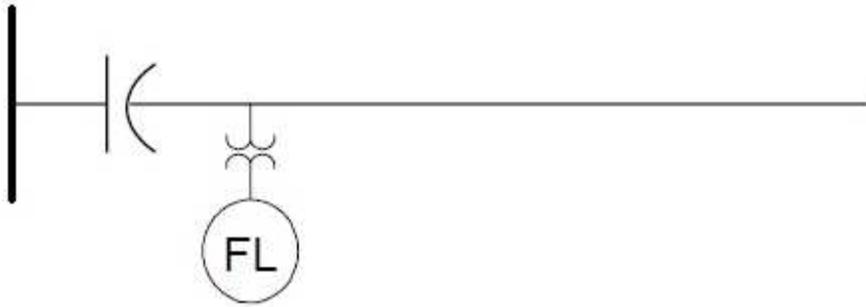
Figure 2.12: Series-compensated line with line-side voltages [17]

In figure 2.12 makes sure that no steady state problem exists in this arrangement.
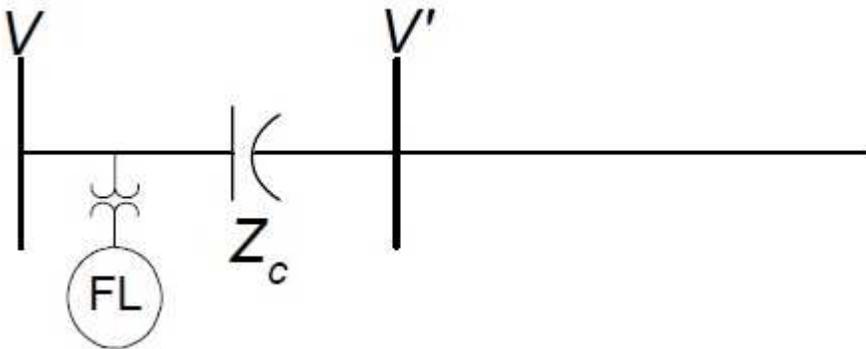
Figure 2.13: Series compensated line with bus side voltage [17]

In figure 2.13 above the arrangement causes a steady-state error due the voltage rise between the measured bus voltage and the line voltage for a fault out on the line.

2.6 Synchrophasor

After the introduction of phasor by Charles Proteus Steinmetz in 1893 the analysis Alternating Current (AC) quantities have been analyzed using this technique. A relatively new variant of this technique that synchronizes the calculation of a phasor to absolute time has been

developed, known as "synchronized phasor measurement" or "synchrophasors." [23]. Figure 2.14 represents a basic block of a PMU.
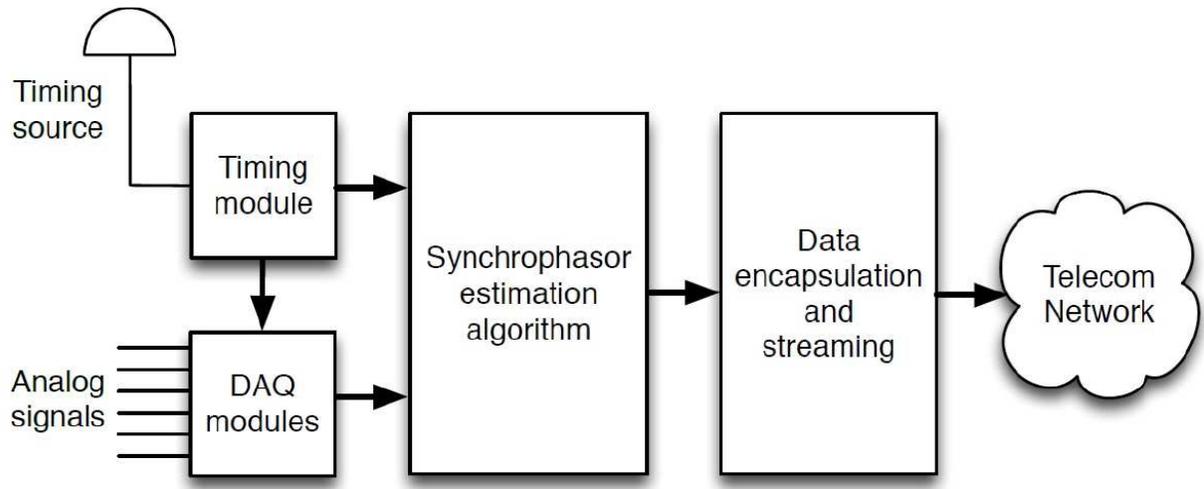
Figure 2.14: Basic block of a PMU

2.6.1 Synchrophasor Definition

The operation of the modern grid is characterized by monitoring voltages, currents and their phases at different locations in the grid. A voltage and current waveform can be mathematically represented by the following equation:

$$x(t) = X_m \cos{(\omega t + \varphi)} \tag{2.10}$$

Where,

X_m = Magnitude of the sinusoidal waveform

ω = Angular frequency $(2\pi f)$, where f is the instantaneous frequency

φ = Angular starting point for the waveform

The effective value or the root mean square value of this sinusoidal voltage is :

$$X = \frac{X_m}{\sqrt{2}} \qquad (2.11)$$

Using Euler's identity,

$e^{j\varphi} = cos\varphi + jsin\varphi$ can be further used to express the sinusoidal in terms of a phasor [24]. The rms phasor representation is:

$$X = \left(\frac{X_m}{\sqrt{2}}\right) e^{j\varphi} \qquad (2.12)$$

$$\left(\frac{X_m}{\sqrt{2}}\right)(cos\varphi + jsin\varphi) \qquad (2.13)$$

$$X_r + jX_i \qquad (2.14)$$

Where, *r* and *i* denotes the real and imaginary components of a complex value in rectangular coordinates. $\frac{X_m}{\sqrt{2}}$ is the rms value of the signal *x(t)* and φ is its instantaneous phase angle relative to a cosine function at nominal system frequency synchronized to UTC. This angle is defined to be 0^0 when the maximum of *x(t)* occurs at the UTC second rollover [1 pulse per second (PPS) time signal], and -90^0 when the positive zero crossing occurs at the UTC second rollover [25]. Adding in the absolute time mark, a synchrophasor is defined as the magnitude and angle of a cosine signal as referenced to an absolute point in time as shown in figure 2.15.
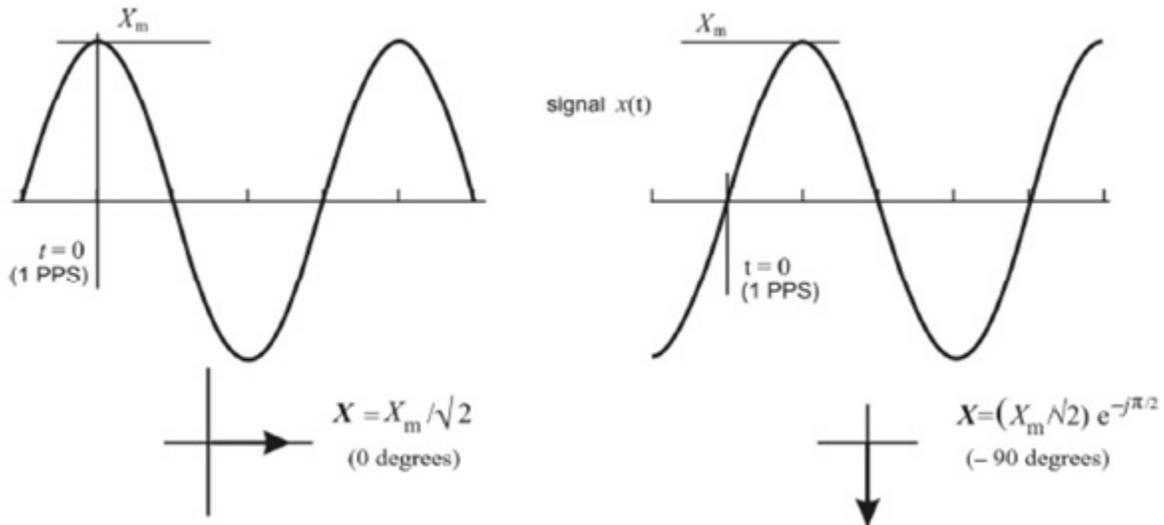
Figure 2.15: Convention for synchrophasor representation [4]

Synchrophasor standard focuses on steady-state signals, that is, signals wherein the frequency of the waveform is constant over the period of measurement but in the real world, the power system seldom operates at the nominal frequency. The calculation of the phase angle therefore need to take into account the actual frequency of the system at the time of measurement. The phasor representation of a sinusoid is independent of its frequency. A sinusoid $x(t) = X_m \cos(\omega t + \varphi)$ has a phasor representation $X = \left(\frac{X_m}{\sqrt{2}}\right) e^{j\varphi}$. The phase angle φ of the phasor is determined by the starting time ($t= 0$) of the sinusoid.

This is equivalent to having the time reference for observation initialized at the beginning of each interval. Consider that such a sinusoid is observed at intervals (0, T_0, $2T_0$, $3T_0$ .....nT_0) , leading to corresponding phasor representations (X_0 , X_1 , X_2 , X_3 ,...) . If the observation interval T_0 is equal to an integer multiple of the period of the sinusoid $T = \frac{1}{f}$ constant phasor is obtained at each observation. On the other hand, if the observation interval T_0 is not an integer multiple of T, the observed phasor has a constant magnitude, but the phase angles of the sequence of phasors (X_0 , X_1 , X_2 , X_3 ,...) will change uniformly at a rate $2\pi(f- f_0) T_0$, where

$f_0 = \frac{1}{T_0}$. This is illustrated in figure 2.16. The observed phasor values over time will increase continuously until they reach *180⁰* , they then wrap around to *-180⁰* and continue to increase as shown in [25].
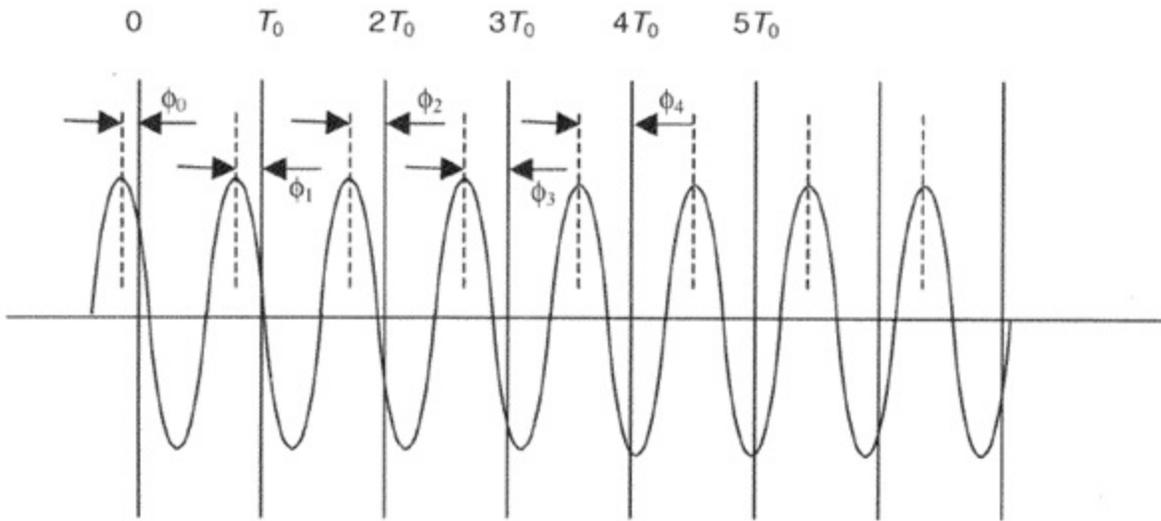
Figure 2.16: A sinusoid with a period of T observed at instants that are multiples of T_0 apart [4]

2.6.2 Evaluation Criteria

The measurement of a synchrophasor must maintain phase and magnitude accuracy over a range of operating conditions. Accuracy for the synchrophasor is measured by TVE and is defined as the square root of the difference squared between the real and imaginary parts of the theoretical actual phasor and the estimated phasor in per unit to the magnitude of the theoretical phasor.

$$TVE = \sqrt{\frac{(X_r(n) - X_r)^2 + (X_i(n) - X_i)^2}{(X_r - X_i)^2}} \tag{2.15}$$

Where $X_r(n)$ and $X_i(n)$ are the measured values, given by the measuring device, and X_r and X_i are the theoretical values of the input signal at the instant of time of measurement. Under steady-state operation a maximum TVE of 1% is allowed to meet the requirements of the synchrophasor standard. In general a phase error of 0.57 degrees (0.01 radians) will cause 1% TVE as defined in equation 2.15. This corresponds to a time error of 26µs in a 60Hz system and 31µs in a 50Hz system [25]. Other measurement criteria to evaluate synchrophasor are the frequency error (FE) and the rate of change of frequency (ROCOF) error (RFE).

The amplitude and the phase estimation have differences between the PMU estimation and the theoretical value. The theoretical values of a synchrophasor representation of a sinusoid and the values obtained from a PMU may include differences in both amplitude and phase. While they could be separately specified, the amplitude and phase differences are considered together in this standard in the quantity called TVE. TVE is an expression of the difference between a perfect sample of a theoretical synchrophasor and the estimate given by the unit under test at the same instant of time. The value is normalized and expressed as per unit of the theoretical phasor [26].
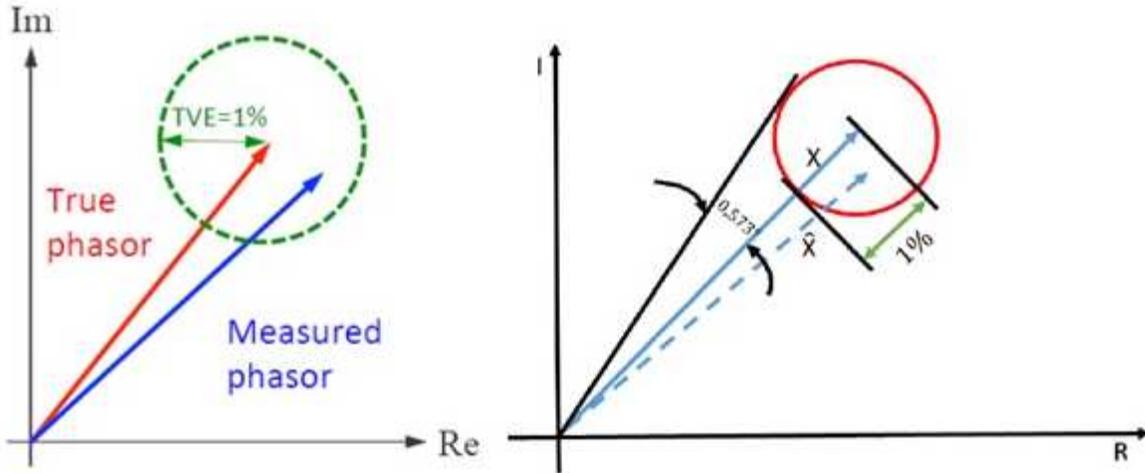
Figure 2.17: Graphical representation of the permitted TVE [27]

Figure 2.17 shows that 1% accuracy limit of the TVE specified in [26] corresponds to a 1% error in the phasor magnitude estimation or to a 0.573 degrees error in the phasor angle estimation. It is worth noting that the TVE limit given by the IEEE Std. C37.118 are conceived for WAMS typically used in transmission networks. Therefore, the application of these limits to distribution networks, which need to be discussed further in detail [28].

The ROCOF is defined as

$$ROCOF(t) = \frac{df(t)}{dt} \tag{2.16}$$

Where,

$$f(t) = \frac{1}{2\pi}\frac{d}{dt}\left(\omega t + \varphi(t)\right) \tag{2.17}$$

At nominal system frequency f_0,

$$\omega t + \varphi(t) = 2\pi f_0 + \varphi(t) = 2\pi \left[f_0 t + \frac{\varphi(t)}{2\pi} \right] \tag{2.18}$$

and the frequency formula becomes

$$f(t) = \frac{d}{dt} \left[\frac{\varphi(t)}{2\pi} \right] = f_0 + \Delta f(t) \tag{2.19}$$

Where $\Delta f(t)$ is the deviation of the frequency from nominal and the ROCOF is given by equation 2.20.

$$ROCOF(t) = \frac{d^2}{dt^2} \left[\frac{\varphi(t)}{2\pi} \right] = \frac{d}{dt} (f_0 + \Delta f(t)) \tag{2.20}$$

2.6.3 Frequency Error (FE)

The measure of error between the theoretical frequency and the measured frequency for the given instant of time [4].

$$FE = |f_{true} - f_{measured}| = |\Delta f_{true} - \Delta f_{measured}| \tag{2.21}$$

2.6.4 Rate of Change of Frequency Error (RFE)

The measure of error between the theoretical ROCOF and the measured ROCOF for the given instant of time [4].

$$RFE = \left| \left(\frac{df}{dt} \right)_{true} - \left(\frac{df}{dt} \right)_{measured} \right| \tag{2.22}$$

The maximum allowed steady-state FE is of 0.005Hz. This corresponds to a time source FE of 0.083MHz in a 60Hz system or a 0.1MHz in a 50Hz system. Essentially, PMU measurements must provide time traceable UTC, with sufficient accuracy to keep the TVE, FE

and RFE, within the required bounds specified by the IEEE C37.118.1-2011 standard. For each measurement, the PMU time tag shall accurately resolve a time measurement to at least 1μs within a 100 year period and it shall include time quality that indicates traceability to UTC, time accuracy, and leap second status [25].

2.6.5 Performance Class of PMUs

The PMUs standard defines two performance classes of PMU, namely P and M. The P class is intended for applications requiring fast measurement response time, especially protections in power system, while the M class should be considered for the cases where measurement accuracy is of crucial importance. The P class, with P to indicate protection, is intended for applications requiring fast response and mandates no explicit filtering. M class, with M to indicate measurement, is intended for applications that could be adversely affected by aliased signals and do not require the fastest reporting speed but high accuracy.

According to this standard, a PMU must meet all the requirements at least for one class. The goal is to provide a comprehensive solution for PMU setups that can guarantee performance compliance with both classes and can thus be used for both protection and measurement application at high reporting rates. This solution thus enables simplifying the setup of a PMU significantly and is aimed at straightforward installations. The main differences between the two performance classes are the test conditions for steady state performance and requirements for dynamic performance, especially as far as frequency and ROCOF estimation are concerned.

Table 2.5: The steady state synchrophasor measurement requirement [4]

Influence quantity	Reference condition	Minimum range of influence quantity over which PMU shall be within given TVE limit			
		P class		M class	
		Range	Max TVE (%)	Range	Max TVE (%)
Signal frequency range—f_{dev} (test applied nominal + deviation: $f_0 \pm f_{dev}$)	$F_{nominal}$ (f_0)	± 2.0 Hz	1	± 2.0 Hz for $F_s < 10$ $\pm F_s/5$ for $10 \leq F_s < 25$ ± 5.0 Hz for $F_s \geq 25$	1
The signal frequency range tests above are to be performed over the given ranges and meet the given requirements at three temperatures: T = nominal (~23 °C), T = 0 °C, and T = 50 °C					
Signal magnitude— Voltage	100% rated	80% to 120% rated	1	10% to 120% rated	1
Signal magnitude— Current	100% rated	10% to 200% rated	1	10% to 200% rated	1
Phase angle with $\lvert f_{in} - f_0 \rvert < 0.25$ Hz (See NOTE 1)	Constant or slowly varying angle	$\pm\pi$ radians	1	$\pm\pi$ radians	1

Influence quantity	Reference condition	Minimum range of influence quantity over which PMU shall be within given TVE limit			
		P class		M class	
		Range	Max TVE (%)	Range	Max TVE (%)
Harmonic distortion (single harmonic)	<0.2% (THD)	1%, each harmonic up to 50th	1	10%, each harmonic up to 50th	1
Out-of-band interference as described below (See NOTES 2 and 3)	<0.2% of input signal magnitude		None	10% of input signal magnitude for $F_s \geq 10$. No requirement for $F_s < 10$.	1.3

Out-of-band interference testing: The passband at each reporting rate is defined as $\lvert f - f_0 \rvert < F_s/2$. An interfering signal outside the filter passband is a signal at frequency f where: $\lvert f - f_0 \rvert \geq F_s/2$

For test the input test signal frequency f_{in} is varied between f_0 and $\pm$ (10%) of the Nyquist frequency of the reporting rate.

That is: $f_0 - 0.1 \ (F_s/2) \leq f_{in} \leq f_0 + 0.1 \ (F_s/2)$

where

F_s = phasor reporting rate
f_0 = nominal system frequency
f_{in} = fundamental frequency of the input test signal

NOTE 1—The phase angle test can be performed with the input frequency f_{in} offset from f_0 where $\lvert f_{in} - f_0 \rvert < 0.25$ Hz. This provides a slowly varying phase angle that simplifies compliance verification without causing significant other effects.

NOTE 2—A signal whose frequency exceeds the Nyquist rate for the reporting rate F_s can alias into the passband. The test signal described for the out-of-band interference test verifies the effectiveness of the PMU anti-alias filtering. The test signal shall include those frequencies outside of the bandwidth specified above that cause the greatest TVE.

NOTE 3—Compliance with out-of-band rejection can be confirmed by using a single frequency sinusoid added to the fundamental power signal at the required magnitude level. The signal frequency is varied over a range from below the passband (at least down to 10 Hz) and from above the passband up to the second harmonic ($2 \times f_0$). If the positive sequence measurement is being tested, the interfering signal is a positive sequence.

2.6.6 Steady State Compliance

The steady state compliance tests for synchrophasor, frequency and ROCOF are summarized in table 2.5. Every row of the table corresponds to a different test with a different influence quantity. The steady state compliance will be verified comparing the measurements of synchrophasor, frequency and ROCOF with the theoretical value of the same quantity, as previously described. For every test, the maximum TVE percentage is equal to 1% for both P and M classes, whereas the frequency and ROCOF requirements depend on the specific test.

2.6.7 Reporting Rates

In Synchrophasor a frequency and ROCOF measurements need to be reported simultaneously at a constant rate, F_s. A given reporting rate F_s, of N frames per second (fps), where N is a positive integer, evenly divides a one second interval into a specified number of sub-intervals. These reporting frames are numbered 0 through $N-1$, and they coincide with the UTC second rollover provided by the GPS [25]. These reporting times are used to determine the instantaneous values of the synchrophasor for any time interval. The reporting rates for 50Hz and 60Hz systems are listed in table 2.6.

Table 2.6: PMU reporting rates [25]

System Frequency	50 Hz			60 Hz					
Reporting rates (Fs, frames per second)	10	25	50	10	12	15	20	30	60

2.6.8 PMU Architecture

The PMU extracts the signals from CT and PT for current and voltage measurement respectively. The signals are then passed through the anti aliasing filter to Analog to Digital (A/D) converter. The GPS receiver receives a signal from GPS (in 1 pulse per second). The microprocessor helps align the signal to be sent to the PDC. The figure 2.18 outlines the process of signal processing.
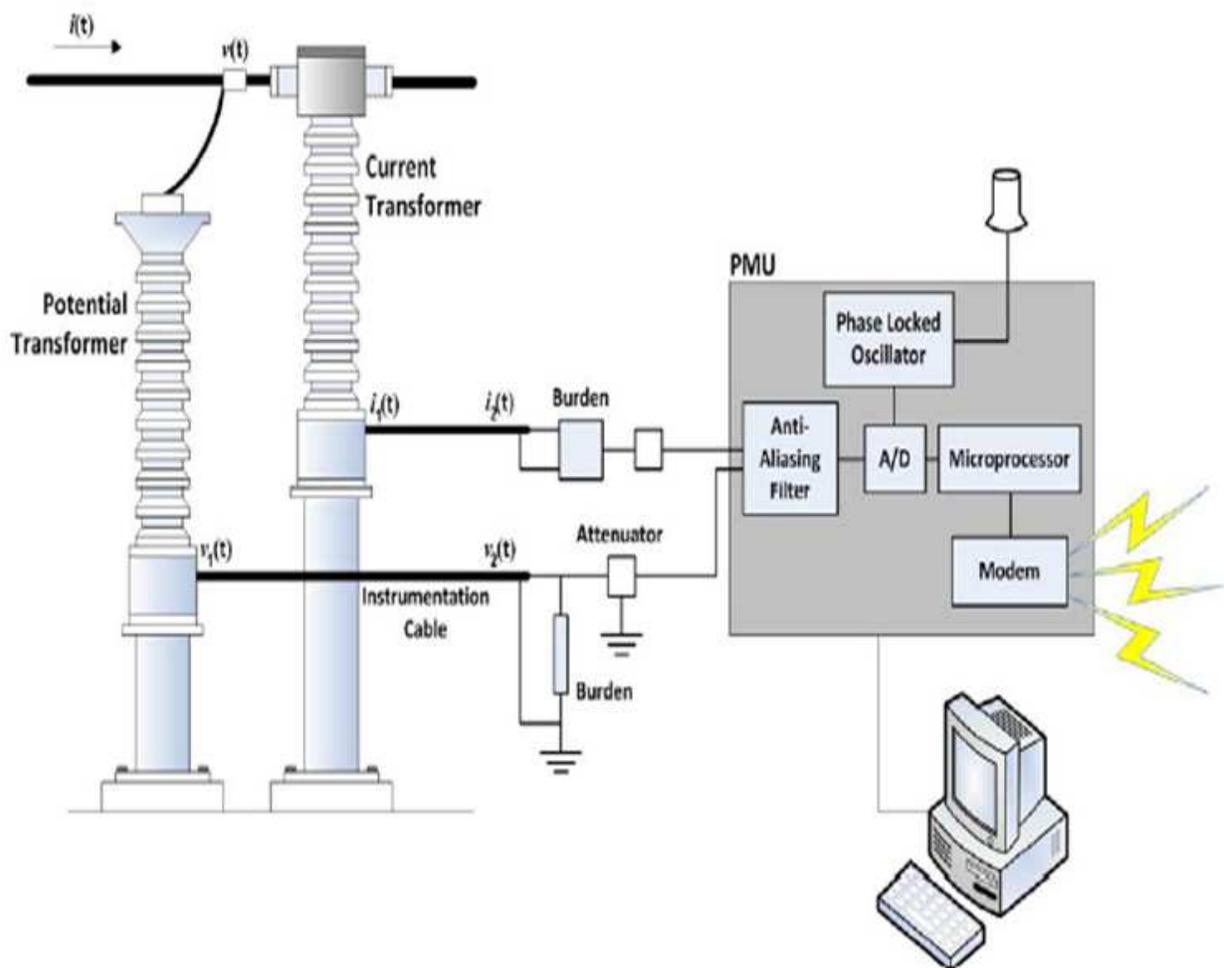
Figure 2.18: PMU architecture [27]

2.6.9 Cost Economization

In [29] A Khanal, G Lebby et. al. worked towards optimizing the electrical network by placing PMUs in efficient way. Integer linear programming was used to arrive at the optimal placement of the PMUs in the network. The following results shows how efficiency was achieved.

Table 2.7: Number and locations of the PMU for an intact system [29]

Bus System	Location of PMUs	Number of PMUs
IEEE 14	2,7,10,13	4
IEEE 30	1,5,6,9,10,12,15,19,25,27	10
IEEE 57	1,6,9,15,19,22,25,27,28,32,36,39,41,44,47,50, 53	17
30 Bus Nigerian Grid	2,3,6,8,10,16,17,21,23,26,27	11

Table 2.8: Number and locations of the PMUs considering one outage [29]

Bus system	Location of PMUs	Number of PMUs
IEEE 14	2,4,5,6,7,8,9,10,13	9
IEEE 30	1,2,3,6,7,9,10,11,12,13,15, 17,19,20,22,23,25,26,27,28,30	21
IEEE 57	1,2,4,6,9,11,12,15,19,20,22,24, 25,27,28,29,30,32,33,35,36,37, 38,39,41,44,46,47,50,51,53,54,56	33
30 Bus Nigerian Grid	1,2,3,6,7,8,10,12,13,14,15,16,17,18, 19,20,21,22,23,24,25,26,27,28,29,30	26

Table 2.9: Comparison of different solvers in terms of CPU clock [29]

Bus System	CPU time for SCIP	CPU time for Tomlab	CPU time for Gurobi
IEEE 14	0.05	0.014	0.00001
IEEE 30	*	0.125	0.0001
IEEE 57	30.14	1.73	0.36
Nigerian 30 Bus	*	1.57	0.05

They found that Python-Gurobi which was used in solving the problem of optimal placement of PMUs in an electric power grid for complete observability and monitoring was indeed fast, reliable and efficient. It was discovered that it achieved the same solution that the other tools had achieved but exceeded them in CPU efficiency.

CHAPTER 3

Literature Review

3.1 Different Fault Location Algorithms

With the principles outlined in the previous chapter, different literary works are contributed from different authors. For this venture , there are some closely related reviews which are described below for more ideas in this field. The methodologies, the computation aspects, the ease of implementations and the drawbacks are pointed out, which are directly related to the problem on our hand. A new methodology based on the combinations of some these previous works have been proposed after the thorough investigation.

3.1.1 Non Synchrophasor Fault Location Algorithms

In [18] the authors used the voltage only method to find the fault location and used the swing angle to screen the impacted area. Areas with the highest change in swing angle were included in the reduced Z bus model. Liao and Elangovan [30] used the algorithms with iterative techniques to locate line to line faults for locating faults on a transmission lines without line parameters. Their techniques failed to locate a balanced three-phase faults. Hlatshwayo, Chowdhury et al. [14] used analytical and Monte Carlo simulation method for the radial network with DG and without DG. They found an increase in the reliability of the network with the DG present but the amount of reliability depended on the location of the placement. Further down from the substation the reliability decreased but remained around the same value as without DG.

Wu [2] proposed a new fault location algorithm based on fault current. In first step they determined the fault channel in the distribution network with DG using the search tree structure

and then they built the fault information matrix using the nodes which strongly correlated to the fault and calculated the accurate fault location using Kirchhoff's current law and principle of phase comparison. Jian, Jianli et al. [31] used unified matrix algorithm for fault section detection and isolation in distribution network with single source. As an improvement to this Fei and Ying [32] used improved matrix algorithm with multi source for locating multiple faulted sections in the network. These two papers had the drawback such that the faulted section could not be determined by these schemes when fault happened at the terminal of one feeder and those algorithms were composed by multiplying of matrices and the process of normalization which needed many steps of operation and correspondingly long time.

RGA improved the fault location accuracy over conventional GA approach and improved matrix approach but in [33] WEI, He et al. had to assume the positive direction of every sources in the network before applying this algorithm and also it took longer computation time. Chao, Xiangjun et al. and Fei and Ying [34] and [32] proposed a new matrix method with network matrix, fault information matrix and fault detection matrix for which the fault detection matrix was the product of network and fault information matrix. This method solved the problem with one step of calculation and simplicity criterion but the two positive directions had to be assumed based on the types of DGs connection for network matrix and fault information matrix respectively. This method did not yield the better solution when the penetration of DGs increased in the network. The disadvantage of all above algorithms was that they dealt with transmission line faults and avoided the complex distribution parameters in their results.

Zhong-xiao, Xiao-bin et al. [35] proposed an heuristic algorithm for distribution system fault location by dividing the fault matrix into several unit matrix and fault current judgment matrix for a quick and reliable fault location but it did not consider and update the changing state

of the switches in the network which would give wrong topology. Wei, Hong et al.[36] used Bayesian and GIS method to find fault location in the distribution network and map it to the GIS but the paper failed to explain the process and still it was only good for the radial network.

3.1.2 Synchrophasor Based Algorithms

Geramian, Abyane [37] used two step procedure to find the fault location on the identified faulted segment. First they placed the optimum number of PMUs for observability and then used synchronized data to calculate fault location. They failed to explain how to find the faulted section. Ren, Venkata et al. [38] presented a new method better than fault impedance method for locating a fault in distribution systems using synchrophasor measurements, for active and passive networks, radial and looped topologies, high impedance faults, and PMU locations independent network. The candidate fault locations were identified by iterating every possible line segment along with the synchronized phasors of voltages and currents. The measurements from remote devices were used to eliminate all non-faulted cases. Although the fault location method provided 1% error, the initial fault location estimation was approximated using apparent fault impedance method.

In [39] the author proposed a fault model using location function based on network correlation coefficient matrix in super-imposed network and used an adaptive search techniques to locate fault branch and fault distance. That method required few PMUs, less calculation burden and were not affected by fault type or fault resistance but the algorithm was affected by element model in power system. The two separate authors in [40] and [38] used methods of locating faults using line parameters estimated from PMU measurements of voltage and current at the line terminals. Those methods had the disadvantage that the line had to be continuously

monitored and the errors in the estimations of the line parameters, particularly those introduced immediately before the fault inception, could have lead to errors in the fault location.

Gelagaev, Vermeyen in [41] used a numerical observability analysis, applicable to distribution systems to the IEEE 34 bus test feeder which was based on the inverse function theory and the Jacobian matrix of the system. By calculating the dependent columns of the Jacobian matrix they determined the unobservable branches in the system. Further that method also gave them an indication of how many linearly independent pseudo-measurements were required to make the distribution system observable. Because the R/X ratio is not negligible in the distribution lines, they used a transformation to simplify the observability analysis.

The above algorithms are specific to transmission network for WAMS and fails to catch the essence for the distribution system requirements. The following algorithms includes the distribution system settings. Some of the synchrophasor evaluation criteria are scrutinized and the recommendations are made towards improvement by different author below.

3.2 Synchrophasor Estimation Algorithm for Distribution System

Ramos and Cruz Serra in [42] used FFT for synchrophasor phase estimation. It is a simple way to estimate a signal and is frequently used method but for time-varying frequency, it has strong limitations because of its spectral resolution. IP can be used to reconstruct IF by using time-warping, was brought forward by Chandrasekhar and Sreenivas in [43] using level crossing algorithm. In the presence of noise, the temporal structure of the level-crossings got distorted. Pradhan, Routray et al. [44] used least mean square error algorithm which was simple in formulation and computational efficiency and also produced satisfactory result in the face of harmonics but higher order harmonics (esp. 5th) adversely affected the convergence. Frequency

jump and dynamic frequency also affected the accuracy. Lee and Kim [45] used Newton method for the same purpose . That algorithm was simple and easy to implement and had high measurement accuracy. The disadvantage of that algorithm was that it was insensitive to high order harmonics. Again the authors in [42] showed the algorithms working using Kalman filtering. It had a good stability due to its linear base and good processing velocity by avoiding matrix inversion but it was sensitive to the initial conditions and its performance was not robust with respect to the variation in the internal parameters of the model.

3.2.1 Total Vector Error

Compared to transmission networks, active distribution networks are characterized by reduced line lengths and limited power flows [8]. With reference to the use of node voltage synchrophasors for the network state estimation, these characteristics result, in general, into very small phase differences between node voltage phasors (generally in the order of tens of m-radians or less). TVE value is affected by both magnitude and phase errors. Synchrophasor estimation involves the calculation of its frequency. A difference between the real and estimated frequencies produce a time varying TVE [46]. Figure 3.1 shows that the 1% accuracy limit of the TVE specified in (IEEE Std C37.118-2005) corresponds to a 1 % error in the phasor magnitude estimation or to a 0.57 degree error in the phasor angle estimation.
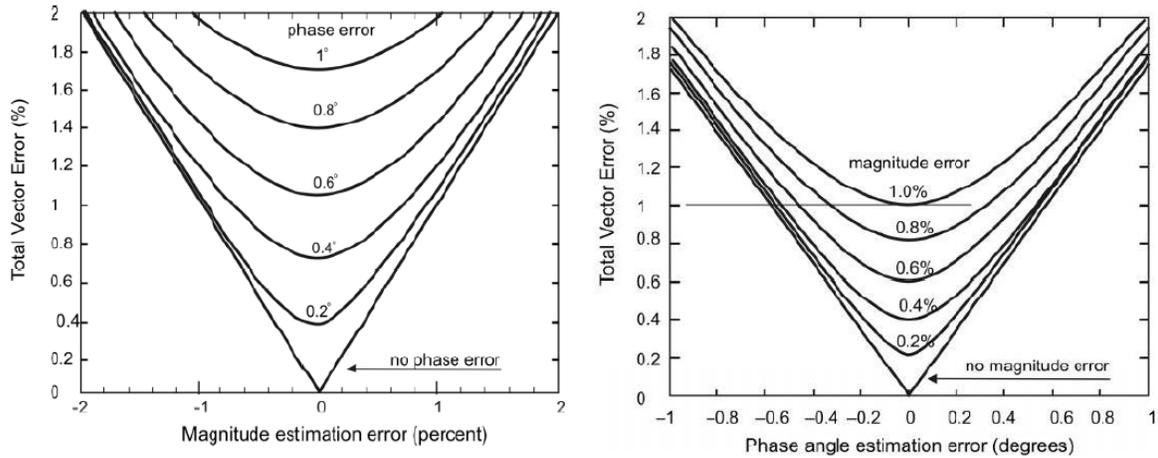
Figure 3.1: Total vector error (magnitude and phase)

With reference to a typical distribution networks values of power flows and feeder impedance, one can generally expect phase differences between bus voltage synchrophasors not exceeding a few degrees [47]. The synchrophasors-based state estimation in distribution networks requires the development of specific algorithm characterized by lower TVE values than about 0.1 %, which corresponds to phase errors in the order of 10^{-2} degrees [8]. The harmonic distortion of phase voltage waveforms is in general non negligible in distribution networks and in this respect, the algorithm for the synchrophasor estimation should implement the extraction of the fundamental frequency waveform avoiding any phase shift. Paolone, Borghetti et al. [8] again proposed a tone-reconstruction algorithm which was based on the use of the Discrete Fourier Transform (DFT), implemented into a specific real-time microcontroller, and took into account the specific requirements for the application in a distribution networks also with the presence of generating units. Further the paper by Borghetti, Nucci [48] aimed at:

- Presenting further improvements of the above mentioned algorithm and the relevant laboratory characterization of the developed PMU

- Showing the results obtained by using three PMUs during the experimental tests of intentional islanding and reconnection maneuvers of a urban distribution network

3.2.2 Spectral Leakage Problem

To apply DFT we need to truncate the length of the discretized signal *x[k]* to a finite number of samples. This is achieved by multiplying the discretized signal by a window of length *N*. The window function is very important in phasor estimation of practical waveforms. The sinusoids with frequency integer multiplication of the fundamental DFT frequency is $\frac{f_s}{N}$. The DFT produces correct results only when the input data sequence contains energy precisely at the frequencies which is an integral multiples of our fundamental frequency $\frac{f_s}{N}$. But, the DFT of sampled real-world signals provides frequency-domain results that can be misleading. This happens because in most cases we don't know a prior information of the input signal characteristics in order to choose the length of a window. If the input has a signal component at some intermediate frequency between our analytical frequencies of $\frac{mf_s}{N}$, say $\frac{1.3f_s}{N}$, this input signal will show up to some degree in all of the *N* output analysis frequencies of our DFT. More specifically the input signal energy shows up in all of the DFT's output bins. This effect, known as leakage causes our DFT results to be only an approximation of the true spectra of the original input signals prior to digital sampling. Furthermore, leakage, took its name because it causes any input signal whose frequency is not exactly at a DFT bin center to leak into all of the other DFT output bins. Although there are ways to minimize leakage, we can't eliminate it entirely. The

best method to reduce this effect is to use a windowing function. Application of a windowing function or a window can be done by multiplying the signal samples with an appropriate sequence of real numbers. A window can be applied in time or in the frequency domain.

When spectral leakage occurs, the DFT spectrum, in most cases, is only an approximation of the signal spectrum and it can easily lead us to make serious mistakes in our estimations. Windows are weighting functions that reduces the discontinuities at the boundaries of the periodic extension and they are applied to the whole length of the observation interval. As a result, they reduce the spectral leakage in frequency response of the input signal and help us to have better approximation of the signal spectrum. There are two ways to perform the windowing:

- Multiplication between the weighting function with the sampled input signal.

- Convolution in the frequency domain. By applying the windowing function in frequency domain, we only need to calculate the frequency values of our interest and then apply the window with the convolution theorem. The main disadvantage of this technique is that we need complex convolution.

CHAPTER 4

Synchrophasor Estimation Techniques

4.1 Discrete Fourier Transform (DFT)

DFT is a mathematical tool used to determine the harmonic, or frequency content of a discrete signal sequence. A discrete signal sequence is a set of values obtained by periodic sampling of a continuous signal in time domain. A unique property of DFT is that it can analyze any discrete sequence regardless of what that sequence actually represents. The DFT which is used for sampled periodic signals, implies that the signal is unchanging for all times.

DFT for synchrophasor application is defined by [49] as the discrete frequency-domain sequence $X(m)$ with the following equation:

$$X_{[k]} \Leftrightarrow X_{[n]} \qquad (4.23)$$

$$X(n) = \sum_{n=0}^{N-1} x(k)e^{-j2\pi kn} \qquad (4.24)$$

$$X(n) = \sum_{n=0}^{N-1} x(k)\left[\cos\left(\frac{2\pi}{N}\right) - j\sin\left(\frac{2\pi}{N}\right)\right] \qquad (4.25)$$

Where,

$X(m) = m^{th}$ DFT output component

m = the index of the DFT output in the frequency domain

$X(n)$ = the sequence of input samples

N = the number of samples of the input sequence and the number of frequency points in the DFT output

The exact frequencies of the different sinusoid depend on both the sampling rate f_s at which the original signal was sampled and the number of samples N . The DFT frequencies which is also called bins are defined as follows:

$$f_{analysis}(m) = \frac{mf_s}{N} \tag{4.26}$$

The ratio $\frac{f_s}{N}$ is called fundamental frequency of the sinusoid or frequency resolution Δf . All the other $X(m)$ analysis frequencies are integral multiples of the fundamental frequency. Frequency resolution represents the distance in frequency between two adjacent DFT coefficient and it is proportional to the acquisition time length and the number of the samples. It depends only on the time needed to acquire all the N samples. We can have the same frequency resolution with different N and F_s as long as T which is a time to acquire all the samples, remains the same.

Magnitude and phase of each $X(m)$ terms are defined as follows:

$$X(m) = X_{real}(m) + jX_{imag}(m) \tag{4.27}$$

$$\frac{|X_k|}{N} = \sqrt{\frac{Re(X_k)^2 + Im(X_k)^2}{N}} \tag{4.28}$$

$$\arg(X_k) = tan^{-1}\left(\frac{Im(X_k)}{Re(X_k)}\right) \tag{4.29}$$

The magnitude and phase response of a sinusoid are shown in figure 4.1 and figure 4.2 respectively.
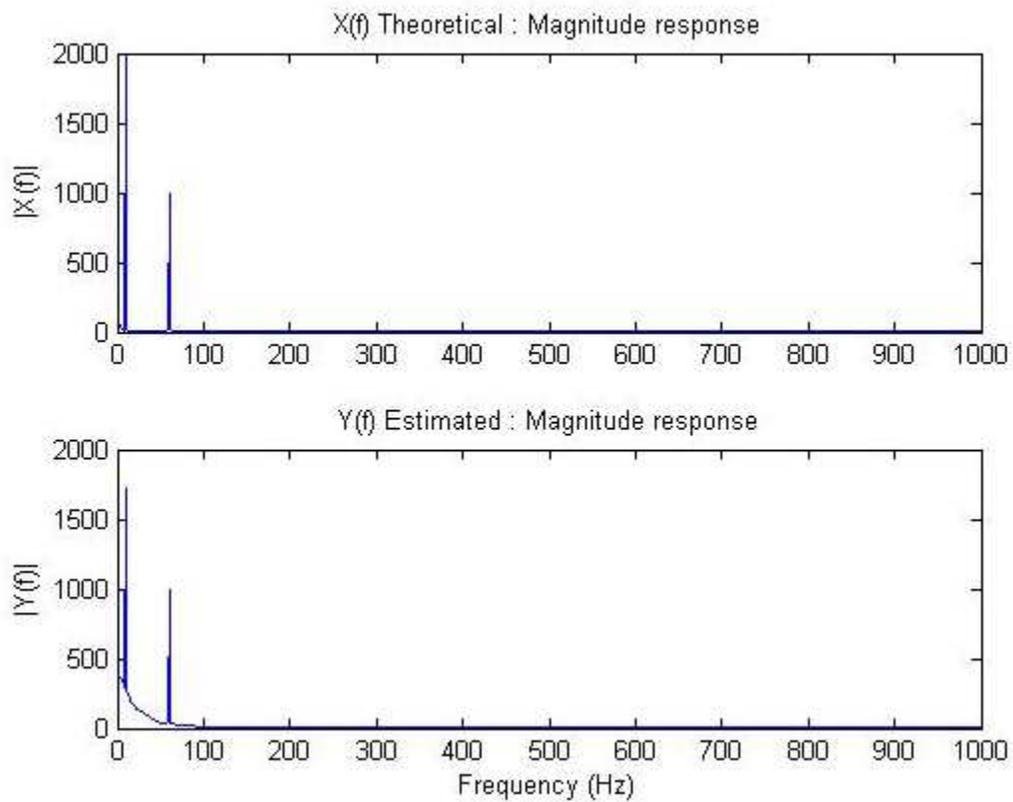
Figure 4.1: DFT of a sinusoid (magnitude response)
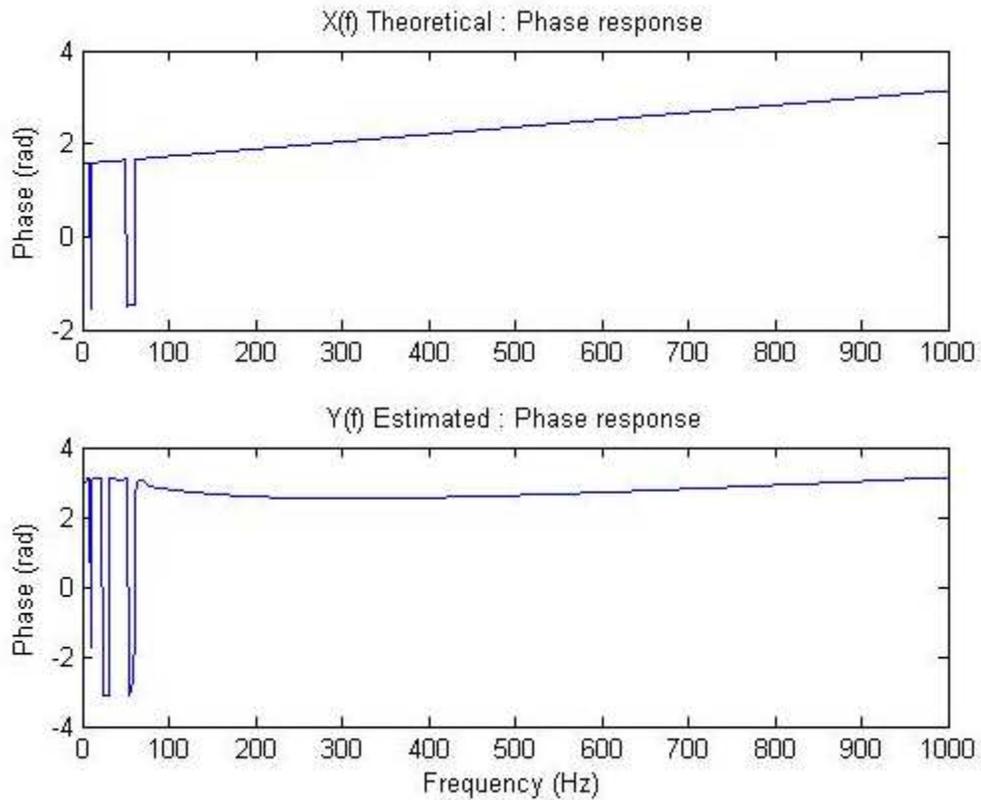
Figure 4.2: DFT of a sinusoid (phase response)

4.2 Windows

When spectral leakage occurs, the DFT spectrum, in most cases, is only an approximation of the signal spectrum and it can easily lead us to make serious mistakes in our estimations. Windows are weighting functions that reduces the discontinuities at the boundaries of the periodic extension and they are applied to the whole length of the observation interval. As a result, they reduce the spectral leakage in frequency response of the input signal and help us to have better approximation of the signal spectrum. There are two ways to perform the windowing.

- Multiplication between the weighting function with the sampled input signal. This means that we have two ways to do it, by having the coefficient on an array or by generating them on the

fly. The time required for coefficient generation is a function of window complexity. Usually the cosine family windows are preferred because of their computational simplicity.

- Convolution in the frequency domain. By applying the windowing function in frequency domain, we only need to calculate the frequency values of our interest and then apply the window with the convolution theorem. The main disadvantage of this technique is that we need complex convolution.

There are really a lot of windowing functions in scientific literature, but the most common windows for power system applications belongs to the cosine window family. Table 1 in Appendix A shows the most common windows used in many similar applications and table 2 shows the selection guide for windows depending on the application. For our application to reduce the effect of the spectral leakage, we chose Hanning window. Next section will describe Hanning window in detail.

4.2.1 Hanning Window

The Hanning window [28]

$$
W_{Hanning}(n) = \begin{cases} 0.5 - 0.5cos\dfrac{2\pi}{N} & 0 \leq n \leq N - 1 \\ 0 & n \geq N \end{cases} \tag{4.30}
$$

The equation for the Hanning window can be also expressed as depending on the nomenclature that we want to use for the first sample of the window.

$$W_{Hanning}(n) = cos^2\left(\frac{n\pi}{N}\right) = \frac{1}{2}\left[1 + cos\frac{2\pi n}{N}\right], n = -\frac{N}{2}, \ldots, -1,0,1, \ldots, \frac{N}{2} \quad (4.31)$$

$$W_{Hanning}(n) = sin^2\left(\frac{n\pi}{N}\right) = \frac{1}{2}\left[1 - cos\frac{2\pi n}{N}\right], n = 0,1, \ldots, N-1 \quad (4.32)$$

The spectrum of Hanning window is:

$$W_{Hanning}(\omega) = \left\{0.5W_R(\omega) - 0.25\left(W_R\left(\omega - \frac{2\pi}{N}\right) + W_R\left(\omega + \frac{2\pi}{N}\right)\right)\right\}e^{-j(N-1)\frac{\omega}{2}} \quad (4.33)$$

Where, $W_R(\omega) = \frac{sin\left(\frac{N\omega}{2}\right)}{sin\left(\frac{\omega}{2}\right)}e^{-j(N-1)\omega/2} = W_0(\omega)e^{-j(N-1)\omega/2}$ and $W_0(\omega)$ is the Dirichlet Kernel.

Other characteristics of the Hanning window are: The main lobe width of the Hanning window is $\frac{8\pi}{N}$, which is twice the size of the rectangular window. The first side lobe maximum of this window is -32 dB, much lower than the rectangular window. The Hanning window achieves side-lobe level reduction by the effect of superposition. From equation 4.33, we can see that the Hanning window is a superposition of the three Dirichlet kernels shifted in frequency by $\frac{2\pi}{N}$, so as to yield partial cancellation of their side lobes.

Figure 4.3 shows the construction of the Hanning window from the three Dirichlet kernels and figure 4.4 shows the application of a Hanning window to a sinusoid along with the frequency spectrum of the signal.
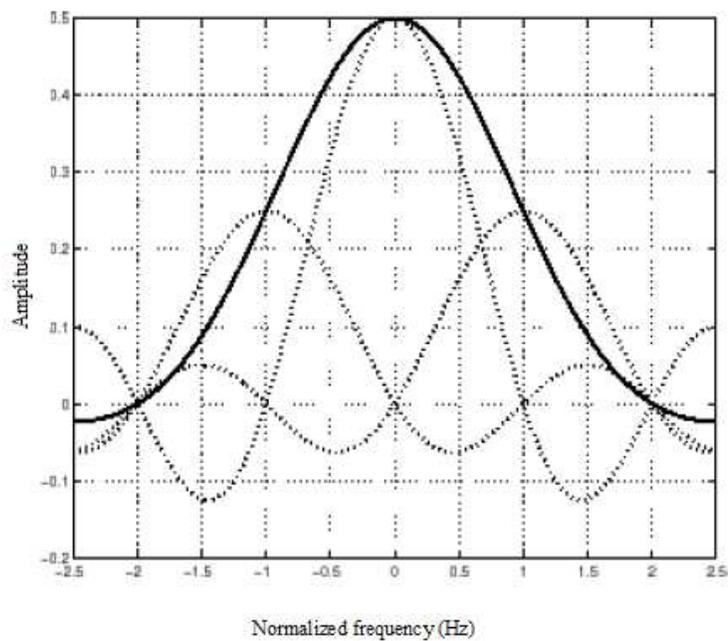
Figure 4.3: Construction of the Hanning window from the 3 Dirichlet kernels
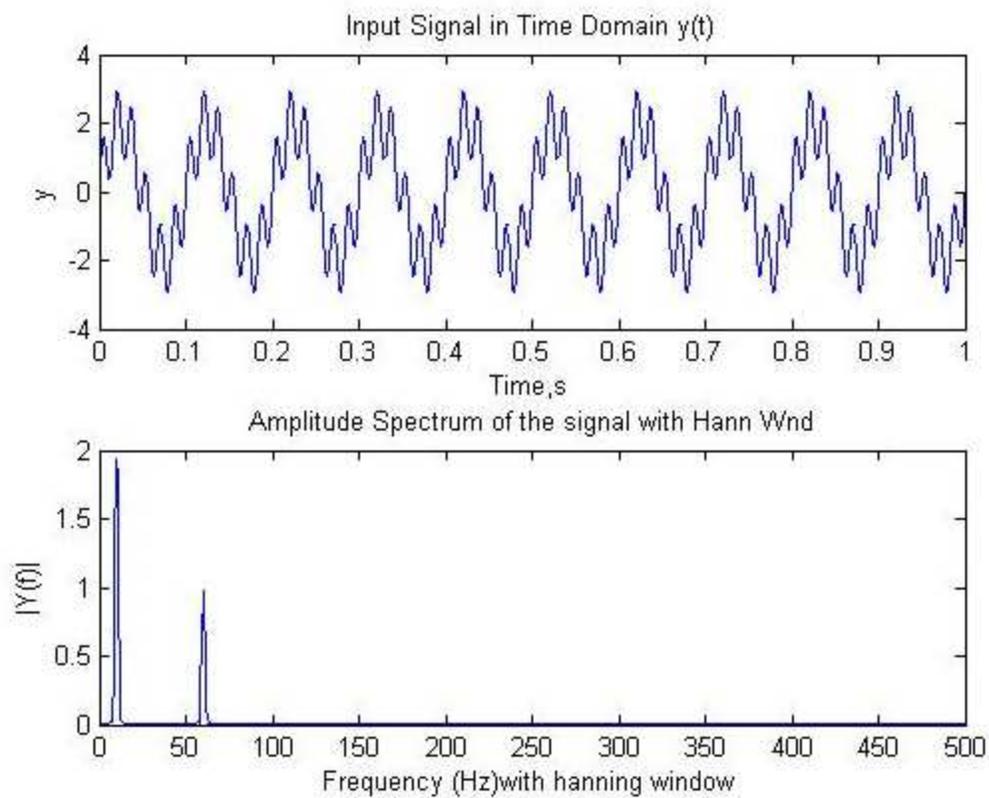
Figure 4.4: Applying Hanning window function to a sinusoid

4.3 One Cycle DFT Based Synchrophasor Estimation

The DFT-based filter is the most popular algorithm and has become a standard in the industry [50], [51]. The computational cost of recursive DFT-based filter is very low and good harmonic immunity can be achieved. The filtering capability of the DFT-based filter depends on its window length. A short data window will give a fast response but unstable output. A long one gives stable output but the response will be delayed. The most suitable window length depends on various factors, such as fault locations, fault types, and fault resistance, etc. This means that a compromise between the filter's delay and its noise suppression capabilities are required. It is possible to select a suitable filtering algorithm and a data window at different stages of a fault to complete fast distribution network protection.

New synchrophasor estimation algorithm is based on one cycle DFT. It is a two step procedure. At the first step the algorithm analyzes the input signal with the proposed algorithm and then performs a time domain analysis of the reconstructed time domain signal that corresponds to the fundamental frequency tone [8]. The algorithms' main steps are as follows:

- Sampling of the three phase voltages in correspondence of the UTC-GPS synchronization signal

- Extraction of the fundamental frequency tone

- Estimation of the synchrophasor amplitude, phase and frequency recursively

This algorithm will allow the use of PMU in an active distribution network, keep the synchrophasor measurement accuracy within specific limits even in presence of a distorted signal waveforms and electromechanical transient as specified in the standard and given in table 2.5.

One cycle 60Hz signal with the Hanning window is shown in figure 4.5 below. The magnitude

spectrum and the magnitude spectrum in dB for the windowed signal is shown in figure 4.6 and

figure 4.7 respectively.
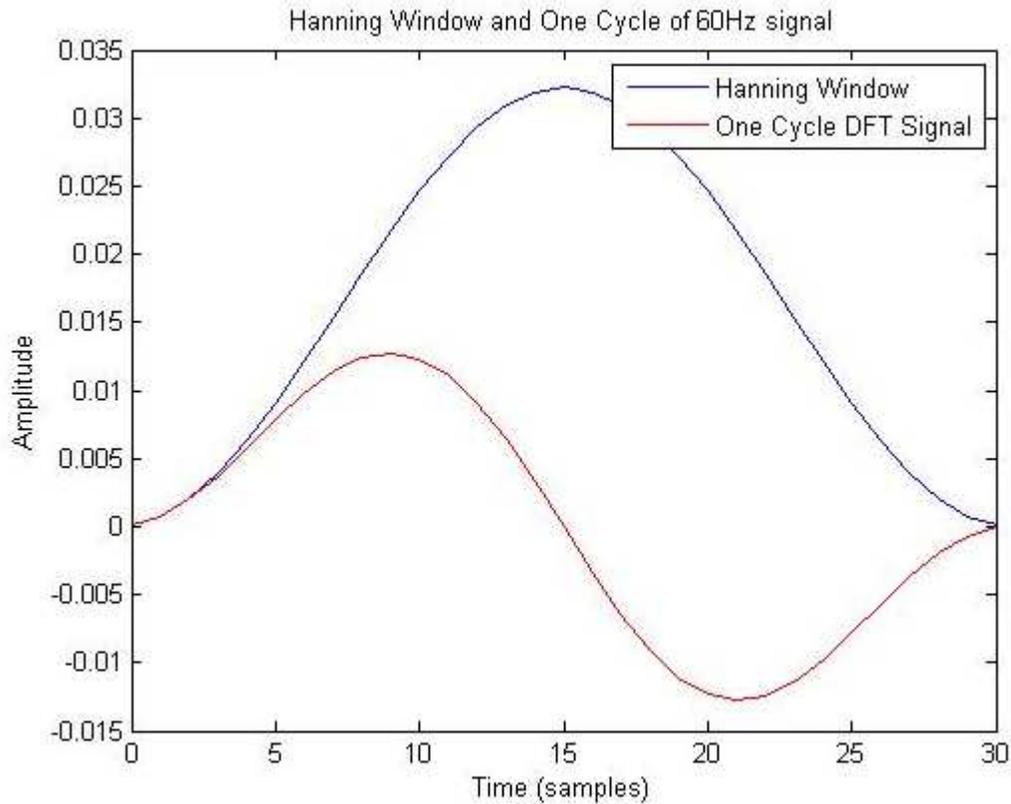
Figure 4.5: One Cycle DFT with Hanning window for P class PMU
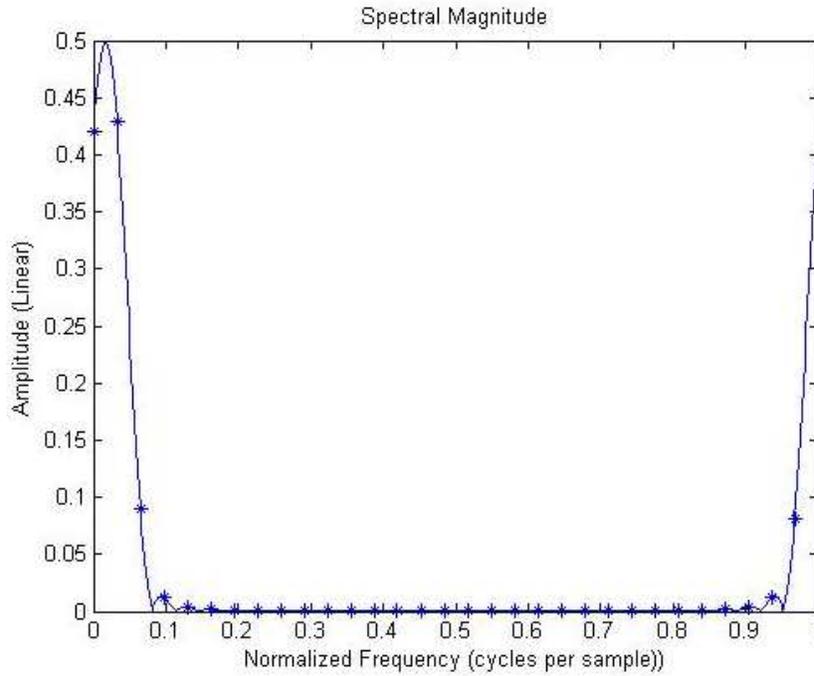
Figure 4.6: Magnitude spectrum of One Cycle DFT signal
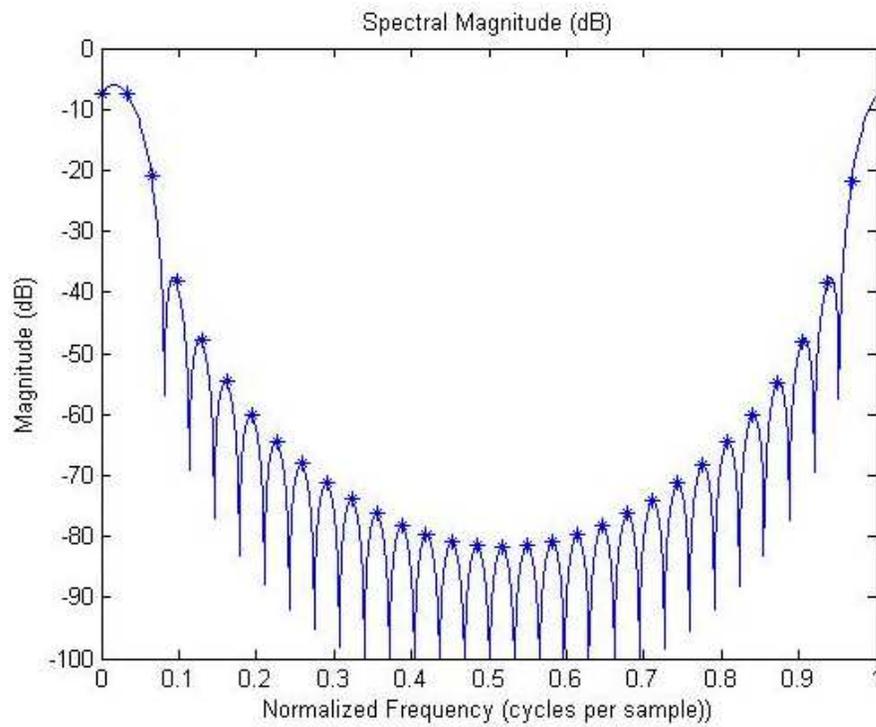
Figure 4.7: Magnitude spectrum (dB) of One Cycle DFT signal

4.3.1 Mathematical Formulation for P Class PMU

The generalized concept of this formulation is derived from [8],[52] and [53].

Let s(t) the PMU input signal expressed as:

$$s(t) = \tilde{s} + \sum_{h=1}^{n} s_h cos(h\omega_0 + \varphi_h) + \varepsilon_t \tag{4.34}$$

where

$\tilde{s}$=DC component within the sampled time window T

s_h = Amplitude of the hth harmonic component

φ_h= Phase of the hth harmonic component

ε_t=Gaussian noise

The DFT of the above signal is given as:

$$G(k\Delta f) = \sum_{h=1}^{n} S_h D_N[(k\Delta f - f_h)T] \tag{4.35}$$

Where,

 N is the number of samples,

$\Delta f = \frac{1}{T}$,

$\Delta t = \frac{T}{N}$,

$k = 0, ... \left(\frac{N}{2}\right) - 1$,

S_h and f_h are the amplitude and frequency of tone h,

D_N =Dirichlet kernel defined by

$$D_N(\vartheta) = \frac{sin(\pi\vartheta)}{Nsin(\pi\vartheta/N)}e^{-j\pi\vartheta\frac{(N-1)}{N}} \qquad (4.36)$$

The identification of the fundamental frequency tone of *s(t)* associated to the identification of the synchrophasor, faces the following two main problems:

- Spectral leakage effects caused by the finite length of time window T

- Identification of the correct frequency value that may fall between two subsequent frequency values provided by the DFT.

Hanning window is used for spectral leakage.

$$G_H(k\Delta f) = \sum_{h=1}^{n} S_h H_N[(k\Delta f - f_h)T] \qquad (4.37)$$

Where,

H_N is the Fourier transform of the Hanning windowed data. Expressing true frequency f_0 of the fundamental frequency tone as the function of DFT frequency step Δf

$$f_0 = (m + \Delta bin)\Delta f \qquad (4.38)$$

Where,

$\Delta bin(0 \leq \Delta bin < 1)$ = Deviation of f_0 from the multiple integer DFT frequency

$m\Delta f(m = 1,2,\ldots\ldots)$.

m and $m+1$ indicate the two DFT tones that delimit the interval in which f_0 is assumed to be.

Since the number N of samples per time window T is very large the *sine* function in the denominator of the Dirichlet kernel can be approximated by its argument as shown in equation 4.39.

$$e^{-j\pi\vartheta\frac{(N-1)}{N}} \approx -1 + \frac{j\pi}{N} \qquad (4.39)$$

The approximation made the $G_H(k\Delta f)$ a linear as a function of Δbin and, as a consequence, the quantity can be approximated as a function of the highest and the second highest tone magnitudes, respectively a and b, in the discrete spectrum of G_H [51].

$$\Delta bin = \pm\frac{a - 2b}{a + b} \qquad (4.40)$$

The complex amplitude of the fundamental frequency tone S_1 at f_0 is estimated as in equation 4.41.

$$S_1 = \frac{2\pi\Delta bin(1 - \Delta bin)}{sin(\pi\Delta bin)}e^{-j\pi\Delta bin}(1 + \Delta bin)G_H(m\Delta f) \qquad (4.41)$$

The estimation of S_1 provides the value of the fundamental frequency tone amplitude s_1 together with its phase ϕ_1. The first step consists into the reconstruction into the time-domain of the fundamental frequency tone given by the equation 4.42

$$s_1(t) = S_1 cos(2\pi f_0 t + \varphi_1) \qquad (4.42)$$

The sampling of $s(t)$ is triggered in correspondence of rise of the time reference pulse per second (PPS) signal. Figure 4.8 shows the procedure to improve the calculation of the synchrophasor phase estimation. The dash-point line represents a generic signal $s(t)$, the continuous line the time-domain reconstructed fundamental frequency tone $s_1(t)$ and the dashed line the PPS signal.
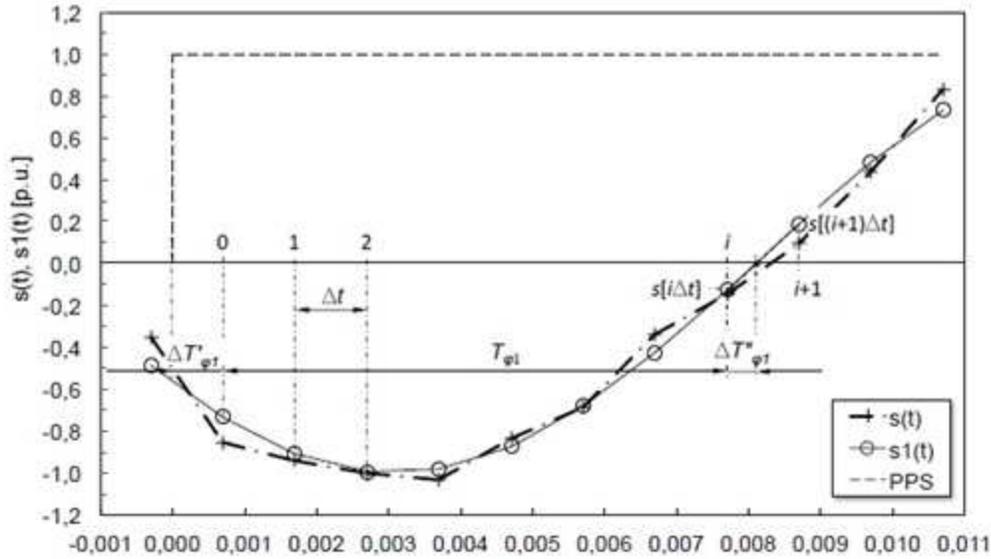
Figure 4.8: Reconstructed signal $s_1(t)$ and redefinition of its phase [52]

By making reference to the figure 4.8, the value of the synchrophasor phase φ_1 is further estimated as in the equation 4.43.

$$\varphi_1 = \frac{3}{2}\pi - 2\pi f_0(T'_{\varphi 1} + \Delta T'_{\varphi 1} + \Delta T''_{\varphi 1}) \tag{4.43}$$

Where,

$$T'_{\varphi 1} = i\Delta t$$

$$\Delta T'_{\varphi 1} = k\frac{1}{f_{clock}}$$

$$\Delta T''_{\varphi 1} = \Delta t \frac{s[i\Delta t]}{|s[i\Delta t] - s[(i+1)\Delta t]|}$$

The estimation of $T'_{\varphi 1}$ is realized by means of a counter that estimates (with the pointer k) the time interval between the PPS rise and the first acquired sample of the $s(t)$. This counter is associated to the clock frequency f_{clock} . The term $\frac{3}{2}\pi$ in equation 4.43 is needed in order to estimate the synchrophasor phase angle in agreement with the time reference defined in [4].

CHAPTER 5

Synchronized Data Sampling

5.1 Setting-free Fault Location Algorithm

The electrical system that uses synchronized or unsynchronized measurements to compute the fault locations based on setting-free algorithm [54] for a transmission line system are already out in the literature. The line parameter are not needed for the fault location calculation using this algorithm. The advantage is that it is weather sensitive and different approximate line parameters are not needed in the calculations. The other useful characteristics of this algorithm is that it does not depend on the values of the fault resistance. When this is applied to an active distribution system, the following two characteristics of the distribution system are not considered. They are 1) Harmonics, 2) Sensitivity of the TVE due to short distribution line length compared to transmission line length. The angle difference between different sectors are well within the limit defined by the IEEE C37.118 so it fails to capture the deviation that occurs in the distribution system [8]. After the post processing of the data with the algorithm defined in chapter 4, it is further implemented here to evaluate its performance.

5.1.1 Mathematical Formulation

5.1.1.1 Asymmetrical Fault

$$V_{s1} - zlI_{s1} = V_{r1} - z(D - l) \tag{5.44}$$

$$V_{s2} - zlI_{s2} = V_{r2} - z(D - l)I_{r2} \tag{5.45}$$

Where,

V_{s1} and V_{r1} =Positive Sequence Sending and Receiving end voltages.

V_{s2} and V_{r2} =Negative Sequence Sending and Receiving end voltages.

z=Line Impedance

l-Fault Distance

D=Length of a line

Solving the above two equations we have,

$$zl = \frac{(V_{s1} - V_{r1})I_{r2} - (V_{s2} - V_{r2})I_{r1}}{(I_{s1}I_{r2} - I_{s2}I_{r1})} \tag{5.46}$$

$$z(D - l)l = \frac{(V_{s1} - V_{r1})I_{s2} - (V_{s2} - V_{r2})I_{s1}}{(I_{s1}I_{r2} - I_{s2}I_{r1})} \tag{5.47}$$

Expressing Fault as a percentage of a Line Length D

$$l\% = \frac{l}{D}100 \tag{5.48}$$

$$l\% = \frac{zl}{zl + z(D - l)}100 \tag{5.49}$$

After substituting for zl and $z(\,D\text{-}l\,)$ from equation 5.46 and equation 5.47 into equation 5.49, we get

$$l\% = \frac{(V_{s1} - V_{r1})I_{r2} - (V_{s2} - V_{r2})I_{r1}}{(V_{s1} - V_{r1})(I_{s2} + I_{r2}) - (V_{s2} - V_{r2})(I_{s1} + I_{r1})} \tag{5.50}$$

The equation 5.50 above gives the estimate of the unsymmetrical fault.

5.1.1.2 Symmetrical Fault
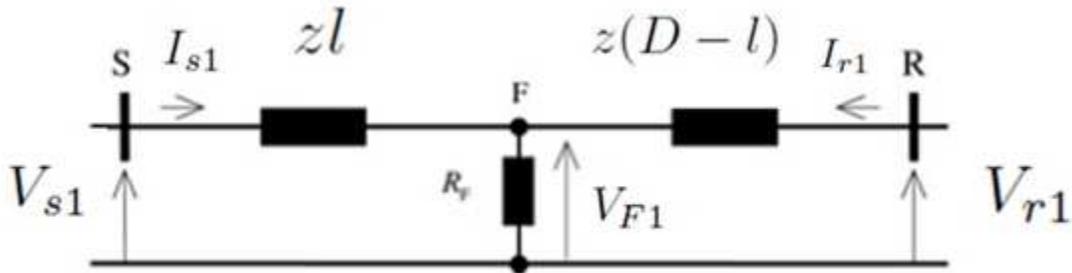
Figure 5.1: Equivalent positive sequence circuit of the faulted line.

Referring to the figure 5.1 and using the relationship given by the equations below we tackle the symmetrical fault problem.

$$V_{s1} - zlI_{s1} - V_{F1} = 0 \tag{5.51}$$

$$V_{r1} - z(D - l)I_{r1} - V_{F1} = 0 \tag{5.52}$$

$$V_{F1} = R_F(I_{s1} + I_{r1}) \tag{5.53}$$

Expressing equation 5.53 into equation 5.51 and equation 5.52 gives

$$zl = \frac{V_{s1}}{I_{s1}} - \frac{I_{s1} + I_{r1}}{I_{s1}}R_F \tag{5.54}$$

$$z(D - l) = \frac{V_{r1}}{I_{r1}} - \frac{I_{s1} + I_{r1}}{I_{r1}} R_F \tag{5.55}$$

Rewriting equation 5.54 and equation 5.55 we have,

$$zl = a_1 + ja_2 + (b_1 + jb_2)R_F \tag{5.56}$$

$$z(D - l) = c_1 + jc_2 + (d_1 + jd_2)R_F \tag{5.57}$$

Where

$$a_1 = Re\left[\frac{V_{s1}}{I_{s1}}\right] \tag{5.58}$$

$$a_2 = Im\left[\frac{V_{s1}}{I_{s1}}\right] \tag{5.59}$$

$$b_1 = Re\left[-\frac{I_{s1} + I_{r1}}{I_{s1}}\right] \tag{5.60}$$

$$b_2 = Im\left[-\frac{I_{s1} + I_{r1}}{I_{s1}}\right] \tag{5.61}$$

$$c_1 = Re\left[\frac{V_{r1}}{I_{r1}}\right] \tag{5.62}$$

$$c_2 = Im\left[\frac{V_{r1}}{I_{r1}}\right] \tag{5.63}$$

$$d_1 = Re\left[-\frac{I_{s1} + I_{r1}}{I_{r1}}\right] \tag{5.64}$$

$$d_2 = Im\left[-\frac{I_{s1} + I_{r1}}{I_{r1}}\right] \tag{5.65}$$

Separating real and Imaginary part of equation 5.56 and equation 5.57 we get,

$$zl = (a_1 + b_1 R_F) + j(a_2 + b_2 R_F) \tag{5.66}$$

$$z(D - l) = (c_1 + d_1 R_F) + j(c_2 + d_2 R_F) \tag{5.67}$$

zl and $z(\ D\text{-}l\ )$ are collinear. Since the impedance z lies in the 1st quadrant of the complex plane, these impedance are located in the same quadrant, as well. Consequently, their real and imaginary components must be greater than zero and the following must hold.

$$a_1 + b_1 R_F > 0 \tag{5.68}$$

$$a_2 + b_2 R_F > 0 \tag{5.69}$$

$$c_1 + d_1 R_F > 0 \tag{5.70}$$

$$c_2 + d_2 R_F > 0 \tag{5.71}$$

Expressing zl and $z(\ D\text{-}l\ )$ in polar form,

$$tan\theta = \frac{a_2 + b_2 R_F}{a_1 + b_1 R_F} \tag{5.72}$$

$$tan\theta = \frac{c_2 + d_2 R_F}{c_1 + d_1 R_F} \tag{5.73}$$

The fault resistance R_F from above can be written as,

$$\frac{a_2 + b_2 R_F}{a_1 + b_1 R_F} = \frac{c_2 + d_2 R_F}{c_1 + d_1 R_F} \tag{5.74}$$

From equation 5.74, the following quadratic equation can be obtained

$$R_F^2 + p R_F + q = 0 \tag{5.75}$$

Where,

$$p = \frac{a_1 d_1 + b_1 c_2 - a_2 d_1 - b_2 c_2}{b_1 d_2 - b_2 d_1} \tag{5.76}$$

$$q = \frac{a_1 c_2 - a_2 c_1}{b_1 d_2 - b_2 d_1} \tag{5.77}$$

Two solutions to the quadratic equation are:

$$(R_F)_1 = \frac{-p + \sqrt{p^2 - 4q}}{2} \tag{5.78}$$

$$(R_F)_2 = \frac{-p - \sqrt{p^2 - 4q}}{2} \tag{5.79}$$

For R_F using equation 5.78 and equation 5.79 gives us following two equations

$$\theta_1 = \arctan\frac{a_2 + b_2 (R_F)_1}{a_1 + b_1 (R_F)_1} \tag{5.80}$$

$$\theta_2 = \arctan\frac{a_2 + b_2 (R_F)_2}{a_1 + b_1 (R_F)_2} \tag{5.81}$$

$$l\% = \frac{l}{D} 100 \tag{5.82}$$

$$l\% = \frac{zl}{zl + z(D - l)} 100 \tag{5.83}$$

$$l\% = \frac{(a_1 + b_1 R_F) + j(a_2 + b_2 R_F)}{(a_1 + b_1 R_F) + j(a_2 + b_2 R_F) + (c_1 + d_1 R_F) + j(c_2 + d_2 R_F)} 100 \tag{5.84}$$

$$l\% = 100 \times \sqrt{\frac{(a_1 + b_1 R_F)^2 + (a_2 + b_2 R_F)^2}{[a_1 + c_1 + (b_1 + d_1)R_F]^2 + [a_2 + c_2 + (b_2 + d_2)R_F]^2}} \tag{5.85}$$

The equation 5.85 above gives the estimate of the fault location for the symmetrical fault.

5.2 Two Machine Infinite Bus Model

The real time synchrophasor data are obtained from the two bus infinite model as shown in figures 5.2 and 5.3. The circuit is simulated using Powerworld [55]. Different fault settings such as single line to ground, line to line, double line to ground faults with different values of fault resistance R_F is defined in the Powerworld. After the required conditions are set for the simulation a transient analysis is run to capture the voltages and currents vectors in the predefined time step from different busses in the network. A screen shot for such settings are depicted in figures 5.4 and 5.5. The vectors generated here is preprocessed and is fed to the One Cycle DFT algorithm previously developed and then the performance is evaluated.
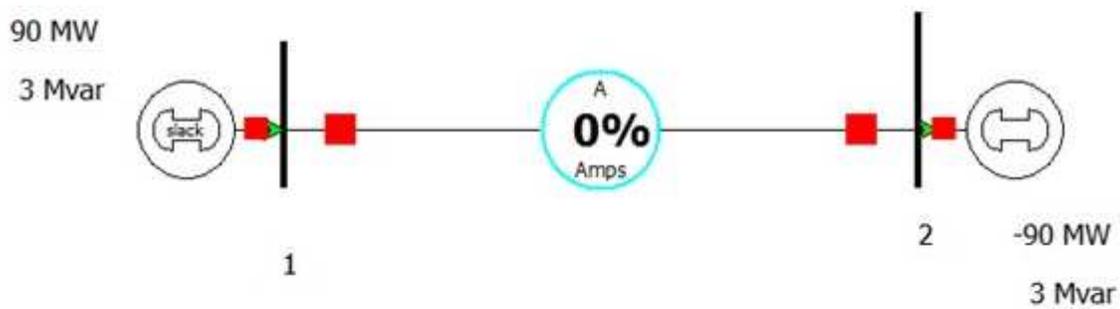
Figure 5.2: Two machine two bus before simulation
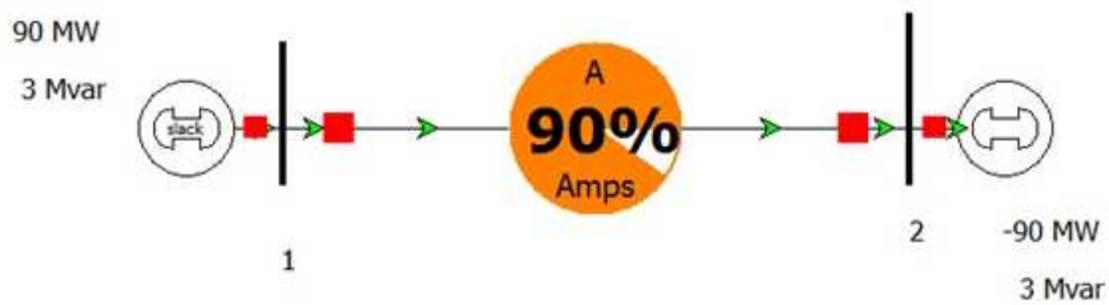
Figure 5.3: Two machine two bus after running the simulation
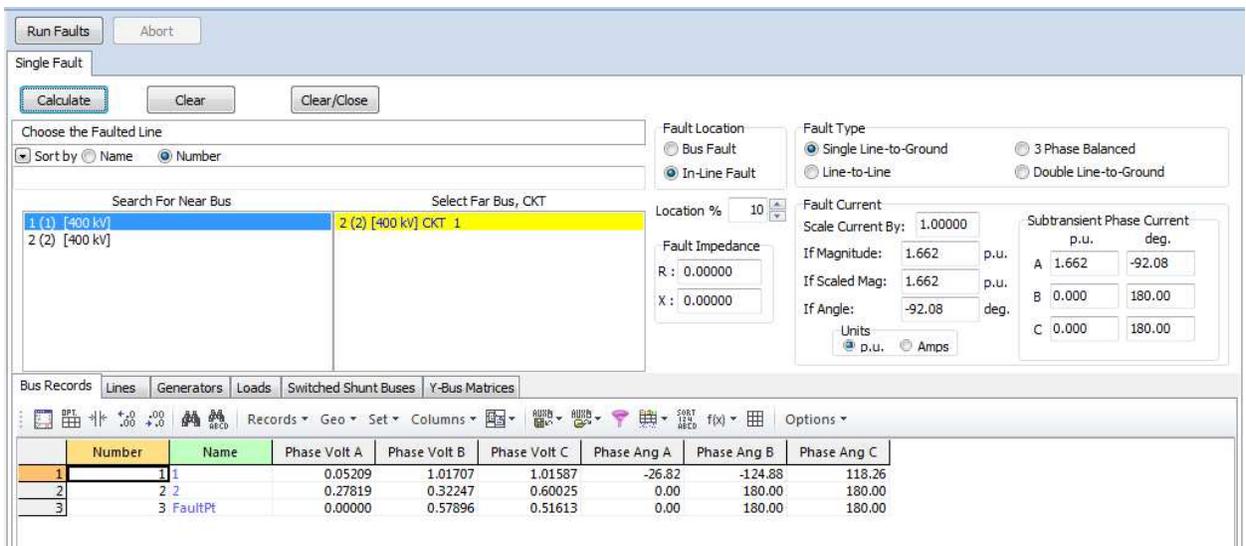
Figure 5.4: Settings for fault
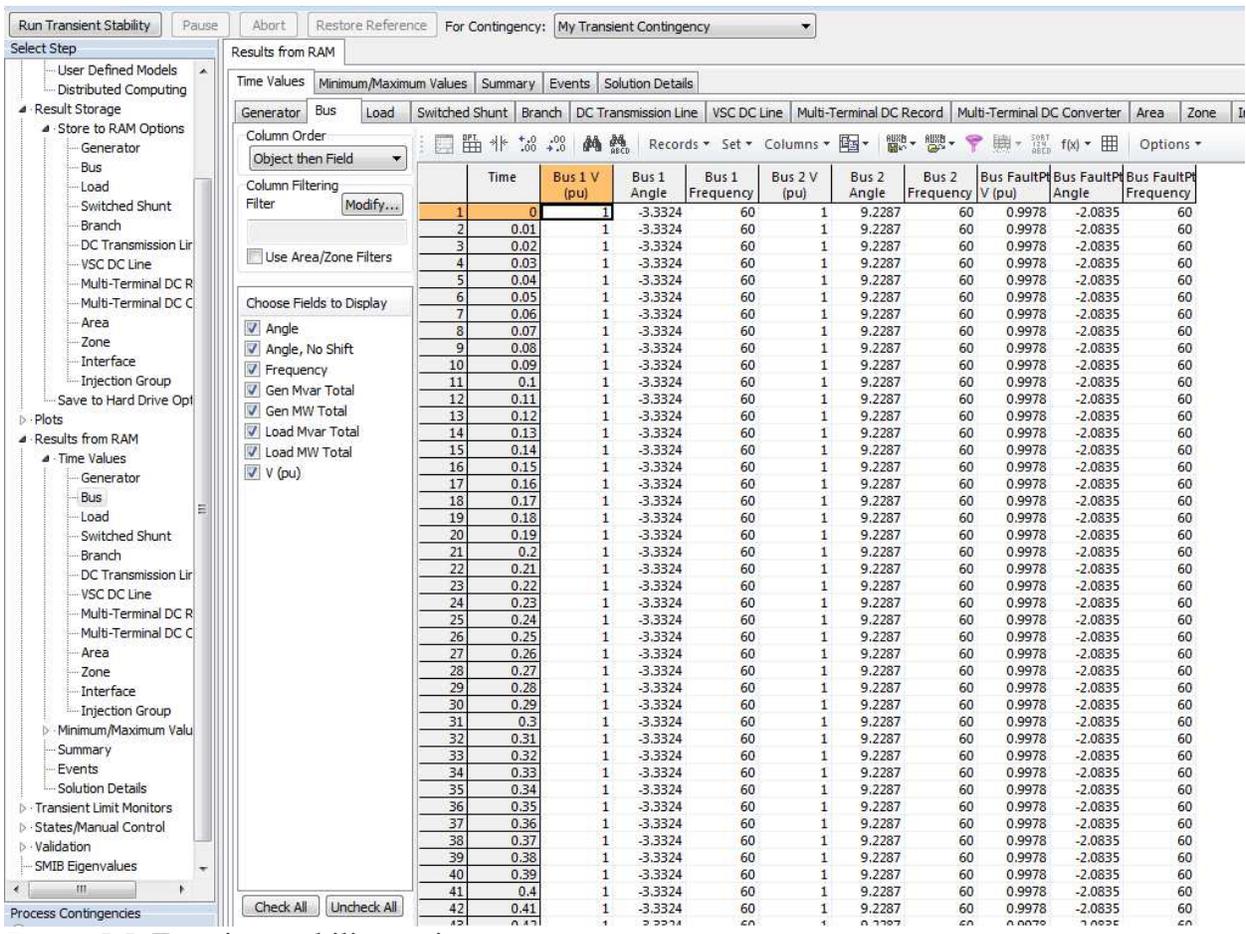
Figure 5.5: Transient stability settings

5.3 Synchrophasor Data Extraction and Preprocessing

The data collection is done by the aid of software and simulations. The required circuit is set-up as per need and the simulation is run. The generated data is saved for later analysis. Since the real time application of control is limited due to the lack of the implementation of the algorithm in the hardware, only post processing analysis is done. Hardware PMUs exists for a transmission line which has a built in capabilities for real time control actions. Devoid of such capabilities and being newer to the field of distribution engineering, this developed synchrophasor algorithm provides only the post processing analysis and the solutions to different transient condition faced during the course of simulation. After the analysis, different remedial schemes are proposed as a solution, which can be further applied for the future uses in the network.

The extracted voltages and currents phasor from the simulation are conditioned to proper format before feeding into the proposed algorithm. The voltage and current magnitude and phases are generated in a vector form. The algorithm for processing takes the input in the rectangular format so these vectors are appropriately converted into the rectangular coordinates and applied to One Cycle DFT algorithm for the analysis.

CHAPTER 6

Results and Implementations

6.1 Results

The results are derived here on parts. First the test signal are subjected to the algorithm to see the performance of the algorithm. When the performance criteria is within the limit, the real world synchrophasor data are tested for the algorithm's efficiency.

6.1.1 Phase Error Performance of the Algorithm

The principal tone reconstruction in time domain depends on the time defined by equation 6.86. The phase error is compensated with these time.

$$\varphi_1 = \frac{3}{2}\pi - 2\pi f_0(T'_{\varphi 1} + \Delta T'_{\varphi 1} + \Delta T''_{\varphi 1}) \tag{6.86}$$

Table 6.1: Phase estimation error performance

$\triangle T'$	T'	$\triangle T''$	φ_1
0.00008	0.6544	0.0039	0.0535
0.000022	0.8458	0.000051	0.0397

The time lag ΔT ' , T' and ΔT" are shown in the table 6.1 and the error performances were evaluated for the efficiency. The error performances were good and stayed below 0.05 percent during the test. The plot for the same is depicted below in figure 6.1. Different sinusoidal signal of known frequencies were subjected for the test and the performance evaluated. Since the signal goes through different filter, the delay is introduced in each filter. The plot of original and estimated signal with the TVE was found below the threshold and is shown in figure 6.2.
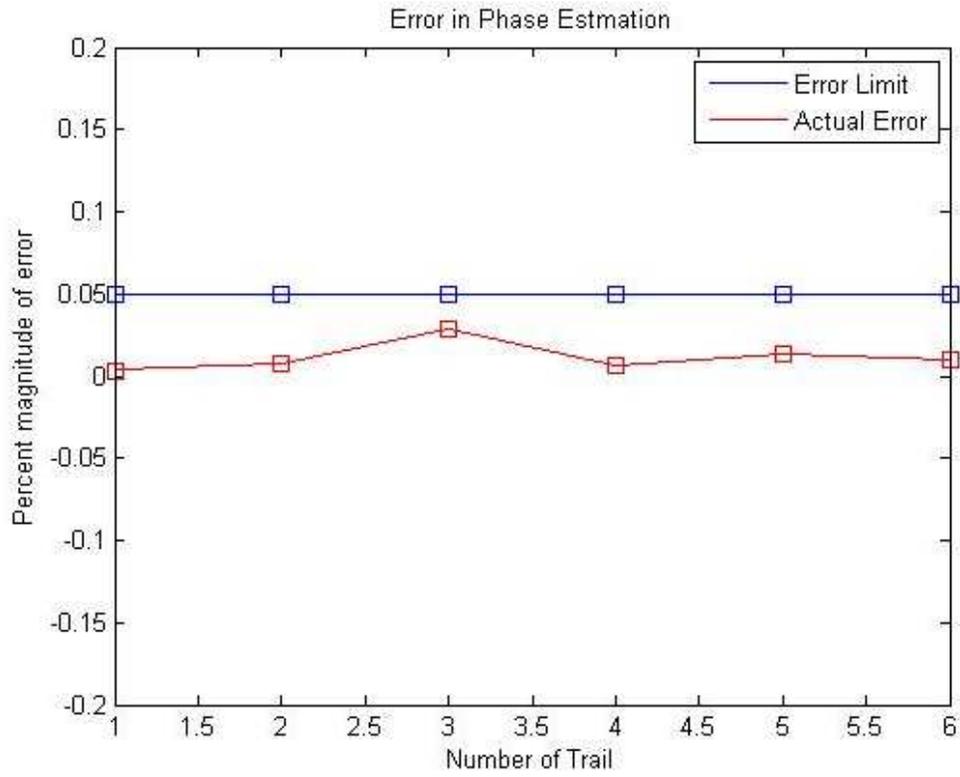
Figure 6.1: Error performance plot
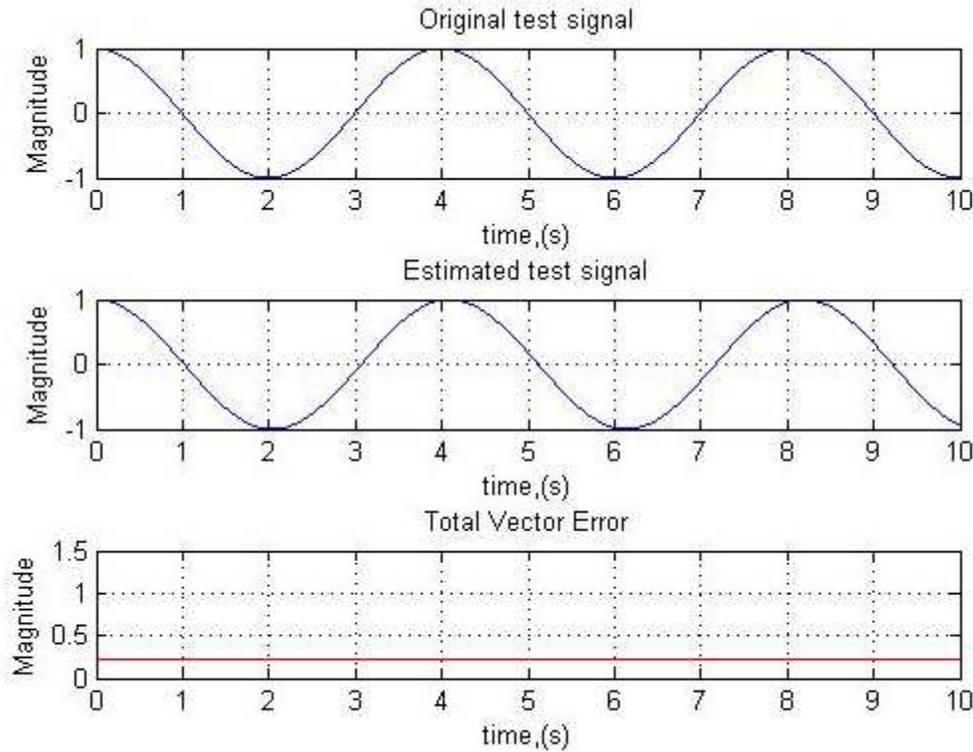
Figure 6.2: TVE performance for the original and estimated signal

6.1.2 Two Machine Infinite Bus System

The synchrophasor data here were obtained using Powerworld simulator [55]. The two bus two machine model in the previous chapter was used to gather the synchrophasor data from the bus and was preprocessed and subjected to the developed algorithm to evaluate its performance. The transient stability analysis was run with the predefined fault settings. The results of the algorithm were further tested for accuracy and efficiency. The TVE for magnitude error, phase error, frequency error and total harmonics distortion error are shown on table 6.2 and are plotted in figure 6.3, figure 6.4, figure 6.5 and figure 6.6 respectively.

Table 6.2: Compensated signal

	Magnitude	Phase	Frequency	Total Harmonic Distortion(THD)
TVE(%)	0.0513	0.0051649	0.0022	0.03658
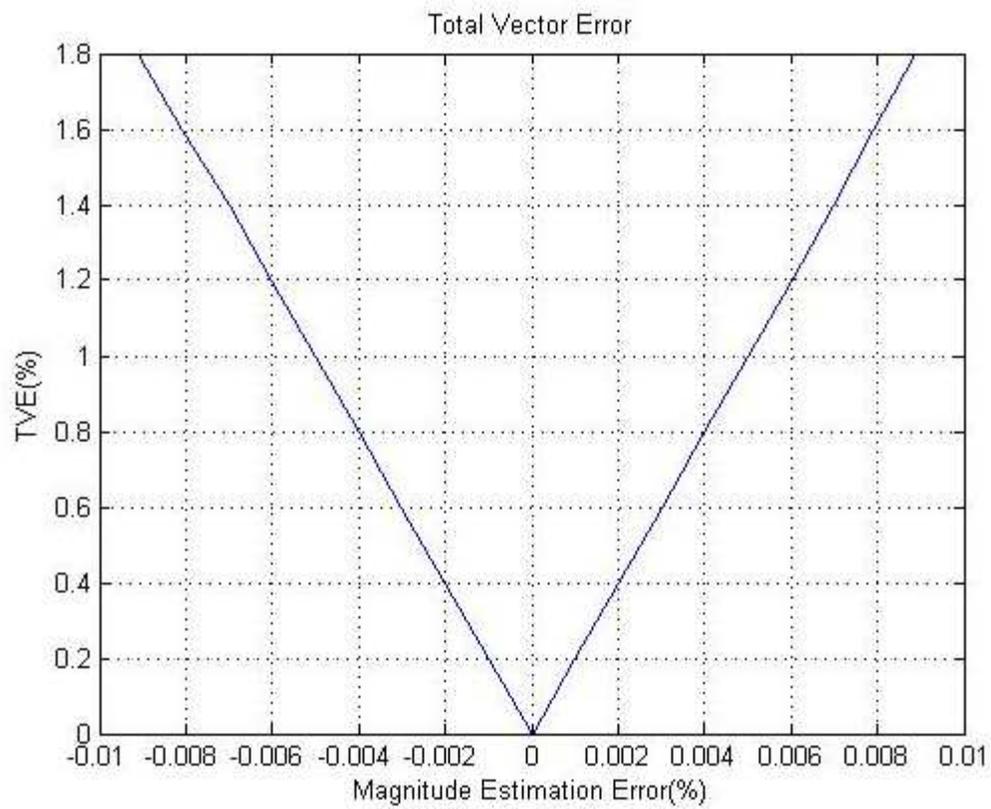
Figure 6.3: TVE magnitude error
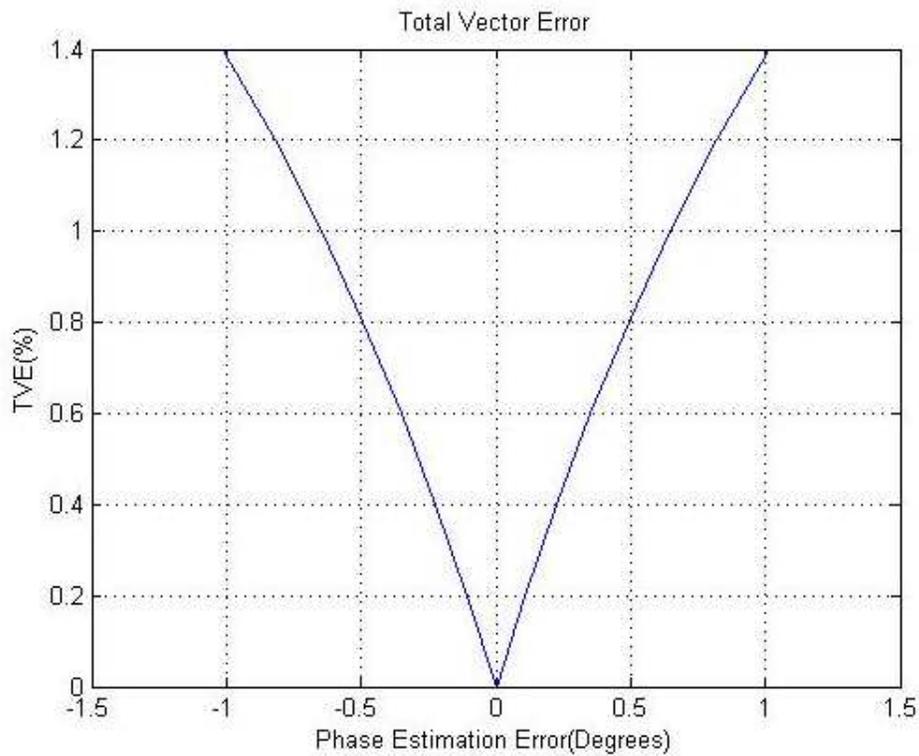
Figure 6.4: TVE phase error
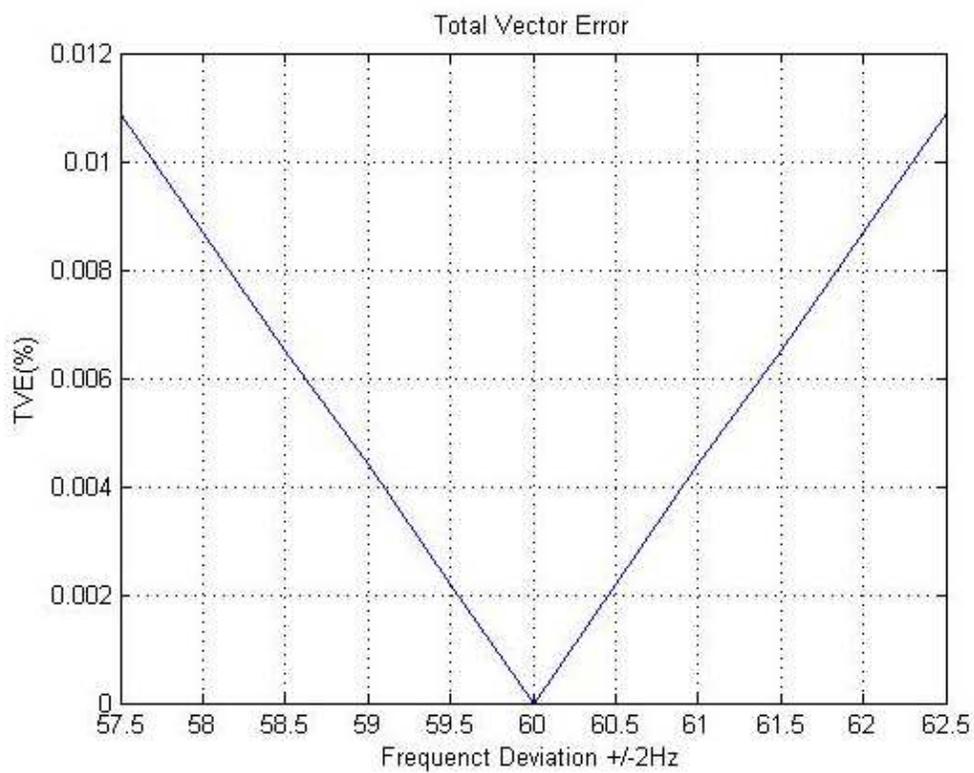
Figure 6.5: TVE frequency error
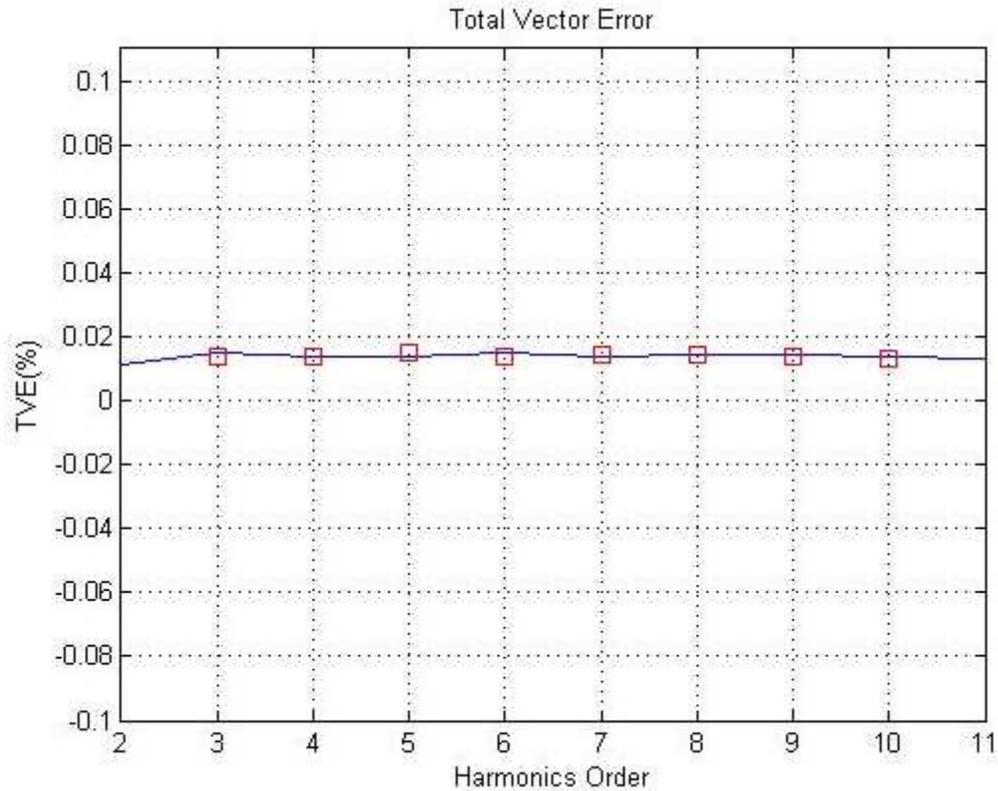
Figure 6.6: TVE for harmonics (up to 11th)

The phase corrected signal is plotted on top of the original signal for phase, magnitude and frequency comparison. The estimated signal had to pass through two filters, Hanning and low pass filter so the delay was introduced in that signal. This signal when processed through the One Cycle DFT algorithm, the TVE for phase, magnitude and frequency came within the permitted limit defined by the synchrophasor standard. The phase uncorrected and the phase corrected signals are shown in figure 6.7 and figure 6.8 respectively.
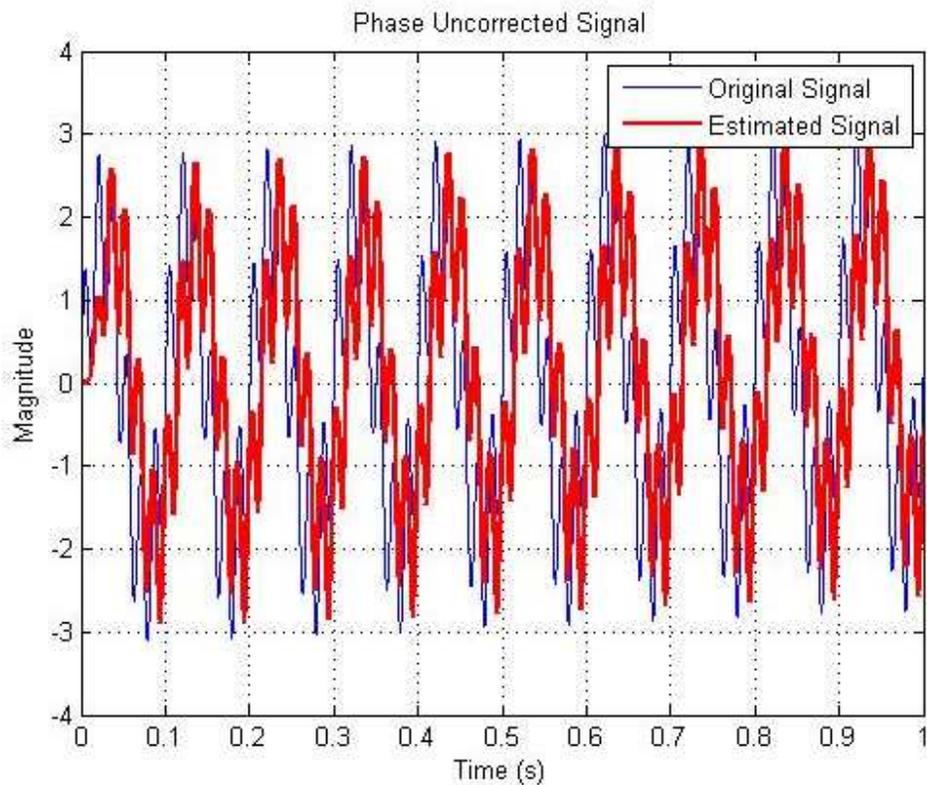
Figure 6.7: Phase uncorrected signal
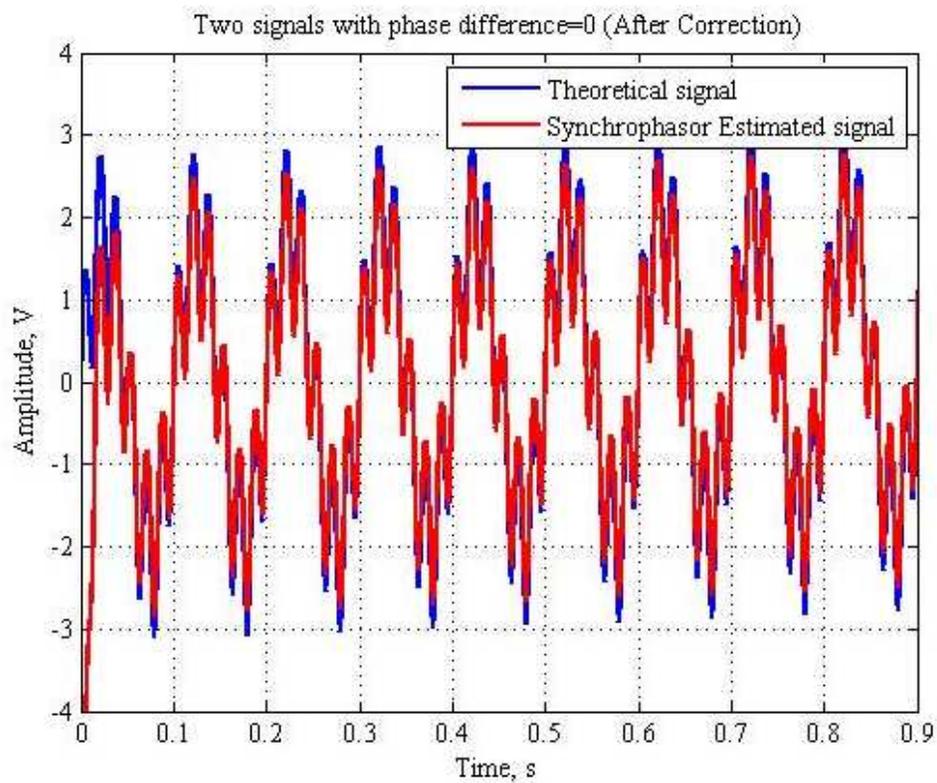
Figure 6.8: Phase corrected signal

6.2 Implementation in IEEE 13 Bus Test Feeder

The performance evaluation of this algorithm is further taken to the next level by testing its performance for efficiency and speed in an IEEE 13 bus test feeder system. The fictitious fault was generated in the network with the procedure mentioned on chapter 5 and the results were extracted for the analysis. The errors were calculated for this procedure after the application of the algorithm. The results from [54] were used as a benchmark data for the performance evaluation. The circuit layout for this experimental procedure is shown in figure 6.8. The different fault type settings were preset and the simulations were run for transient stability analysis. After the simulation, the synchrophasor data were extracted from every bus in the system along with the precise time stamp.

Figure 6.9: IEEE 13 bus test feeder depicted using Powerworld

6.2.1 Fault Performance

The following set of fault location analysis were performed for the line length of 50 km and 100 km. The fault settings were defined as outlined on chapter 5 and transient stability analysis were run. After the execution the generated data for fault were extracted and evaluated. The simulations were performed for single line to ground, line to line and double line to ground for the fault resistance value of R_F equal to 0, 10 and 100 ohms. The final error after this procedure are shown in the table 6.3. The plots for the error performance are further shown in figures 6.9, 6.10, 6.11, 6.12, 6.13, 6.14.

Table 6.3: Simulation result from different network condition

Fault Type			Fault simulated				
		10	15	35	60	75
$R_F = 0\Omega$	D=50km	0.0078	0.0084	0.0085	0.0099	0.0104
$R_F = 10\Omega$	SLG	0.0098	0.0098	0.0099	0.01	0.01
$R_F = 100\Omega$		0.0098	0.0098	0.0099	0.01	0.01
$R_F = 0\Omega$	LL	0.0096	0.0098	0.0099	0.0099	0.01
$R_F = 100\Omega$		0.0101	0.0101	0.0102	0.0097	0.0099
$R_F = 0\Omega$	LLG	0.0086	0.0092	0.0098	0.01	0.0101
$R_F = 100\Omega$		0.0096	0.0098	0.0099	0.0099	0.01
$R_F = 0\Omega$	D=100km	0.000247	0.0092	0.0093	0.0105	0.0098
$R_F = 10\Omega$	SLG	0.000114	0.0099	0.0099	0.01	0.01
$R_F = 100\Omega$		0.000125	0.0098	0.0099	0.01	0.01
$R_F = 0\Omega$	LL	0.0096	0.0097	0.0099	0.01	0.01
$R_F = 100\Omega$		0.0101	0.0101	0.0102	0.0097	0.0099
$R_F = 0\Omega$	LLG	0.0087	0.0092	0.0098	0.01	0.0101
$R_F = 100\Omega$		0.0096	0.0097	0.0099	0.01	0.01
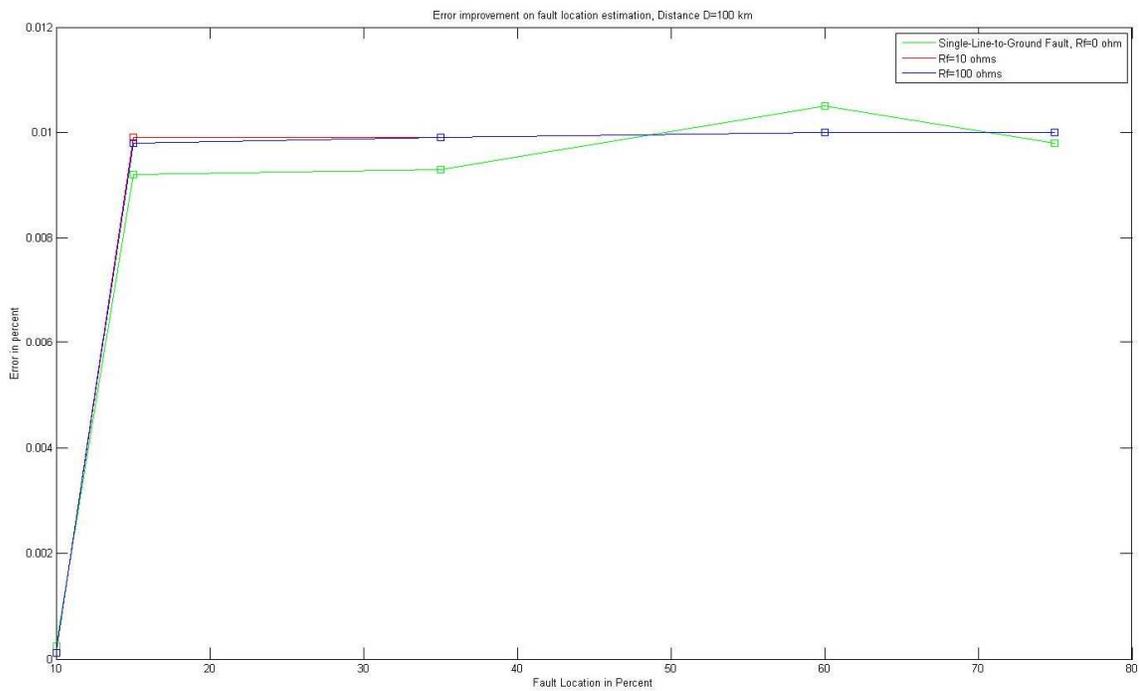
Figure 6.10: Error for single line to ground (D=100 km)
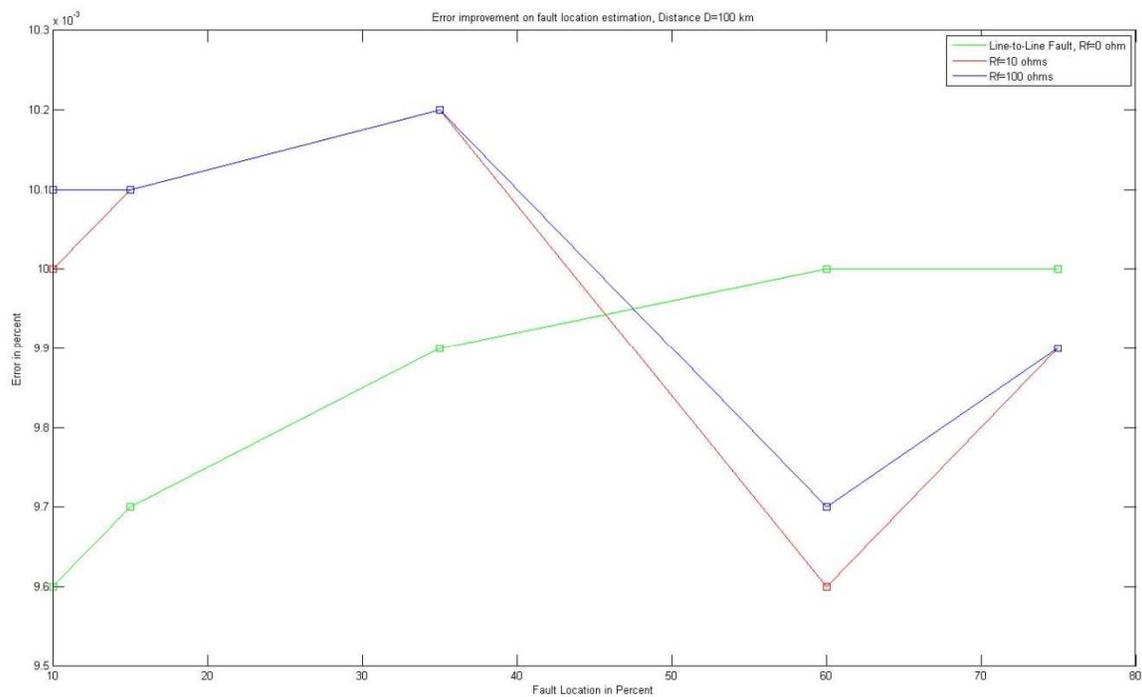
Figure 6.11: Error for line to line (D=100 km)
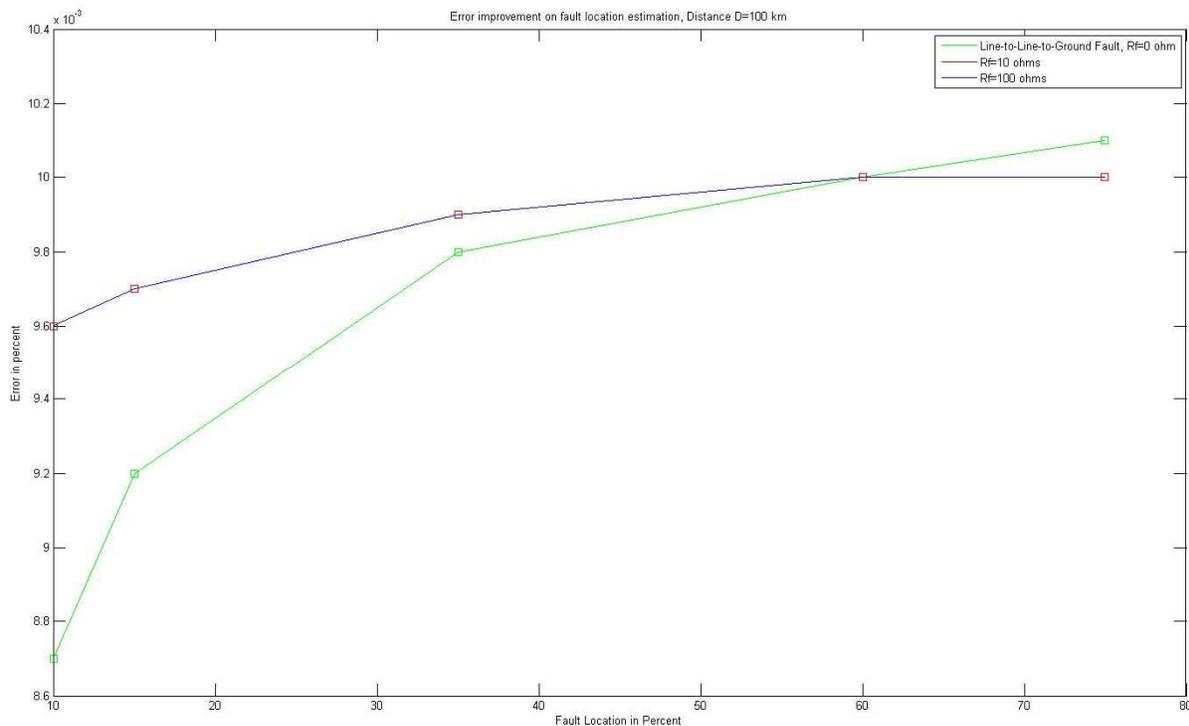
Figure 6.12: Error for double line to ground (D=100 km)
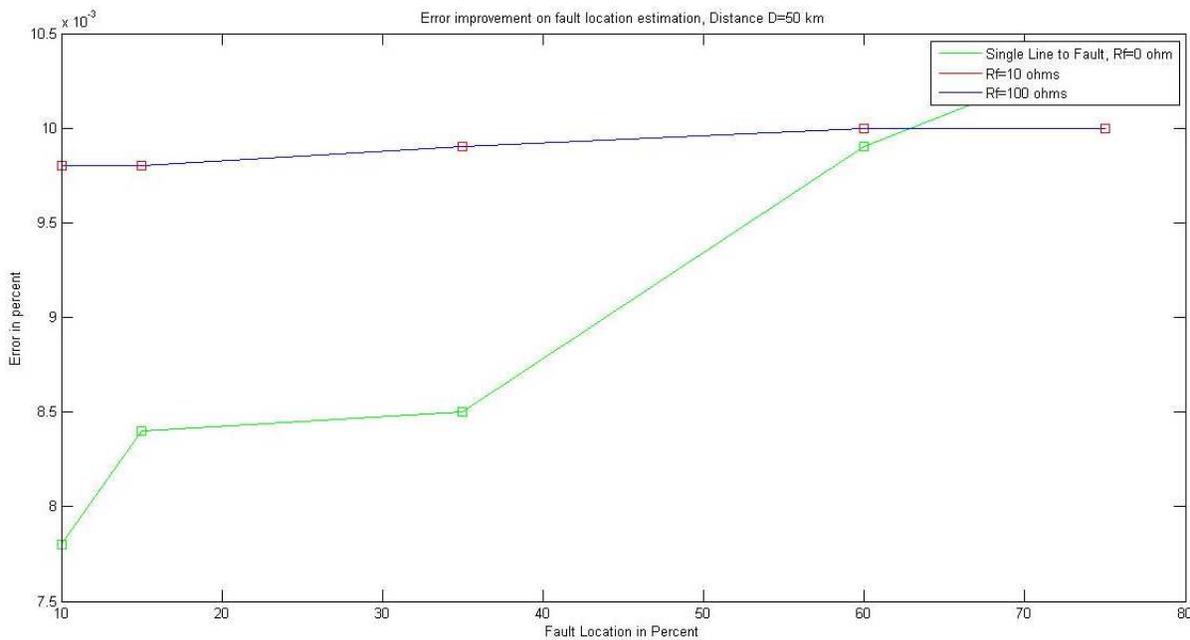
Figure 6.13: Error for single line to ground (D=50 km)
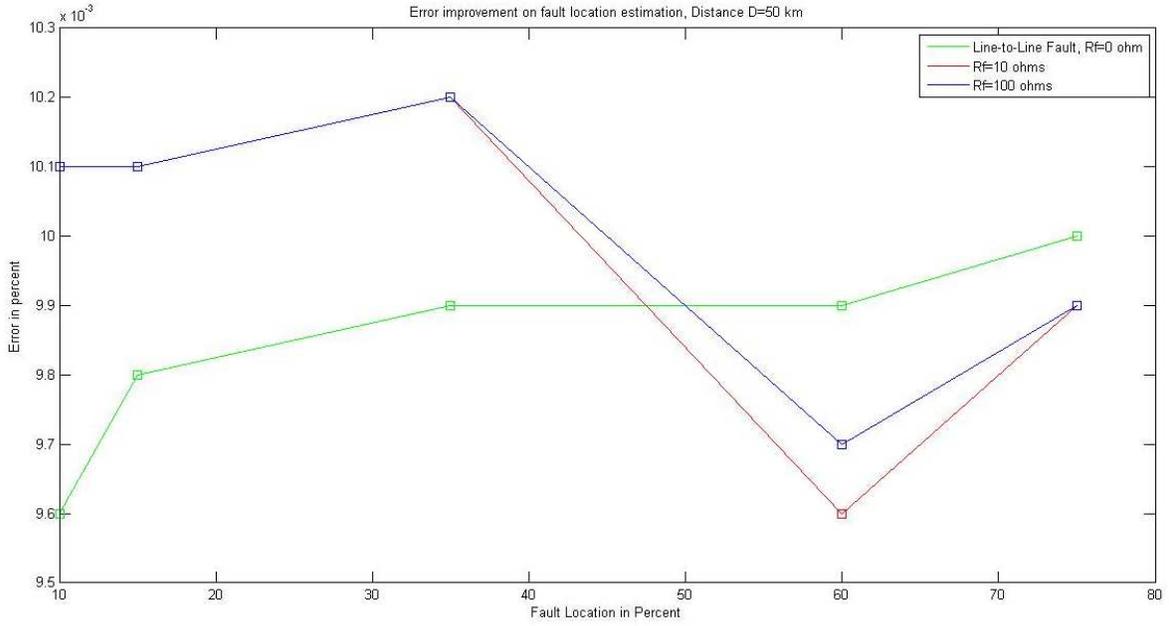
Figure 6.14: Error for line to line (D=50 km)
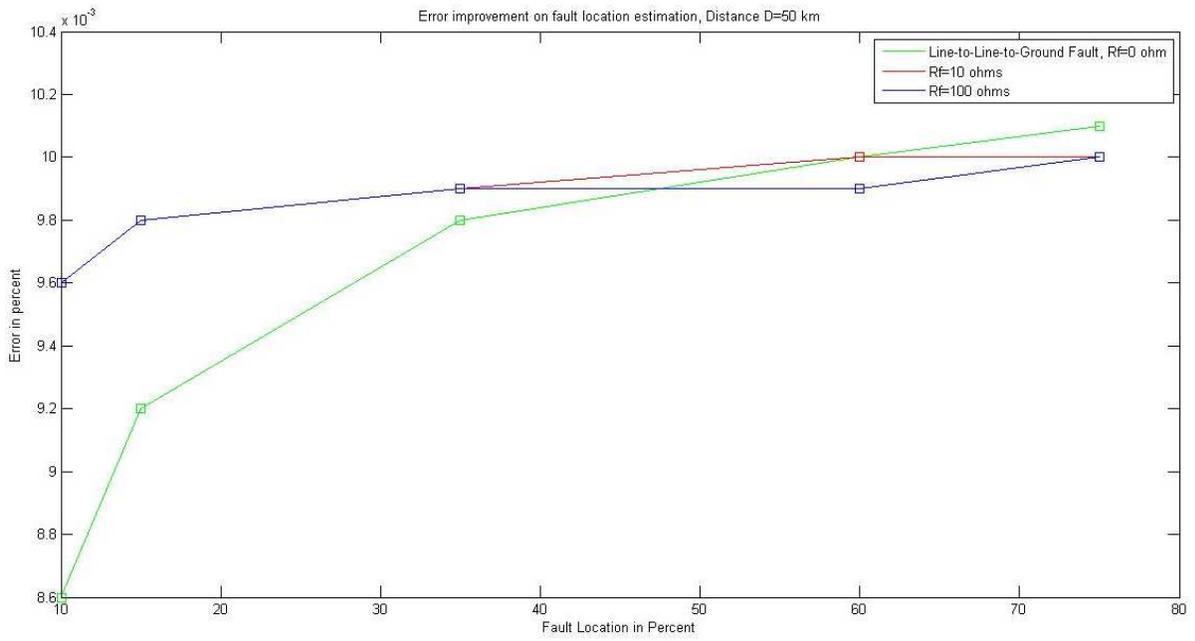
Figure 6.15: Error for double line to ground (D=50 km)

6.3 Statistical Significance

6.3.1 Parametric t-statistics

The statistical tools were used to analyze the benchmark data and the new generated data. The hypothesis are defined as.

The null hypothesis: H_0 : Both methods gives similar result

The Alternative Hypothesis: H_a : Improved method gives better result

At the significance level (α)=0.05

The data were checked for the normalcy using 1 sample KS (Kolmogorov–Smirnov) test. When it was found to be normal, the parametric t-test was performed on the existing data and the improved data with the new algorithm. It was found that, p-value < α. The null hypothesis is rejected in the favor of the alternative. In other word we have a significant evidence to show that the new improved algorithm gives better result than the existing one.

CHAPTER 7

Conclusion and Future Work

7.1 Conclusion

This study looked into the synchrophasor technology with a deeper prospect of utilizing it to its full extent into a distribution network. To make this application possible, a signal processing techniques were addressed and analyzed to derive new efficient algorithm which would allow synchrophasor to be deployed widely into the distribution network and without which it would not have been possible. For that reason different signal processing techniques were considered as a potential candidate for the job. With all the best reason stated in the literature review, One Cycle DFT approach was chosen for its speed which was the desired characteristics of a P class PMU. The time domain reconstruction of the principal tone frequency was considered as the measure to mitigate the phase error.

When the test for efficiency were performed on a standard test signal and real network signal, the TVE, phase error, magnitude error, frequency error and THD error were well within the limit as stated in the synchrophasor standard. A further implementation of this algorithm were carried out in a two machine infinite bus and an IEEE 13 bus test feeder. It was found that all the above mentioned performance criteria were satisfied and were well within the given boundary for the proper operation. As an application to the efficient fault location technique it was found that the fault location errors were significantly reduced. This claim is further substantiated by the statistical hypothesis testing. When the hypothesis tests were performed it was found that the new algorithm outperformed the benchmark algorithm significantly.

The developed algorithm is efficient, fast and complies with the synchrophasor standard so it can be implemented in the hardware for the real time processing of the synchrophasor data.

7.2 Future Work

After working with the synchrophasor for the distribution system applications for the post processing of the data, the next level would be to process the data continuously in a real time and provide necessary control action required by the system during the fault. Such control action is only possible when this algorithm is implemented in a hardware and deployed out in the field. Most power system control equipments are already out there on the field doing their predefined jobs. To replace them with the capability of this new signal processing algorithm would mean astronomical economic burden.

Moreover the smart grid realization initiative also means replacing such legacy power system equipments from the root on and replace them with the contemporary ones. Since economy-wise this action is not feasible so the alternative has to be sought. One of the alternative to cut cost but yet get covered with the technologically advanced equipments is by Substation Asset Optimization.

The hardware implementation of the above algorithm is made possible by considering the retrofit design of the hardware. These hardware can then just piggy-ride on the existing PMU devices and perform their job in the distribution system which would save tremendous amount of resources.

After the synopses on the cost part I would like my future work to be in the optimization area but not only limited to the area summarized below:

- Continue working at this end for even better and faster result

- Consider working on Substation Asset Optimization front

- Consider working with micro-PMUs suited only for the distribution system

References

[1]   D. A. Haughton, "State estimation for enhanced monitoring, reliability, restoration and control of smart distribution systems," Arizona State University, 2012.

[2]   N. Wu, "A new fault location algorithm for distribution network with DG," in *Electricity Distribution (CICED), 2010 China International Conference on*, 2010, pp. 1-7.

[3]   EPA. *Climate Change Indicators*. Available: http://www.epa.gov/climate/climatechange/science/indicators/ghg/index.html

[4]   "IEEE Standard for Synchrophasor Measurements for Power Systems," *IEEE Std C37.118.1-2011 (Revision of IEEE Std C37.118-2005),* pp. 1-61, IEEE Std C37.118.1-2011.

[5]   Y. Cunjiang, Z. Huaxun, and Z. Lei, "Architecture Design For Smart Grid," *Energy Procedia,* vol. 17, Part B, pp. 1524-1528, // 2012.

[6]   V. Tamilmaran and K. Dwarkadas Pralhadas, "Smart grid: an overview," *Smart Grid and Renewable Energy,* vol. 2011, 2011.

[7]   D. Elmakias, *New computational methods in power system reliability* vol. 111: Springer, 2008.

[8]   M. Paolone, A. Borghetti, and C. Nucci, "Development of an RTU for synchrophasors estimation in active distribution networks," in *PowerTech, 2009 IEEE Bucharest*, 2009, pp. 1-6.

[9]   P. Dondi, D. Bayoumi, C. Haederli, D. Julian, and M. Suter, "Network integration of distributed power generation," *Journal of Power Sources,* vol. 106, pp. 1-9, 4/1/ 2002.

[10]   G. Pepermans, J. Driesen, D. Haeseldonckx, R. Belmans, and W. D'haeseleer, "Distributed generation: definition, benefits and issues," *Energy policy,* vol. 33, pp. 787-798, 2005.

[11]   Y. Makarov, S. Lu, B. McManus, and J. Pease, "The future impact of wind on BPA power system ancillary services," in *Transmission and Distribution Conference and Exposition, 2008. T&# x00026; D. IEEE/PES*, 2008, pp. 1-5.

[12]   P. P. Barker and R. W. de Mello, "Determining the impact of distributed generation on power systems. I. Radial distribution systems," in *Power Engineering Society Summer Meeting, 2000. IEEE*, 2000, pp. 1645-1656.

[13]   C. J. Mozina, "A Tutorial on the Impact of Distributed Generation (DG) on Distribution Systems," in *Protective Relay Engineers, 2008 61st Annual Conference for*, 2008, pp. 591-609.

[14]   M. Hlatshwayo, S. Chowdhury, S. Chowdhury, and K. Awodele, "Impacts of DG penetration in the reliability of Distribution Systems," in *Power System Technology (POWERCON), 2010 International Conference on*, 2010, pp. 1-8.

[15]   "IEEE Recommended Practices and Requirements for Harmonic Control in Electrical Power Systems," *IEEE Std 519-1992,* pp. 1-112, IEEE 519 1993.

[16]   "IEEE Guide for the Application of Neutral Grounding in Electrical Utility Systems, Part IV - Distribution," *IEEE Std C62.92.4-1991,* p. 0_1, IEEE Std C62.92.4-1991 1992.

[17]   "IEEE Guide for Determining Fault Location on AC Transmission and Distribution Lines," *IEEE Std C37.114-2004,* pp. 0_1-36, 2005.

[18]   E. Nashawati, R. Garcia, and T. Rosenberger, "Using synchrophasor for fault location identification," in *Protective Relay Engineers, 2012 65th Annual Conference for*, 2012, pp. 14-21.

[19]   E. Nashawati, "Dynamic System Reduction And Fault Location Identification Using Synchrophasors," 2012.

[20]   K. Zimmerman and D. Costello, "Impedance-based fault location experience," in *Protective Relay Engineers, 2005 58th Annual Conference for*, 2005, pp. 211-226.

[21]   T. Takagi, Y. Yamakoshi, M. Yamaura, R. Kondow, and T. Matsushima, "Development of a new type fault locator using the one-terminal voltage and current data," *power apparatus and systems, ieee transactions on,* pp. 2892-2898, 1982.

[22]   L. Ericksson, G. Rockefeller, and M. Saha, "An accurate fault locator with compensation for apparent reactance in the fault resistance resulting from remote-end infeed," ASEA AB, Vasteras1985.

[23]   M. Adamiak, B. Kasztenny, and W. Premerlani, "Synchrophasors: definition, measurement, and application," *Proceedings of the 59th Annual Georgia Tech Protective Relaying, Atlanta, GA,* 2005.

[24]   J. D. Glover, M. Sarma, and T. Overbye, *Power System Analysis & Design, SI Version*: Cengage Learning, 2011.

[25]   "IEEE Standard for Synchrophasors for Power Systems," *IEEE Std C37.118-2005 (Revision of IEEE Std 1344-1995),* pp. 0_1-57, IEEE Std C37.118-2005.

[26]   P. Castello, J. Liu, C. Muscas, P. A. Pegoraro, F. Ponci, and A. Monti, "A fast and accurate PMU algorithm for P+ M class measurement of synchrophasor and frequency," 2014.

[27] Z. Huang, B. Kasztenny, V. Madani, K. Martin, S. Meliopoulos, D. Novosel, *et al.*, "Performance evaluation of phasor measurement systems," in *Power and Energy Society General Meeting-Conversion and Delivery of Electrical Energy in the 21st Century, 2008 IEEE*, 2008, pp. 1-7.

[28] P. Romano and M. Paolone, "Enhanced interpolated-DFT for synchrophasor estimation in FPGAs: Theory, implementation, and validation of a PMU prototype," 2014.

[29] A. Khanal, E. Oleka, A. Osareh, and G. Lebby, "Optimal Placement of Phasor Measurement Units for Maximum Network Observability Using Python-Gurobi."

[30] Y. Liao and S. Elangovan, "Unsynchronised two-terminal transmission-line fault-location without using line parameters," in *Generation, Transmission and Distribution, IEE Proceedings-*, 2006, pp. 639-643.

[31] L. Jian, N. Jianli, and D. Yu, "Du Yu. A unified matrix algorithm for fault section detection and isolation in distribution system," *Automation of Electric Power Systems,* vol. 23, pp. 31-33, 1999.

[32] W. Fei and S. Ying, "An Improved Matrix Algorithm for Fault Location in Distribution Network of Power Systems [J]," *Automation of Electric Power Systems,* vol. 24, 2003.

[33] Z.-n. WEI, H. He, and Y.-p. ZHENG, "A refined genetic algorithm for the fault sections location [J]," *Proceedings of the Csee,* vol. 4, p. 025, 2002.

[34] Y. Chao, Z. Xiangjun, and X. Yunfeng, "Improved algorithm for fault location in distribution network with distributed generations," in *Intelligent Computation Technology and Automation (ICICTA), 2008 International Conference on*, 2008, pp. 893-896.

[35]   C. Zhong-xiao, Z. Xiao-bin, and C. Xing-yu, "Study of Fault Location Algorithm in Distribution Network Based on Fault Matrix," in *Engineering and Technology (S-CET), 2012 Spring Congress on*, 2012, pp. 1-3.

[36]   W. Li, H. Chen, and B. Xiang, "The Study for GIS-based Distribution Network Monitoring and Control Area Fault Location Methods," in *Computer Science & Service System (CSSS), 2012 International Conference on*, 2012, pp. 1758-1761.

[37]   S. Geramian, H. A. Abyane, and K. Mazlumi, "Determination of optimal PMU placement for fault location using genetic algorithm," in *Harmonics and Quality of Power, 2008. ICHQP 2008. 13th International Conference on*, 2008, pp. 1-5.

[38]   J. Ren, S. Venkata, and E. Sortomme, "An Accurate Synchrophasor Based Fault Location Method for Emerging Distribution Systems," 2014.

[39]   J. Ma, J.-l. Li, Z.-P. Wang, and Q.-x. Yang, "A novel wide-area fault location algorithm based on fault model," in *Power and Energy Engineering Conference (APPEEC), 2010 Asia-Pacific*, 2010, pp. 1-4.

[40]   C.-S. Chen, C.-W. Liu, and J.-A. Jiang, "A new adaptive PMU based protection scheme for transposed/untransposed parallel transmission lines," *Power Delivery, IEEE Transactions on,* vol. 17, pp. 395-404, 2002.

[41]   R. Gelagaev, P. Vermeyen, J. Vandewalle, and J. Driesen, "Numerical observability analysis of distribution systems," in *Harmonics and Quality of Power (ICHQP), 2010 14th International Conference on*, 2010, pp. 1-6.

[42]   P. M. Ramos and A. Cruz Serra, "Comparison of frequency estimation algorithms for power quality assessment," *Measurement,* vol. 42, pp. 1312-1317, 2009.

[43] S. Chandrasekhar and T. V. Sreenivas, "Instantaneous frequency estimation using level-crossing information," in *Acoustics, Speech, and Signal Processing, 2003. Proceedings.(ICASSP'03). 2003 IEEE International Conference on*, 2003, pp. VI-141-4 vol. 6.

[44] A. Pradhan, A. Routray, and A. Basak, "Power system frequency estimation using least mean square technique," *Power Delivery, IEEE Transactions on,* vol. 20, pp. 1812-1816, 2005.

[45] J.-H. Lee and H.-T. Kim, "Application of Newton method to natural frequency estimation," in *Aerospace and Electronics Conference (NAECON), Proceedings of the IEEE 2010 National*, 2010, pp. 212-214.

[46] M. A. Donolo and V. A. Centeno, "Accuracy Limits for Synchrophasor Measurements and the IEEE standard," *Power Delivery, IEEE Transactions on,* vol. 23, pp. 504-505, 2008.

[47] W. H. Kersting, "Radial distribution test feeders," *Power Systems, IEEE Transactions on,* vol. 6, pp. 975-985, 1991.

[48] A. Borghetti, C. A. Nucci, M. Paolone, G. Ciappi, and A. Solari, "Synchronized phasors monitoring during the islanding maneuver of an active distribution network," *Smart Grid, IEEE Transactions on,* vol. 2, pp. 82-91, 2011.

[49] A. G. Phadke and J. S. Thorp, *Synchronized phasor measurements and their applications*: Springer, 2008.

[50] A. G. Phadke, "Synchronized phasor measurements-a historical overview," in *Transmission and Distribution Conference and Exhibition 2002: Asia Pacific. IEEE/PES*, 2002, pp. 476-479.

[51]   T. Grandke, "Interpolation algorithms for discrete Fourier transforms of weighted signals," *Instrumentation and Measurement, IEEE Transactions on,* vol. 32, pp. 350-355, 1983.

[52]   M. Paolone, A. Borghetti, and C. A. Nucci, "A synchrophasor estimation algorithm for the monitoring of active distribution networks in steady state and transient conditions," in *Proc. of the 17th Power Systems Computation Conference (PSCC 2011), Stockholm, Sweden,* 2011.

[53]   A. Carta, N. Locci, C. Muscas, and S. Sulis, "A flexible GPS-based system for synchronized phasor measurement in electric distribution networks," *Instrumentation and Measurement, IEEE Transactions on,* vol. 57, pp. 2450-2456, 2008.

[54]   G. Preston, Z. Radojevic, C. Kim, and V. Terzija, "New settings-free fault location algorithm based on synchronised sampling," *Generation, Transmission & Distribution, IET,* vol. 5, pp. 376-383, 2011.

[55]   *Power World Simulator.* Available: http://www.powerworld.com/products/simulator/overview

Appendix A

Table A.1: Most common windows used for DSP.

Window Type		Highest sidelobe level (dB)	Sidelobe falloff (dB/octave)	Coherent gain	Equivalent noise BW (bins)	3.0-dB BW (bins)	Scallop loss (dB)	Worst-case process loss (dB)	6.0-dB BW (bins)	Overlap correlation (%) 75% OL	50% OL
Rectangle		−13	−6	1.00	1.00	0.89	3.92	3.92	1.21	75.0	50.0
Triangle		−27	−12	0.50	1.33	1.28	1.82	3.07	1.78	71.9	25.0
RVCI	α=1.0	−23	−12	0.64	1.23	1.20	2.10	3.01	1.65	75.5	31.8
	α=2.0	−32	−18	0.50	1.50	1.44	1.42	3.18	2.00	65.9	16.7
	α=3.0	−39	−24	0.42	1.73	1.66	1.08	3.47	2.32	56.7	8.5
	α=4.0	−47	−30	0.38	1.94	1.86	0.86	3.75	2.59	48.6	4.3
Hamming		−43	−6	0.54	1.36	1.30	1.78	3.10	1.81	70.7	23.5
Parabolic		−21	−12	0.67	1.20	1.16	2.22	3.01	1.59	76.5	34.4
Riemann		−26	−12	0.59	1.30	1.26	1.89	3.03	1.74	73.4	27.4
Cubic		−53	−24	0.38	1.92	1.82	0.90	3.72	2.55	49.3	5.0
Tukey	α=0.25	−14	−18	0.88	1.10	1.01	2.96	3.39	1.38	74.1	44.4
	α=0.50	−15	−18	0.75	1.22	1.15	2.24	3.11	1.57	72.7	36.4
	α=0.75	−19	−18	0.63	1.36	1.31	1.73	3.07	1.80	70.5	25.1
Bohman		−46	−24	0.41	1.79	1.71	1.02	3.54	2.38	54.5	7.4
Poisson	α=2.0	−19	−6	0.44	1.30	1.21	2.09	3.23	1.69	69.9	27.8
	α=3.0	−24	−6	0.32	1.65	1.45	1.46	3.64	2.08	54.8	15.1
	α=4.0	−31	−6	0.25	2.08	1.75	1.03	4.21	2.58	40.4	7.4
Hamming,Poisson	α=0.5	−35	−18	0.43	1.61	1.54	1.26	3.33	2.14	61.3	12.6
	α=1.0	−39	−18	0.38	1.73	1.64	1.11	3.50	2.30	56.0	9.2
	α=2.0	none	−18	0.29	2.02	1.87	0.87	3.94	2.65	44.6	4.7
Cauchy	α=3.0	−31	−6	0.42	1.48	1.34	1.71	3.40	1.90	61.6	20.2
	α=4.0	−35	−6	0.33	1.76	1.50	1.36	3.83	2.20	48.8	13.2
	α=5.0	−30	−6	0.28	2.06	1.68	1.13	4.28	2.53	38.3	9.0
Taylor	α=2.0	−40	−6	0.57	1.30	1.25	1.91	3.06	1.74	75.7	28.3
	α=2.5	−50	−6	0.51	1.43	1.36	1.60	3.15	1.90	71.3	21.4
	α=3.0	−60	−6	0.47	1.55	1.47	1.37	3.26	2.06	67.0	16.1
	α=3.5	−70	−6	0.44	1.66	1.58	1.20	3.40	2.21	62.9	12.1
	α=4.0	−80	−6	0.41	1.76	1.67	1.06	3.52	2.35	59.1	9.1
Gaussian	α=2.5	−42	−6	0.51	1.39	1.33	1.69	3.14	1.86	67.7	20.0
	α=3.0	−55	−6	0.43	1.64	1.55	1.25	3.40	2.18	57.5	10.6
	α=3.5	−69	−6	0.37	1.90	1.79	0.94	3.73	2.52	47.2	4.9
Dolph-Chebyshev	α=2.5	−50	0	0.53	1.39	1.33	1.70	3.12	1.85	69.6	22.3
	α=3.0	−60	0	0.48	1.51	1.44	1.44	3.23	2.01	64.7	16.3
	α=3.5	−70	0	0.45	1.62	1.55	1.25	3.35	2.17	60.2	11.9
	α=4.0	−80	0	0.42	1.73	1.65	1.10	3.48	2.31	55.9	8.7
Kaiser-Bessel	α=2.0	−46	−6	0.49	1.50	1.43	1.46	3.20	1.99	65.7	16.9
	α=2.5	−57	−6	0.44	1.65	1.57	1.20	3.38	2.20	59.5	11.2
	α=3.0	−69	−6	0.40	1.80	1.71	1.02	3.56	2.39	53.9	7.4
	α=3.5	−82	−6	0.37	1.93	1.83	0.89	3.74	2.57	48.8	4.8
Barcilon-Temes	α=3.0	−53	−6	0.47	1.56	1.49	1.34	3.27	2.07	63.0	14.2
	α=3.5	−58	−6	0.43	1.67	1.59	1.18	3.40	2.23	58.6	10.4
	α=4.0	−68	−6	0.41	1.77	1.69	1.05	3.52	2.36	54.4	7.6
Exact Blackman		−68	−6	0.46	1.57	1.52	1.33	3.29	2.13	62.7	14.0
Blackman		−58	−18	0.42	1.73	1.68	1.10	3.47	2.35	56.7	9.0
Minimum 3-sample Blackman-Harris		−71	−6	0.42	1.71	1.66	1.13	3.45	1.81	57.2	9.6
Minimum 4-sample Blackman-Harris		−92	−6	0.36	2.00	1.90	0.83	3.85	2.72	46.0	3.8
62-dB-3-Sample Blackman-Harris		−62	−6	0.45	1.61	1.56	1.27	3.34	2.19	61.0	12.6
74-dB-4-Sample Blackman-Harris		−74	−6	0.40	1.79	1.74	1.03	3.56	2.44	53.9	7.4
4-sample-Kaiser–Bessel	α=3.0	−69	−6	0.40	1.80	1.74	1.02	3.56	2.44	53.9	7.4

Table A.2: Selection guide for windows depending on the application

Type of Signal	Window
Transients whose duration is shorter than the length of the window	Rectangular
Transients whose duration is longer than the length of the window	Exponential, Hanning
General-purpose applications	Hanning
Spectral analysis (frequency-response measurements)	Hanning (for random excitation), Rectangular (for pseudorandom excitation)
Separation of two tones with frequencies very close to each other, but with widely differing amplitudes	Kaiser-Bessel
Separation of two tones with frequencies very close to each other, but with almost equal amplitudes	Rectangular
Accurate single-tone amplitude measurements	Flat top
Sine wave or combination of sine waves	Hanning
Sine wave and amplitude accuracy is important	Flat top
Narrowband random signal (vibration data)	Hanning
Broadband random (white noise)	Uniform
Closely spaced sine waves	Uniform, Hamming
Excitation signals (hammer blow)	Force
Response signals	Exponential
Unknown content	Hanning

Appendix B

Sample Matlab Codes

Synchrophasor Signal Processing

```matlab
clear all; close all;clc;
% Analysis parameters:

M = 31;                 % Window length (we'll use a "Hanning window")
N = 31;                 % FFT length (zero padding around a factor of 2)
n = [0:N-1];            % time indices for sinusoid and FFT

%% Two machine infinite bus model

s=xlsread('2bus.xlsx');             % Load Synchrophasor Data simulated from
Powerworld
R=s(:,2);                           % Voltage Magnitude Column
theta=s(:,3);                       % Phase Angle Column
x = R.*exp(theta*sqrt(-1));         % Convert into Phasor form
x=x';
X=real(x);                          % Real part of original signal
figure;plot(X);
Y=imag(x);                          % Imaginary part of the original signal

%% Compute Hanning window:

nm = [0:M-1];                                   % time indices for window
computation
w = (1/M) * (cos((pi/M)*(nm-(M-1)/2))).^2;  % Hanning window
wzp = [w,zeros(1,N-M)];                         % zero-pad out to the length of x
xw = x .* wzp;                                  % apply the window w to the
signal x

%% Plots Time Domain

% Display real part of windowed signal and the Hanning window:

figure;
plot(n,wzp,'-'); hold on;
plot(n,real(xw),'r-');
title('Hanning Window and One Cycle of 60Hz signal');
xlabel('Time (samples)'); ylabel('Amplitude');
legend('Hanning Window','One Cycle DFT Signal');

%stem(n,real(xw));
hold off;
%% Discrete Fourier Transform
Xw = fft(xw);                       % FFT of windowed data
fn = [0:1.0/N:1-1.0/N];             % Normalized frequency axis
spec = 20*log10(abs(Xw));           % Spectral magnitude in dB
```

```matlab
% Since the zeros go to minus infinity, clip at -100 dB:
spec = max(spec,-100*ones(1,length(spec)));
phs = angle(Xw);                                % Spectral phase in radians
phsu = unwrap(phs);                             % Unwrapped spectral phase
(using matlab function)
Nzp = 16;                                       % Zero-padding factor
Nfft = N*Nzp;                                   % Increased FFT size
xwi = [xw,zeros(1,Nfft-N)];                     % New zero-padded FFT buffer
Xwi = fft(xwi);                                 % Take the FFT
fni = [0:1.0/Nfft:1.0-1.0/Nfft];                % Normalized frequency axis
speci = 20*log10(abs(Xwi));                     % Interpolated spectral
magnitude in dB
speci = max(speci,-100*ones(1,length(speci)));  % clip at -100 dB
phsi = angle(Xwi);                              % Phase
phsiu = unwrap(phsi);                           % Unwrapped phase


%%
% [g]=FFTPF1D(Xwi, M, f0, P); figure;
% plot(n,g);
% Plot spectral magnitude
%
%% Plots Frequency Domain

figure;
plot(fn,abs(Xw),'*'); hold on; plot(fni,abs(Xwi));
title('Spectral Magnitude');
xlabel('Normalized Frequency (cycles per sample))');
ylabel('Amplitude (Linear)');
%% Plot in dB
figure;
plot(fn,spec,'*'); hold on; plot(fni,speci);
title('Spectral Magnitude (dB)');
xlabel('Normalized Frequency (cycles per sample))');
ylabel('Magnitude (dB)');
amp=Xw;
amp1=amp(1:2);
```

Magnitude-TVE plot

```matlab
close all;clear all;clc;
a1=xlsread('TVE_mag_data.xlsx');        % Load TVE data from excel file
a=a1(:,1); b=a1(:,2);                   % Data columns for TVE(magnitude)
tve=0:0.2:1.8;                          % Range
%% Plot
plot(a,tve)                             % Plot magnitude against the given
range
hold on;
plot(b,tve)                             % Plot magnitude against the given
range
xlabel('Magnitude Estimation Error(%)');
ylabel('TVE(%)');
title('Total Vector Error')
grid on;
```

```matlab
hold off;
```

Phase-TVE plot

```matlab
close all;clear all;clc;
a1=xlsread('TVE_Phase_data.xlsx');     % Load TVE data from excel file
a=a1(:,1); b=a1(:,2);                  % Data columns for TVE(phase)
tve=0:0.2:1.4;                         % Range
%% Plots
plot(a,tve)                            % Plot phase against the given range
hold on;
plot(b,tve)                            % Plot phase against the given range
xlabel('Phase Estimation Error(Degrees)');
ylabel('TVE(%)');
title('Total Vector Error')
grid on;
hold off;
```

Frequency-TVE plot

```matlab
close all;clear all;clc;
a1=xlsread('frequency_tve.xlsx');   % Load TVE data from excel file
a=a1(:,1); b=a1(:,2);               % Data columns for TVE(frequency)
tve=0:0.2:2;                        % Range
%% Plots
plot(a,b)                           % Plot frequency against the given range
xlabel('Frequency Deviation +/-2Hz');
ylabel('TVE(%)');
title('Total Vector Error')
grid on;
```

Harmonics-TVE plot

```matlab
close all;clear all;clc;
a1=xlsread('harmonics_tve.xlsx');   % Load TVE data from excel file
a=a1(:,1); b=a1(:,2);               % Data columns for TVE(Harmonic Number)
%% Plot
plot(a,b)
xlabel('Harmonics Order');
ylabel('TVE(%)');
title('Total Vector Error')
ylim([-0.1 0.11])
xlim([2 11])
hold on;
plot(b,'rs')
grid on;
```

Fault Location Techniques (Positive, Negative and Zero Sequence data)

```matlab
close all;clear all;clc;
a=xlsread('75_100dlg_busvoltage.xlsx');     % Load Voltage Data
b=xlsread('75_100dlg_current.xlsx');        % Load Current Data
%ls=10;
ls=75;
% ls=35;
%ls=60;
%ls=75;


%% Sending End Voltages
a1=a(1,1);%a2=a(1,4);
b1=a(1,2);%b2=a(1,5);
c1=a(1,3);%c2=a(1,6);
Vas= a1%*exp(i*a2);%z1= a1*exp(i*a2);
Vbs= b1%*exp(i*b2)%z2= b1*exp(i*b2);
Vcs= c1%*exp(i*c2);%z3= c1*exp(i*c2);
% spv=[z1 z2 z3];


%% Receiving End Voltages
a11=a(2,1);%a22=a(2,4);
b11=a(2,2);%b22=a(2,5);
c11=a(2,3);%c22=a(2,6);
Var= a11%*exp(i*a22);%z11= a11*exp(i*a22);
Vbr= b11%*exp(i*b22);%z22= b11*exp(i*b22);
Vcr= c11%*exp(i*c22);%z33= c11*exp(i*c22);
%rpv=[z11 z22 z33];


%% Voltage phasor in Rectangular System
%volp=[spv;rpv]
%% Sending End Current
a3=b(1,1);%a4=b(1,4);
b3=b(1,2);%b4=b(1,5);
c3=b(1,3);%c4=b(1,6)
Ias= a3%*exp(i*a4);%z4= a3*exp(i*a4);
Ibs= b3%*exp(i*b4);%z5= b3*exp(i*b4);
Ics= c3%*exp(i*c4);%z6= c3*exp(i*c4);
%spc=[z4 z5 z6];
%% Receiving End Current
a31=b(2,1);%a41=b(2,4);
b31=b(2,2);%b41=b(2,5);
c31=b(2,3);%c41=b(2,6);
Iar= a31%*exp(i*a41);%z44= a31*exp(i*a41);
Ibr= b31%*exp(i*b41);%z55= b31*exp(i*b41);
Icr= c31%*exp(i*c41);%z66= c31*exp(i*c41);
%rpc=[z44 z55 z66];
%% Zero Sequence Voltage
r=-25.7300;rs=(-26.3700)^2;
```

```matlab
Vos=(1/3)*(Vas+Vbs+Vcs)
Vps=(1/3)*(Vas+r*Vbs+rs*Vcs)
Vns=(1/3)*(Vas+rs*Vbs+r*Vcs)
%% Zero Sequence Voltage
%r=-26.3700;rs=(-26.3700)^2;
Vor=(1/3)*(Var+Vbr+Vcr)
Vpr=(1/3)*(Var+r*Vbr+rs*Vcr)
Vnr=(1/3)*(Var+rs*Vbr+r*Vcr)
%% Zero Sequence Current
ir=-125.5100;irs=(ir)^2;
Ior=(1/3)*(Iar+Ibr+Icr)
Ipr=(1/3)*(Iar+ir*Ibr+irs*Icr)
Inr=(1/3)*(Iar+irs*Ibr+ir*Icr)
%% Zero Sequence Current
%ir=-125.1600;irs=(ir)^2;
Ios=(1/3)*(Ias+Ibs+Ics)
Ips=(1/3)*(Ias+ir*Ibs+irs*Ics)
Ins=(1/3)*(Ias+irs*Ibs+ir*Ics)
%% Current in Rectangular System
%curp=[spc;rpc]
%% Nevative Sequence Voltage and Current
% snv=[z1 z3 z2];rnv=[z11 z33 z22];
% snc=[z4 z6 z5];rnc=[z44 z66 z55];
% voln=[snv;rnv]
% curn=[snc;rnc]
%%
%l=((V_s1-V_r1 ) I_r2-(V_s2-V_r2)I_r1)/((V_s1-V_r1 ) (I)_s2+I_r2)-(V_s2-V_r2
)
(I)_s1+I_r1))*100
l=((Vps-Vpr)*Inr-(Vns-Vnr))/((Vps-Vpr)*(Ins+Inr)-(Vns-Vnr)*(Ips+Ipr))
error=abs((l-ls)/(ls*100))
```

Filtering, DFT, Reconstruction

```matlab
close all;clc; clear all;
%% Testing with the known test signals
%load sineWave

Fs=2000;
t=0:1/Fs:1;
npts = length(t);            % number of points
f0=60;
sineWave = sin(2*pi*f0*t)+2*sin(2*pi*10*t);
%plot(t,sineWave)

%% Plot the sineWave Signal in Time Domain
plot(t,sineWave, 'b');
xlabel('Time(s)');
ylabel('Magnitude');
hold on ;
grid on;

%% Detrend the sineWave Signal.
```

```matlab
xn= detrend(sineWave);
plot(t,xn ,'r');
legend({'Before De-trending', 'After De-trending'});
grid on;
%% Plot the Power Spectral Density of sineWave Signal
[pxx,fx] = pwelch(xn,[],[],[],Fs);
plotsineWave(fx,pxx,' :: Before Filtering');
xlabel('Frequency(Hz)');
ylabel('Magnitude');

%% Low Pass Filtering
N = 7;
Fp = 75;
Ap = 1;
h = fdesign.lowpass('N,Fp,Ap', N, Fp, Ap, Fs);
e = design(h, 'cheby1');
%% Apply the filter to Smooth out the sineWave Signal
xfilter = filter(e,xn);
%% Visualize PSD of the sineWave signal before and after Filtering
[pff,ff] = pwelch(xfilter,[],[],[],Fs);
plotsineWave(fx,pxx,'compare', ff,pff);
xlabel('Frequency(Hz))');
ylabel('Magnitude');

%% Overlay the filtered signal on the original sineWave signal.

% Filtered signal is delayed
figure;
plot(t, xn, 'b',t, xfilter,'r');title('Signals After Applying the
Algorithm');
grid on;

% legend({'Original Signal','Estimated Signal','PPS Signal'});
set(gcf,'NumberTitle','Off', 'Name','Filtered Signal vs. Actual Signal');
xlabel('Time(s)');
ylabel('Magnitude');


%% Defining PPS
%% Reference wave:
% Fc = 60;                      % hertz
% x = cos(2*pi*Fc*t);          % Plot the signal versus time:
% figure;
% plot(t,x);
% xlabel('time (in seconds)');
% title('Reference Cosine Wave');
% zoom xon;


w = 0.01;                       %pulse width
d= w/2:w*100:1;                 %delay vector
y2=3*pulstran(t,d,'rectpuls',w);
%figure;
hold on;
plot(t,y2,'g--','linewidth',2);
```

```matlab
set(gca,'Ylim',[-4 4]);
legend({'Original Signal','Estimated Signal','PPS Signal'});
xlabel('Time(s)');
ylabel('Magnitude');
%legend({'PPS Signal'});
hold off;


%% Calculate Phase Difference
PhDiff = phdiffmeasure(xn, xnn);
% display the phase difference
PhDiffstr = num2str(PhDiff);
disp(['Phase difference xn->xfilter = ' PhDiffstr ' deg'])


% plot the signals
figure;
plot(t, xn, 'b', 'LineWidth', 2)
grid on
hold on
plot(t, xnn, 'r', 'LineWidth', 2)
xlim([0 0.9])
ylim([-4 4])
set(gca, 'FontName', 'Times New Roman')
xlabel('Time, s')
ylabel('Amplitude, V')
title('Two signals with phase difference=0 (After Correction)')
legend('Theoretical signal', 'Synchrophasor Estimated signal')


%% Magnitude and Phase difference computation
X=fft(xn); % take the DFT
Y=fft(xnn); % take the DFT
NumUniquePts = ceil((npts+1)/2); % Calculate the numberof unique points

%%
figure;
subplot(211);
f = (0:NumUniquePts-1)*Fs/npts;
plot(f,abs(X(1:NumUniquePts)));
title('X(f) Theoretical : Magnitude response');
ylabel('|X(f)|')
subplot(212)
plot(f,abs(Y(1:NumUniquePts)));
title('Y(f) Estimated : Magnitude response')
xlabel('Frequency (Hz)');
ylabel('|Y(f)|')

%%
figure;
subplot(211)
plot(f,angle(X(1:NumUniquePts)));
title('X(f) Theoretical : Phase response');
ylabel('Phase (rad)');
subplot(212)
```

```matlab
plot(f,angle(Y(1:NumUniquePts)));
title('Y(f) Estimated : Phase response');
xlabel('Frequency (Hz)');
ylabel('Phase (rad)');


%%
% Determine the max value and max point. This is where the sinusoidal is
located.
[mag_xn idx_xn] = max(abs(X));
[mag_xnn idx_xnn] = max(abs(Y));

% determine the phase difference at the maximum point.
px = angle(X(idx_xn));
py = angle(Y(idx_xnn));
phase_lag = py - px

% determine the amplitude scaling
amplitude_ratio = mag_xnn/mag_xn
amplitude_diff = mag_xnn-mag_xn;
%% Total Vector Error
```

Appendix C

Publications

- (A. Khanal, G. Lebby et. al) Optimal Placement of Phasor Measurement Units for Maximum Network Observability Using Python Gurobi. *Conference: IAJC Orlando Fl, 25th Sep - 27th Sep2014.*

- (A. Khanal, G. Lebby et. al) Impact of Wind Energy on Cost and Balancing Reserves. *Conference, ICEEE, Miami Fl, 09thMar - 10th Mar2015*